Proceedings from the workshop on Neutron, Neutrino, Nuclear, Muon and Medical Physics at ESS,

2-4 December 2009, Lund, Sweden

Introduction

ESS organized a 3-day workshop in December 2009 in Lund on the broader physics programme at ESS. The workshop was named Neutron, Nuclear, Neutrino, Muon and Medical Physics at ESS or simply 3N2MP at ESS. The proceedings that are now finally available reflect the status and thinking of the different topics at the time of the workshop, and are not necessarily up to date. Still, making them available is important for the on-going work on the European science strategy, in the design update projects at ESS and for the planning of the future ESS science programme.

Lund, 11th of April 2012
Johan Rathsman (Lund University), Peter Christiansen (Lund University) and Mats Lindroos (ESS).

Thanks to Esben Klinkby for proofreading.

Table of Content

Title	page
Fundamental Science at ESS	7
Workshop Program	9
Neutron Physics Possibilities at ESS	13
Neutrino Physics Possibilities at ESS	27
Nuclear Physics Possibilities at ESS	53
Muon Physics Possibilities at ESS	69
Medical Opportunities at ESS	95

Fundamental Science at ESS

The ESS project will maintain Europes leadership in the use of neutrons for both materials sciences and for fundamental physics studies. The ESS project has been in preparation for 15 years or more, with initial operations planned for 2019. However, it will not be fully operational before 2023-2025. ESS is primarily designed for neutron scattering science, but it would also be possible to do other neutron related physics at ESS. It is even possible to share the proton driver linac of ESS with other intense proton users such as neutrino physics. An attempt was made at the 3N2MP workshop to make an overview of the opportunities for non-scattering Neutron physics applications, Nuclear, Neutrino, Muon and Medical Physics at ESS. The objective was to identify unique opportunities for such physics at ESS. The scope of the workshop was very broad, in order to avoid missing any unique opportunity for physics at ESS. These proceedings present an overview of the science discussed at the workshop.
New results have been obtained in a number of areas, since the workshop. Most notably, the last unknown mixing angle for neutrino physics, θ_{13}, has been measured and found to be as large as 8.8 degrees ($\sin^2 2\theta_{13} = 0.092 \pm 0.016(\text{stat}) \pm 0.005(\text{syst})$) [1]. This would make a neutrino superbeam at ESS a possible tool to search for CP violation in the weak sector. Tord Ekelöf and co-workers at Uppsala University have recently made such a proposal [2].

The ESS Scientific Advisory Committee advises ESS management on the science program. The work to define the future science program at ESS continues, and we hope that other workshops will follow. Great opportunities for world class physics at ESS should not be missed!

[1] Recent result from the Daya Bay Reactor Neutrino Experiment: `http://arxiv.org/abs/1203.1669`

[2] For more information, see:
`https://indico.nbi.ku.dk/contributionDisplay.py?contribId=83&sessionId=1&confId=380`

Workshop Program

Wednesday 02 December 2009

The European Spallation source - Grand Hotel, Piratensalen (10:00-11:10)

- Conveners: Dr. Lindroos, Mats

time	title	presenter
10:00	Welcome	
10:10	This is ESS!	Dr. CARLILE, Colin
10:50	The present planned science programme at ESS	Dr. VETTIER, Christian

Neutron Physics 1 - Grand Hotel, Piratensalen (11:10-12:15)

- Conveners: Dr. Zimmer, Oliver

time	title	presenter
11:10	Neutrons and the New Standard Model	Prof. RAMSEY-MUSOLF, Michael
11:50	Ultracold Neutron Sources and Physics with UCN	Prof. KIRCH, Klaus

Neutron Physics 2 - Grand Hotel, Piratensalen (13:30-17:00)

- Conveners: Dr. Zimmer, Oliver

time	title	presenter
13:30	Search for new short range interactions with neutrons	Dr. PIGNOL, Guillaume
13:55	The Beta Decay of the Neutron	Dr. ABELE, Hartmut
14:20	Quantum Optical Phenomena Studied with Neutrons	Dr. HASEGAWA, Yuji
14:45	Break	
15:15	A Search for neutron-antineutron oscillations at the ESS	Prof. SNOW, William
15:35	Transverse electron polarization from neutron decay – 2nd generation experiments with pulsed beams	Prof. BODEK, Kazimierz
15:55	Storage modification of the crystal-diffraction nEDM experiment	Dr. VORONIN, Vladimir
16:15	A phase-space-transformer based ultracold neutron source for the European Spallation Source	Dr. ZSIGMOND, Geza
16:35	Neutron-induced single event effects in electronic components and systems: possibilities for studies and testing at ESS	Dr. PROKOFIEV, Alexander
16:45	Polarization of 3He for neutron applications at JCNS	Dr. BABCOCK, Earl

Thursday 03 December 2009

Neutron Physics 3 - Grand Hotel, Piratensalen (08:30-09:20)

- Conveners: Dr. Zimmer, Oliver

time	title	presenter
08:30	Testing Beta Decay Oscillations with Spallation Neutrons	Mr. LUND, Gustav
08:50	An experiment to measure the bound-β- decay of the free neutron	Dr. SCHOTT, Wolgang

Neutrino Physics - Grand Hotel, Piratensalen (09:20-12:40)

- Conveners: Prof. Mezzetto, Mauro

time	title	presenter
09:20	Experience from the LSND experiment, with connections with MiniBooNE and OscSNS	Dr. MILLS, Geoffrey
09:45	Experience from the Karmen Experiment	Dr. STEIDL, Markus
10:10	Why is it so important to measure neutrino cross sections in the ten MeV range	Dr. JACHOVICZ, Natalie
10:35	break	
11:00	Coherent Elastic Netrino Nucleus Scattering	Prof. SCHOLBERG, Kate
11:25	Status of Neutrino Oscillations and Sterile Neutrinos	Dr. MALTONI, Michele
11:50	Physics Potential of an ESS Based Neutrino Experiment	Dr. VOLPE, Cristina
12:15	Rare Decays with Muons	Prof. KUNO, Yoshikata

Nuclear Physics - Grand Hotel, Piratensalen (14:00-17:00)

- Conveners: Prof. Butler, Peter

time	title	presenter
14:00	Nuclear astrophysics using n-TOF facilities	Dr. REIFARTH, Rene
14:30	Radioactive Ion Beam Physics @ MYRRHA	Prof. VAN DUPPEN, Piet
15:00	EURISOL: A Multi-Megawatt Facility for Nuclear Physics	Dr. BLUMENFELD, Yorick
15:30	Coffee break	
16:00	The European Spallation as Source of Neutrinos for Nuclear Astrophysics Applications	Dr. MARTINEZ, Gabriel
16:30	Muonic Radioactive Atoms	Dr. STRASSER, Patrick

Friday 04 December 2009

Muon Physics - PALESTRA building, at Lund University area, Lundagård (09:00-11:00)

- Conveners: Prof. Jungmann, Klaus

time	title	presenter
09:00	Muon Physics Possibilities at ESS in Comparison to other Activities in the Field	Prof. NAGAMINE, Kanetada
09:30	Muons and Slow Muons and Their Physics Prospects	Dr. MORENZONI, Elvezio
10:00	A Condensed Matter Muon Spin Relaxation Facility at ESS	Dr. LORD, James
10:30	Compact storage ring to search for the muon electric dipole moment	Dr. ONDERWATER, Cornelis

Medical applications - PALESTRA building, at Lund University area, Lundagård (11:30-12:30)

- Conveners: Prof. Peach, Ken

time	title	presenter
11:30	Production of radioisotopes for medical applications	KOESTER, Ulli
12:05	Medical applications at a neutron source	Prof. PEACH, Ken

Conclusions - PALESTRA building, at Lund University area, Lundagård (12:30-13:30)

time	title	presenter
12:30	Concluding remarks: Nuclear, Medicine and Neutron Physics	Prof. CHOMAZ, PHILIPPE
12:50	Concluding remarks: Muon and Neutrino Physics	Dr. MCELRATH, Bob
13:10	Closing of the workshop	

Neutron Physics Possibilities at ESS

H. Abele,[1] E. Babcock,[2] K. Bodek,[3] Y. Hasegawa,[4] K. Kirch,[5]
G. Lund,[6] G. Pignol,[7] A. Prokofiev,[6] M. Ramsay-Musolfs,[8]
W. Schott,[7] W. Snow,[9] V.V. Voronin,[10] and G. Zsigmond[11]

[1] *Vienna University of Technology, Vienna, Austria*

[2] *JCNS, Garching, Germany*

[3] *Jagiellonian University Institute of Physics, Cracow, Poland*

[4] *Atominstitut TU-Wien, Vienna, Austria*

[5] *ETH Zurich, Villigen PSI, Switzerland*

[6] *Uppsala University, Uppsala, Sweden*

[7] *TU München, Garching, Germany*

[8] *University of Wisconsin-Madison, Madison, United States of America*

[9] *Indiana University, Bloomington, United States of America*

[10] *Petersburg Nuclear Physics Institute, Gatchina, Russia*

[11] *Paul Scherrer Institut, Villigen PSI, Switzerland*

I. THE NEUTRON AS AN ELEMENTARY PARTICLE

We stand at a crossroads moment at the interface of particle physics with nuclear physics, astrophysics, and cosmology. For three decades, the Standard Model of particle physics has successfully provided our framework for explaining phenomena involving three of the four known forces of nature. However, there exist many reasons to believe that the SM is not the complete theory. Besides the energy frontier, there exists another frontier in the search for what I will call the new Standard Model (NSM): the high precision, high sensitivity frontier. The pattern of deviations (or their absence) that emerges from precision experiments is like a set of footprints of new forces.

A. Neutron EDM and the Origin of Matter

The search for the neutron EDM is already shedding light on one of the outstanding puzzles at the interface of particle and nuclear physics with cosmology: Why is there more

visible matter than antimatter in the universe?

There are three necessary ingredients for successful baryogenesis the process whereby something (net baryon number) was created out of nothing: (a) violation of baryon number (B); (b) violation of both C and CP symmetry; and (c) a departure from equilibrium dynamics. The observation of a non-zero EDM of the neutron could signal the presence of CP-violating interactions needed to produce the early universe charge asymmetries (e.g. [1, 2]).

To date, we have only upper limits on the magnitude of the neutron EDM and on the EDMs of other systems, such as neutral atoms from which one deduces an upper limit on the electron EDM. Since we do not know where the CP-violation needed for the abundance of matter might live, it is important to search for EDMs of a variety of systems. Consequently, one should view the neutron EDM program in the broader context of EDM searches. Nonetheless, the neutron EDM holds a special place as the simplest system involving quarks and gluons that could have a non-vanishing EDM (d = 2.9 x 10^{-26} e-cm; [3]).

The current neutron EDM limit is, nevertheless, compatible with successful supersymmetric electroweak baryogenesis under the right conditions for the superpartner spectrum. It would likely take future EDM searches with two orders of magnitude better sensitivity to conclusively test this possibility [2]. Experiments underway at the ILL in Grenoble, PSI in Switzerland, and Spallation Neutron Source in the U.S. are working their way toward this horizon. It may be that a future experiment at the ESS, with the significantly higher neutron flux, could push the neutron EDM program across the finish line in the search for cosmologically relevant CP-violation.

V.V. Voronin proposed an alternative method for a precise determination of an electric dipole moment of the neutron. This method uses the strong internal electrical fields of noncentro symmetric crystals which may reach values up to 6.5x10^8 V/cm (in BeO). A proposed crystal resonator system can uses the pulse structure of the ESS source due to a multiple transit of the beam through such a crystal [4].

B. Neutron decay

A beam position for particle physics with cold neutrons strongly profits from ESS. A gain factor of 30 compared to ILL is expected, if a LPTS with 16 2/3 Hz repetition rate and a pulse length of 2 ms is realized. On the time scale of the ESS, one will anticipate a robust

and high impact program of neutron decay studies, building on the vast experience and ongoing progress at ILL, FRM2, NIST, Los Alamos, and the SNS. The physics programme is rich and includes the following precision tests of the Standard Model and search for physics beyond the Standard Model:

- An improved determination of Standard Model parameters. With a new and precise value of λ, the ratio of the axial-vector to vector-coupling, one will cover the demand from particle physics, astro-particle physics, where this quantity is needed for calculations of the nucleosynthesis after the big bang, the energy production in the sun, the formation of neutron stars, and the calibration of neutrino- LHC-detectors. A new value for $V_{\rm ud}$, the first element of the Cabibbo-Kobayashi-Maskawa (CKM) matrix gives better insight into quark mixing, allowing precise tests of CKM unitarity.

- A search for right-handed admixtures to the left-handed feature of the Standard model. They are forbidden in the Standard-Model, but, as a natural consequence of symmetry breaking in the early universe, they should be found in neutron b - decay. Signatures are a WR mass with mixing angle ζ.

- A search for scalar and tensor admixtures $g_{\rm S}$ and $g_{\rm T}$ to the electroweak interaction. $g_{\rm S}$ and $g_{\rm T}$ are also forbidden in the Standard model but supersymmetry contributions to correlation coefficients or the Fierz interference term b can approach the 10^3 level, a factor of five away from the current sensitivity limit. See Section III for an experimental proposal.

- A precision measurement of the weak-magnetism form factor f_2 prediction of electroweak theory. Such an experiment would be one of the rare occasions, where a strong test of the underlying structure itself of the Standard model becomes available.

In contrast to the EDM experiments, precise studies of neutron decay parameters, such as the neutron lifetime and decay correlation coefficients, start off by measuring quantities that are not suppressed in the Standard Model. In this case, the goal is to look for exquisitely small deviations from the non-zero SM predictions that could signal the presence of virtual new particles that were more active as real particles in the early universe.

To illustrate, consider tests of the unitarity of the Cabibbo-Kobayashi-Maskawa matrix, for which superallowed nuclear β-decay provides the most input in the guise of $V_{\rm ud}$. Combin-

ing the results of an extensive program of experimental lifetime, branching ratio, and Q-value measurements with recent progress in computing hadronic contributions to SM electroweak radiative corrections, one obtains a value for $V_{\rm ud}$ with a precision of a few times 10^{-4} [1, 5].

Looking to the future, if progress is made in reducing the uncertainties associated with $V_{\rm us}$, the limit in CKM unitarity tests may again be set by $V_{\rm ud}$. In this respect, a program of neutron decay studies that include a more precise determination of the lifetime and one or more of the decay correlation coefficients, may provide a path forward. The nuclear decay determinations of $V_{\rm ud}$ are likely to hit an irreducible uncertainty associated with nuclear structure corrections to the ft values. In addition, certain neutron decay correlations may provide information about new interactions that do not have pure left- or right-handed character or exotic particles such as leptoquarks.

A new perspective aspect comes in due to the recent observation of a modulated electron decay process in hydrogen-like ions in storage rings [6]. There is no clear theoretical explanation for such an oscillation. The suspicious scale 10^3 eV has shown up in seemingly unrelated experiments repeatedly. This scale belongs to the average temperature and density of the universe as well as several unexplained experimental anomalies: neutrino mass and cosmological constant and it is related through the Planck scale to the Hubble constant, Pioneer anomaly and the MOND acceleration parameter, none of which are fully understood at present. It is proposed to test the possibility that it is the electron that is oscillating, by removing it from the initial state in the neutron-hydrogen-atom decay channel. The installation of a neutron-hydrogen atom decay spectroscopy system is recommended.

C. Neutron-antineutron oscillations

An observation of neutron-antineutron oscillations would constitute a discovery of fundamental importance for particle physics and cosmology. The required change in baryon number by 2 units with no change in lepton number would signal physics beyond the Standard Model and could be relevant for understanding the matter-antimatter asymmetry of the universe. We mention recent developments in cold neutron technology which can make possible improvements in the sensitivity to the free neutron oscillation probability by factors of 100-1000. For these sensitivities a null result would place the most stringent limit on this possible mode of matter instability. At an intense pulsed source such as the ESS one can

imagine reducing the transverse size of the beam (and therefore the cost of the experiment) using a phased supermirror reflector array.

What physics might a search for neutron-antineutron oscillations address? One issue is the ultimate stability of matter. Since there are many particles lighter than nucleons there is no obvious physical principle that forbids them from disappearing. In the Standard Model (SM) there seem to be two globally-conserved quantum numbers: baryon number B and lepton number L. Extensions to the Standard Model are not expected to conserve either B or L, however, and B violation leads to matter instability. Proton decay has never been seen: typical upper limits for the proton decay rate into different modes range from $10^{32} - 10^{33}$ years. If a neutron oscillates into an antineutron inside a nucleus, the antineutron annihilates and the nucleus explodes: this phenomenon also has never been observed. SM extensions can lead to B violation by 2 units and not 1 unit [7].

The probability for a neutron to oscillate into an antineutron at time t is

$$P = \frac{\delta^2}{\delta^2 + V^2} \sin^2 \left(\sqrt{\delta^2 + V^2}\, t/\hbar \right) \tag{1}$$

where δ is the off-diagonal piece of the Hamiltonian in neutron-antineutron state space which induces the oscillation and V incorporates the effects of all interactions which are different for the neutron and the antineutron. The oscillation time τ is simply $\tau = h/\delta$. The neutron-antineutron energy splitting 2V from both the difference in the neutron and antineutron optical potential in the residual gas of a vacuum chamber and from the Zeeman energy difference 2μB in a magnetically-shielded volume is orders of magnitude larger than the neutron-antineutron transition energy d for any conceivable experiment. Therefore the experiment must be operated in the quasifree limit corresponding to $Vt < h$: in this limit the antineutron transition probability is still $(\delta t/h)^2$ as can be seen above. Thus high vacuum and suppressed magnetic fields are mandatory.

A search for oscillations using free neutrons therefore possesses decisive experimental advantages. The last experiment in the free neutron system set an upper limit of 8.6 x 10^7s (90 % confidence level) on the oscillation time [8]. A schematic view of a related instrument is shown in Fig. 1.

An elliptical mirror assembly and piezo-controlled reflecting plates could reduce the transversal gravity spreading of the beam and increase the sensitivity of the method. The improvements in sensitivity that can be reached, when expressed in terms of the instability

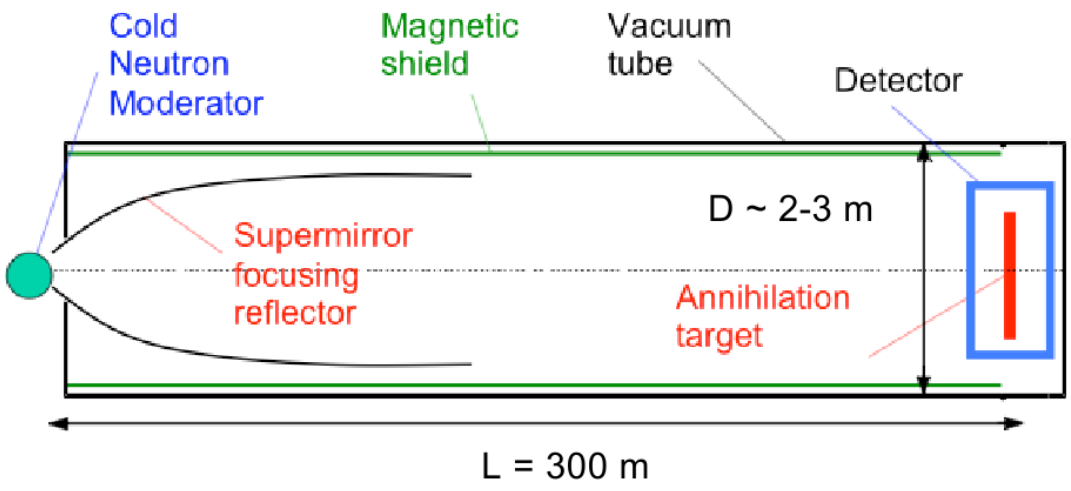

FIG. 1. Proposed layout of a new neutron-antineutron oscillation experiment.

of matter, approach the 10^{36} year range. A null result would therefore place the most stringent existing limit on a possible decay mode for the "normal" matter whose mass dominates our everyday world.

II. THE NEUTRON AS A QUANTUM WAVE

As massive particles neutrons exhibit all quantum effects and can be used to get new insight into the quantum world. Many neutron interference experiments have been performed with perfect crystal interferometers and various Larmor interferometer methods [9]. Since several interpretations of quantum physics are at the table new experiments should decide whether a more complete theory exists and can be formulated in the future. Questions about reality, locality and causality can be tackled by neutron quantum optics methods. Entanglement, contextuality and gravity quantization experiments are interesting topics for related experiments at a pulsed high flux spallation source. Many of such experiments need ultra-cold neutrons which can be produced at such sources rather effectively.

A. Neutron quantum optics

There are arguments to extend and reorganize quantum mechanics by a deterministic theory underlying it. Two major schemes refuting those theories are a violation of Bells

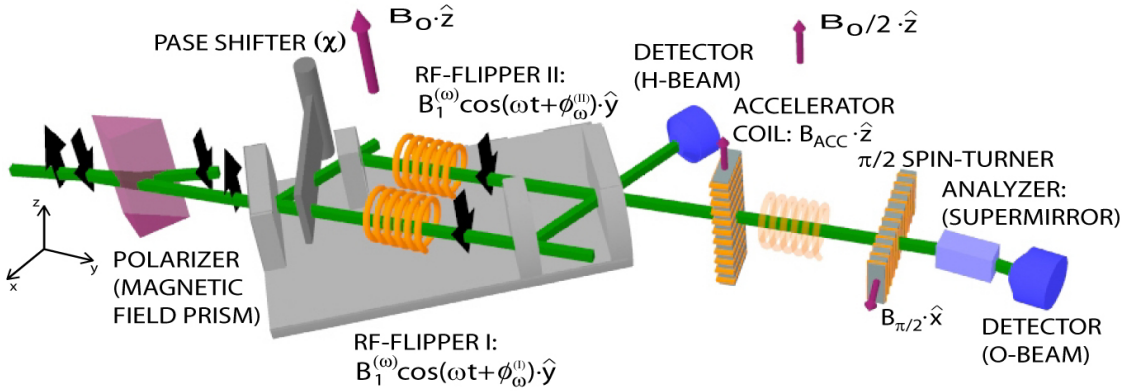

FIG. 2. Neutron interferometric set-up for triply entanglement of neutron quantum states.

inequality [10], and the Kochen-Specker theorem [11]. The former discards local hidden-variable theories, and the latter stresses the incompatibility of quantum mechanics with a large class of hidden-variable theories. Such theories assume that the result of a measurement of an observable is predetermined and independent of a suitable (previous or simultaneous) measurement of any other compatible observable. While the original proof of the Kochen-Specker theorem is rather complicated, an experimentally testable inequality can be achieved by neutron interferometry. Figure 2 shows how neutrons can be manipulated to achieve and analyze a spin-beam path-energy entanglement [12]. For such experiments optical benches, clean room conditions and vibration isolations are requested.

Exploiting two beams in interferometers, which are really separated in a macroscopic scale, or the interference between two spin eigenstates , neutron optical methods, i.e., neutron interferometry as well as neutron polarimetery, are established as very useful strategies for the investigation of quantum theory. Such studies are of relevance for quantum information and communication technologies. Further applications like a quantum/wave calculation and resources for spectroscopic improvements are anticipated.

B. Gravity quantization

The neutron is an appropriate particle to investigate gravity effects in detail. That can be done by means of neutron interferometry where the quantum phase is influenced by gravity and any non-inertial phenomenon, and by means of ultra-cold neutrons where the gravity

effects become comparable with the kinetic energy of these neutrons. Recently the quantization of neutrons within the Earth gravity field has been observed (Nesvizhevsky et al. 2002) and transitions between these levels can be induced [13]. This opens the field of peV-physics which will become an important branch of neutron physics in the future. The search for additional terms to the Newtonian one for small distances will become an interesting topic for such investigations. The idea is to explore a unique system consisting of a particle, the neutron, and a macroscopic object, the mirror. Such measurements with ultracold neutrons will offer high sensitivity to various gravity terms (e.g.Yukawa-like contributions at small distances).

$$V(r) = -G\frac{m_i m_j}{r}\left(1 + \alpha e^{-r/\lambda}\right) \tag{2}$$

To date neutron physics experiments provide the most stringent limits at very short distances around 1- 100 nm.

III. NEUTRON BOUND β- DECAY- BOB

The neutron decay is for many years subject of intense studies, as it reveals detailed information about the structure of the weak interaction. Using the two-body neutron β-decay into a hydrogen atom (H) and an electron antineutrino ($\bar{\nu}$)

$$n \rightarrow H + \bar{\nu} \tag{3}$$

the hyperfine population of the emerging hydrogen atom can be investigated [15]. The challenge lies in the very small branching ratio BR $= 4 \cdot 10^{-6}$ of the total neutron β-decay rate. Hydrogen atoms from this decay have 326.3 eV kinetic energy corresponding to $\beta = 0.83 \cdot 10^{-3}$. Only states with zero angular momentum in the hydrogen atom are populated, the 1s and the metastable 2s with 83.2% and 10.4% probability, respectively.

According to [16]- [17] for a purely left-handed V-A interaction three hydrogen hyperfine spin states associated with the antineutrino helicity $H_{\bar{\nu}}$ =1 exist with populations depending only on one variable $\chi = (1+g_S)/(\lambda - 2g_T)$, $\lambda = g_A/g_V = -1.2695 \pm .0029$ [18]. g_A, g_V, g_S, g_T are the axial, vector, scalar and tensor coupling constants. Thus, by measuring the three spin state populations, a combination of g_S and g_T can be obtained. A fourth spin state can only be populated by the emission of right-handed neutrinos resulting in $H_{\bar{\nu}} < 1$. Thus,

by measuring this spin state, beyond Standard Model quantities, as the V+A model η and ζ are obtained [19]. η is the mass ratio squared of two intermediate charged vector bosons and ζ the boson mass eigenstate mixing angle.

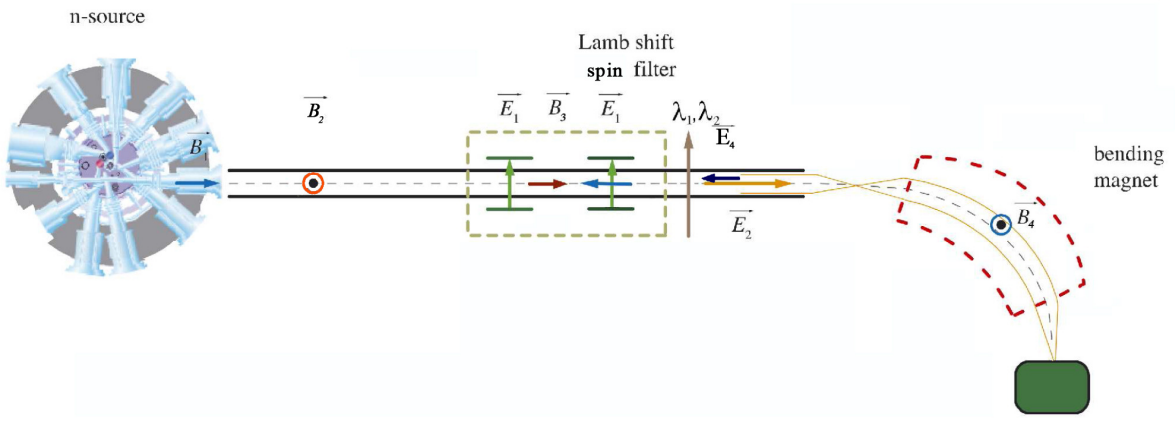

FIG. 3. Sketch of the experimental setup for measuring hydrogen atoms from neutron bound-β-decay at an intense neutron source.

A. Experiment

At an intense thermal neutron source through-going beam tube, e. g., at the FRM2 with $1.4 \cdot 10^{14}$ neutrons/(cm^{2}s)(Fig. 3), a $3\,\mathrm{s}^{-1}$ background free bound β- decay rate can be obtained. The small axial $\vec{B_1}$ field keeps the initial H(2s) spin configuration. The three-body neutron β-decay protons and electrons are shielded by the transverse magnetic field B_2= 100 Gauss. Other charged and neutral particles moving in transverse directions are suppressed by diaphragm absorbers on both sides of the through- going beam pipe. One of the four metastable H(2s) hyperfine state atoms are selected by a Lamb shift spin filter and subsequently excited to a Rydberg state within two crossed perpendicular curved mirror laser resonators and ionized by the axial $\vec{E_2}$ field by means of which the resulting protons are accelerated and focused by the transverse $\vec{B_4}$ field(magnet with wedges) onto a detector [20]. In a first experiment, the bound β-decay H(2s) atom yield is obtained by quenching the H(2s) atoms with an axial $\vec{E}$ field and measuring the resulting Lyman- α photons. Alternatively, the H(2s) atoms after the spin filter are charge exchanged into H^- within a 1 mbar Ar cell, selected from H^- produced by H(1s) by the axial field $\vec{E_4}$, accelerated by $\vec{E_2}$

and focused by $\vec{B}_4$ onto a detector.

In a mock- up experiment outside a neutron facility, an ionizer was set up, by means of which a 50 nA 550 eV proton beam was produced and separated from other ions by a Wien filter. The protons were partially exchanged into H(2s) within a Cs cell. One of four hyperfine spin states was selected by a spin filter. After the spin filter the H(2s) atoms were either quenched by means of an $\vec{E}$ field, and the Lyman- α photons measured by a solar blind photo multiplier, or the H(2s) were charge exchanged within an Ar cell into H^- which were then analyzed by an electric counter field, accelerated and focused onto a detector. Figure 4 shows the Lyman- α intensity produced by quenching the H(2s) atoms after the spin filter vs. the spin filter field $\vec{B}_3$. The peaks correspond to the $\alpha(1,1)$ and $\alpha(1,2)$ H(2s) hyperfine spin states [20].

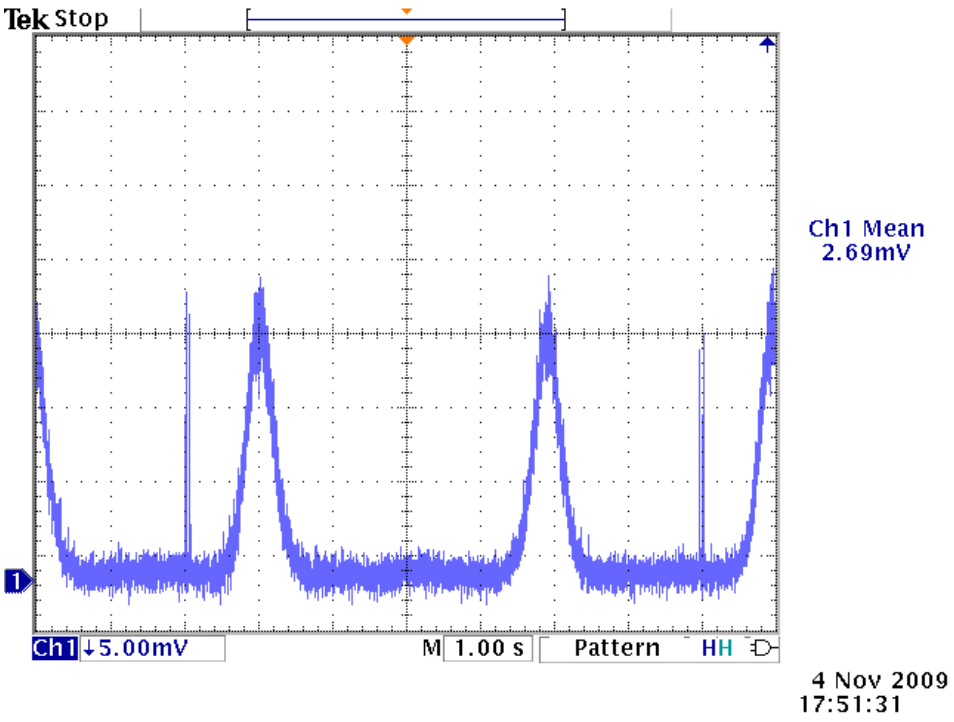

FIG. 4. Photo multiplier current vs. spin filter quantization field B_3

B. Perspectives at ESS

For BOB and other neutron decay experiments, as, e. g., the measurement of the neutron β- decay asymmetry[21], an extremely low neutron and γ background is important. This can be achieved, if the experiment is mounted at a beam pipe going through the moderator tank at the thermalization length distance(0.33 m) away from the neutron source. Neutrons and γ rays are absorbed on both sides of the beam pipe outside of the moderator tank by traps consisting of a widened beam tube and orifices with successively smaller apertures.

In order to do this type of experiments at ESS, such a beam pipe should be intgegrated. At ESS, a larger bound β hydrogen rate $\dot{N}_H$ than at other intense neutron sources can be obtained yielding for the $3.1 \cdot 10^{14}\, n/(cm^2 s)$ T=300K ESS average thermal neutron flux at ca. 0.3 m away from the target $(\dot{N}_H)_{ESS} \approx 2 \cdot (\dot{N}_H)_{FRM2}$ and for a T=20K ESS moderator with the same average flux $(\dot{N}_H)_{ESS} \approx 8 \cdot (\dot{N}_H)_{FRM2}$. The background can be further reduced by triggering the experiment(e. g., the lasers) with the ESS long and short proton pulses yielding 150 μs long thermal neutron pulses of $1.0 \cdot 10^{16}\, n/(cm^2 s)$ and $1.3 \cdot 10^{17}\, n/(cm^2 s)$ peak fluxes, respectively, being 65 and 840 times larger than the FRM2 average flux.

By measuring the neutron bound- β- decay, the g_S or g_T upper limits should be reduced by a factor 10 and $H_{\bar{\nu}}$ obtained with 10^{-3} accuracy.

IV. SUMMARY AND CONCLUSIONS

The workshop Neutrino, Neutron, Nuclear, Medical and Muon Physics at ESS in Lund in December 2009 was a very useful meeting in order to identify opportunities for nonscattering activities. Especially the higher intensity and the pulse structure of the ESS provide new possibilities for fundamental neutron physics experiments. The next step is certainly their consideration during the design phase of ESS. On focus are the Day-One-Instruments, which strongly profit from the opportunities at ESS. To strengthen the case for particle and fundamental physics at ESS, we would like to suggest the following Day-One-Installations at ESS, where the expected benefit factor compared to ILL can reach 30 or more:

- Beam station for particle physics with cold neutrons

  Requirements: cold neutron supermirror guide coupled to LPTS with 16 2/3 Hz rep-

etition rate and a pulse length of 2 ms for an expected gain factor of 30 compared to ILL. The area required for the experiments should be about 10 m in width, 15 m in length and 6 m in height, floor load approx. 10 t/m^2, crane load of 5t.

- Beam station for particle physics with ultra-cold neutrons
  Requirements: An ultra-cold neutron station driven by a separate target and the installation of an advanced phase space transformer [14]. Area requirement 42 m^2 (including UCN-source).

- Beam station for quantum optics experiments with thermal neutrons
  Requirements: Supermirror guide, optical bench, clean room, air conditioning, vibration isolation area 36 m^2.

These installations can contribute to make ESS unique and more attractive for a broad community of scientists.

V. ACKNOWLEDGMENTS

Wolfgang Schott would like to thank his collaborators: S. Paul, M. Berger, R. Emmerich, R. Engels, T. Faestermann, P. Fierlinger, F. J. Hartmann, R. Hertenberger, J Schön, W. Schott, U. Schubert, A. Trautner, and T. Udem.

[1] H. Abele, The neutron. Its properties and basic interactions, Prog. Part. Nucl. Phys **60**, 1-81 (2008)

[2] V. Cirigliano, Y. Li, S. Profumo, and M. J. Ramsey-Musolf, MSSM Baryogenesis and Electric Dipole Moments: An Update on the Phenomenology, accepted for publication in JHEP [arXiv:0910.4589/hep-ph] (2009).

[3] C. A. Baker et al, An Improved Experimental Limit on the Electric Dipole Moment of the Neutron Phys Rev. Lett. **97**:131801 (2006).

[4] V.V. Fedorov, I.A. Kuznetsov, E.G. Lapin, et al., Nucl. Instr. and Meth., **B252** (1) (2006) 131-135.

[5] S. Profumo, M. J. Ramsey-Musolf and S. Tulin, Supersymmetric Contributions to Weak Decay Correlation Coefficients, Phys. Rev. **D75**:075017 (2007)

[6] P. A Vetter et.al, Search for oscillation of the Electron-Capture decay probability of 142Pm. Phys.Lett.**B670**:196, (2008).

[7] H. V. Klapdor-Kleingrothaus, E. Ma, and U. Sarkar, Mod. Phys. Lett. **A17**, 2221 (2002).

[8] M. Baldo-Ceolin et al., Z. Phys. **C 63**, 409 (1994).

[9] H. Rauch, S.A. Werner, Neutron Interferometry, Clarendon Press, Oxford 2000.

[10] J. S. Bell, Physics (Long Island City, N.Y.) **1** (1964) 195

[11] S. Kochen and E. Specker, J. Math. Mech. **17** (1967) 59

[12] H. Bartosik, J. Klepp, C. Schmitzer, S. Sponar, A. Cabello, H. Rauch and Y. Hasegawa, Phys. Rev. Lett. **103** (2009) 040403.

[13] H. Abele et al., QuBounce: the dynamics of ultra-cold neutrons falling in the gravity potential of the Earth, Nuclear Physics **A827**, 593c (2009).

[14] S. Mayer, H. Rauch, P. Geltenbort, P. Schmidt-Wellenburg, P. Allenspach, G. Zsigmond, New aspects for high-intensity neutron beam production, Nucl.Instr.Meth. A **608** (2009) 434

[15] L. L. Nemenov, Sov. J. Nucl. Phys. **31**, 115 (1980).

[16] L. L. Nemenov and A. A. Ovchinnikova, Sov. J. Nucl. Phys. **31**, 659 (1980).

[17] W. Schott et al., Eur. Phys. J. A **30**, 603 (2006).

[18] S. Eidelman *et al.*, Phys. Lett. B **592**, 1 (2004) and 2005 partial update for edition 2006.

[19] J. Byrne, Eur. Phys. Lett. **56**, 633 (2001).

[20] W. Schott et al., Hyperfine Interact, DOI 10.1007/s10751-009-0011-z, Springer Science+Business Media B. V. 2009.

[21] H. Abele et al., Phys. Rev. Lett. **88**, 211801(2002).

Neutrino Physics Possibilities at ESS

Markus Steidl,[1] N.Jachowicz,[2] Kate Scholberg,[3]
R. Lazauskas,[4] C. Volpe,[5] and Michele Maltoni[6]

[1]*Institut fr Kernphysik, Karlsruhe Institute of Technology, 76344 Eggenstein, Germany*

[2]*Ghent University, Department of Physics and Astronomy,*
Proeftuinstraat 86, B-9000 Gent, Belgium

[3]*Duke University, Durham, United States of America*

[4]*IPHC, IN2P3-CNRS/Université Louis Pasteur BP 28, F-67037 Strasbourg Cedex 2, France*

[5]*Institut de Physique Nucléaire, F-91406 Orsay cedex,*
CNRS/IN2P3 and University of Paris-XI, France

[6]*Instituto de Física Teórica UAM/CSIC,*
Universidad Autónoma de Madrid, Cantoblanco, E-28049 Madrid, Spain

This summary of the neutrino part of the workshop consists of individual contributions for each talk.

I. EXPERIENCES FROM THE KARMEN EXPERIMENT

The KARMEN (KArlsruhe Rutherford Medium Energy Neutrino) experiment has been performed at the neutron spallation facility ISIS of the Rutherford Appleton Laboratory (Chilton,UK) over the period of time from 1990-2001. Due to a clean neutrino beam provided by ISIS, which is well characterized in time, energy and flavour content unique neutrino-nucleus cross section measurements were performed. Furthermore, searches for physics beyond the standard model have been carried out, in particular searches for neutrino oscillations. Neutrino-nucleus interactions in the energy range of several MeV are of special interest in astrophysical calculations, e.g. as outlined in this conference [1]. In case of neutrino oscillations special emphasis had been on the $\bar{\nu}_\mu \rightarrow \bar{\nu}_e$ appearance channel due to a claim of evidence by the LSND experiment for such oscillations [2]. Such a claim is of special importance as a global parameter fit to all available neutrino oscillation data can not be reconciled within the standard model of three neutrino flavors [3]. Whereas in this short contribution not all results and experiences can be presented, a complete description

of KARMEN and its results is given in [4].

A. Source and detector

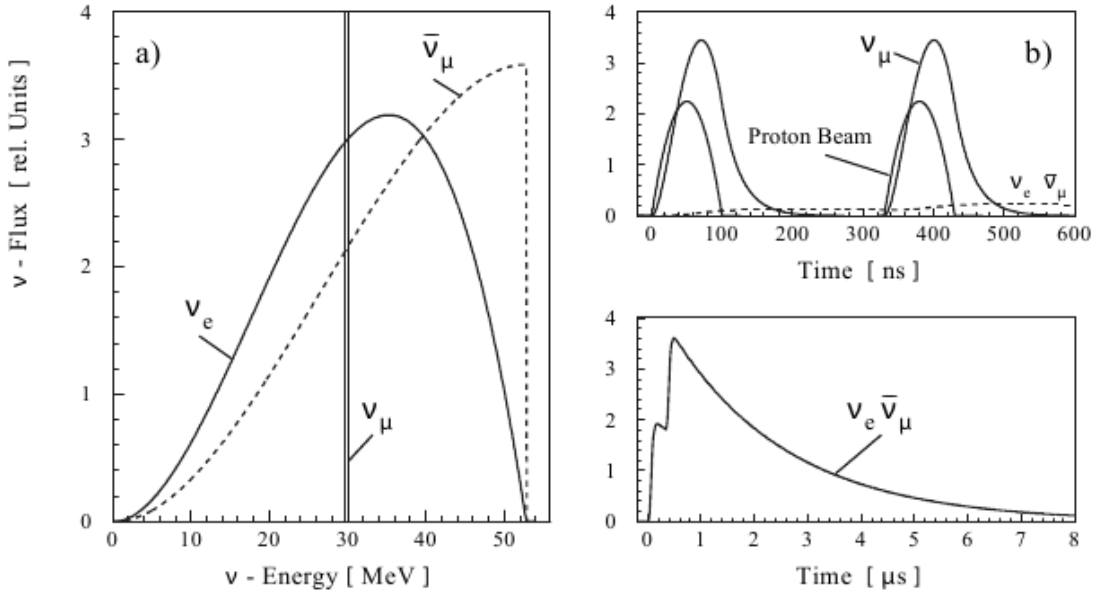

FIG. 1. (a) energy and (b) time structure of produced neutrinos at ISIS

The neutrinos were produced at ISIS by stopping 800 MeV protons in a beam dump Ta-D^2O-target (see Fig. 1): ν_e, ν_μ, and $\bar{\nu}_\mu$ emerge with equal intensities from the decay chain of primarily produced π^+. The ν_μ from π^+ -decay at rest are monoenergetic ($E_0 = 30$ MeV) whereas the continuous energy distributions of ν_e and $\bar{\nu}_\mu$ up to 52.8 MeV can be calculated using the V-A theory. Two parabolic proton pulses of 100 ns base width and 325 ns apart are produced by the ISIS machine with a repetition frequency of 50 Hz. The different lifetimes of π^+ ($\tau = 26$ ns) and μ^+ ($\tau = 2.2\ \mu s$) allow a clear separation in time of the ν_μ-burst from the following ν_e and $\bar{\nu}_\mu$ and provide duty cycles of 10^{-5} and 5x10^{-4} respectively. The impressive duty cycle led to high signal to background ratios in the neutrino-nucleus analysis up to 60:1.

The neutrinos are detected in a 56 tonnes liquid scintillation calorimeter with an active volume of 96 % [5]. The KARMEN detector is segmented into 512 optically individual modules by double acrylic walls with an air gap allowing efficient light transport via total internal reflection. Gd2O3 coated paper within the module walls provide efficient detection

of thermal neutrons via Gd(n,g) capture. A massive 7000 ton iron blockhouse in combination with three layers of active anti counters provides shielding against beam correlated spallation neutron background and suppression of hadronic and muonic cosmic background. The third veto counter has been commissioned in Feb. 1997 leading to a cosmic background reduction of a factor 40 [6] compared to the previous configuration.

B. Neutrino Nucleus Interactions

The following table shows a compilation of measured charged and neutral current reactions. The major systematical uncertainty arises from the uncertainty on the total neutrino flux, reflecting the uncertainty of π^+ production simulations, which take the detailed geometry of the target into account. In the third column the original references are quoted, a complete update taking all data from the KARMEN era into account can be found in [4].

Reaction	Cross Section in 10^{-42} cm^2	Original reference
^{12}C$(\nu,\nu')^{12}$C'	10.2 ± 0.4 stat. ± 0.8 syst.	PLB332 (1994) 251
^{12}C$(\nu_\mu,\nu'_\mu)^{12}$C'	3.2 ± 0.5 stat. ± 0.4 syst.	PLB423 (1998) 15
^{12}C$(\nu_e,e^-)^{12}$N$_{gs}$	9.6 ± 0.3 stat. ± 0.7 syst.	PLB339(1994)215
^{12}C$(\nu_e,e^-)^{12}$N*	4.8 ± 0.6 stat. ± 0.5 syst.	Progr.Part.Nucl.Phys 40 (1998) 183
^{13}C$(\nu_e,e^-)^{13}$N*	50 ± 25 stat. ± 6 syst.	[4]
^{56}Fe (ν_e,e^-)X	217 ± 35 stat. +27 syst. -65 syst.	Progr.Part.Nucl.Phys 40 (1998) 183

TABLE I. Compilation of measured charged and neutral current reactions.

C. Search for $\bar{\nu}_\mu \to \bar{\nu}_e$ oscillations

The signature for $\bar{\nu}_e$ detection is a spatially and delayed correlated coincidence between a high energetic positron from the p($\bar{\nu}_e$, e^+)n reaction and the subsequent γ-emission from neutron capture. The positrons show the 2.2 μs exponential decrease due to the μ^+ decay and are therefore expected in a time window of several microseconds after beam on target. The energies of the positrons reach up to 51 MeV. The shape of the expected energy spectrum strongly depends on Δm^2, reflecting the dependence of the oscillation formula on Δm^2

and an excellent energy resolution of the detector. Neutrons are captured either on protons, emitting a single monoenergetic 2.2 MeV gamma, or they are captured on Gd, emitting on average 3 quanta with a sum energy of 8 MeV. The time difference between e^+ and γs from neutron capture shows an exponential decrease of 120 ms lifetime. A delayed coincidence is accepted in a delayed time window of 5-300 ms after the prompt event and to be within a coincidence volume of 1.3 m.

In total, 15 candidates fulfill all conditions for the $\bar{\nu}_e$ signature, in agreement with the background expectation of 15.8 ± 0.5 events, yielding no indication for oscillations. A single event based likelihood analysis leads to upper limits on the oscillation parameters: $\sin^2(2\Theta) < 1.7 \times 10^{-3}$ for $\Delta m^2 \geq 100$ eV and $\Delta m^2 < 0.055$ eV^2 for $\sin^2(2\Theta) = 1$ at 90 % confidence [6]. Thus, KARMEN does not confirm the LSND experiment and restricts significantly its favored parameter region for Δm^2 and $\sin^2(2\Theta)$. Other searches The neutrino beam purity and good energy resolution of the KARMEN detector allowed for further sensitive searches for non SM physics:

Search	Result	Original reference
Test of (V-A) structure in m-decay	$\omega_L < 0.113$ (90%CL)	PRL81(1998) 520
Weak charge radius of 12C nucleus	R_A = (3.8 +1.4/-1.8) fm	PLB339(1994) 215
NC/CC flavour universality	R =1.07 0.6 stat. 0.01 syst.	PLB332(1994) 251
Lepton flavour violation in μ^+ decays	BR $< 0.9(1.7)^{-3}$ (90%CL)	PRL90(2003) 181804
$\nu_e \rightarrow \nu_\tau(\nu_x)$	$\Delta m^2 < 0.77$ eV^2 (90%CL)	PRC57 (1998) 3414
$\bar{\nu}_e \rightarrow \bar{\nu}_\mu$	$\sin^2(2\Theta) < 1.7 \times 10^{-3}$ (90%CL)	PRD66(2002)013001

TABLE II. Compilation of measured charged and neutral current reactions.

D. Conclusions

The time structure of the ISIS beam in combination with an active and passive shielded massive detector allowed for neutrino-nucleus investigations especially on ^{12}C with signal to background ratios up to 60:1. It was even possible to measure for the first time neutrino

induced charged current reaction on ^{56}Fe, which is of special interest in astrophysical processes. The well characterized neutrino beam together with its very low $\bar{\nu}_e$ contamination allowed for sensitive searches for non-SM physics. Especially in the $\bar{\nu}_\mu \rightarrow \bar{\nu}_e$ appearance channel KARMEN was able to exclude nearly all of the LSND parameter space for oscillations and therefore eliminated the needs for sterile or additional neutrinos to get conformity with neutrino oscillation experiments on the solar and atmospheric sector.

II. NEUTRINO CROSS-SECTIONS IN THE TENS-OF-MEV ENERGY RANGE

Neutrinos are produced in a variety of phenomena and at various sites in the universe, and hence come in different flavours and with a broad range of energies. A lot of them however, have energies below 100 MeV. Learning from these neutrinos involves the need to detect them in their interactions with matter. Neutrino-electron scattering cross sections are theoretically well-known, but have the disadvantage that cross sections are very small. Scattering off nuclei results in larger cross sections. At the energies considered here, the interaction process is however very sensitive to details in nuclear structure and correlations in the nucleus. This results in theoretical predictions [7–11] that are subject to model dependences, while experimental data are scarce [12–16], mainly because the experimental situation is complicated by the fact that cross sections are small and monochromatic neutrino beams not available.

Still, as they are the only particles interacting solely by means of the weak interaction, neutrinos can reveal information about e.g. the structure of nuclei or the strange quark content of the nucleon, that is difficult to obtain otherwise. The prominence of the axial current contribution in weak interactions hereby plays a key role. Figure 2 shows an example, investigating the influence of the strange quark content of the nucleus on cross sections. Whereas the influence of vector strangeness is very small at these energies, the axial has a non-negligible influence. In general the net strangeness effect would vanish for isoscalar targets, but close to particle knockout threshold the influence becomes larger due to binding energy differences between protons and neutrons. As a consequence the differential cross sections differ, and the energies of reaction products can be very different. Traditionally it is assumed that vector strangeness form factors can be determined in parity violating electron scattering whereas the axial contribution should be studied in neutrino-scattering

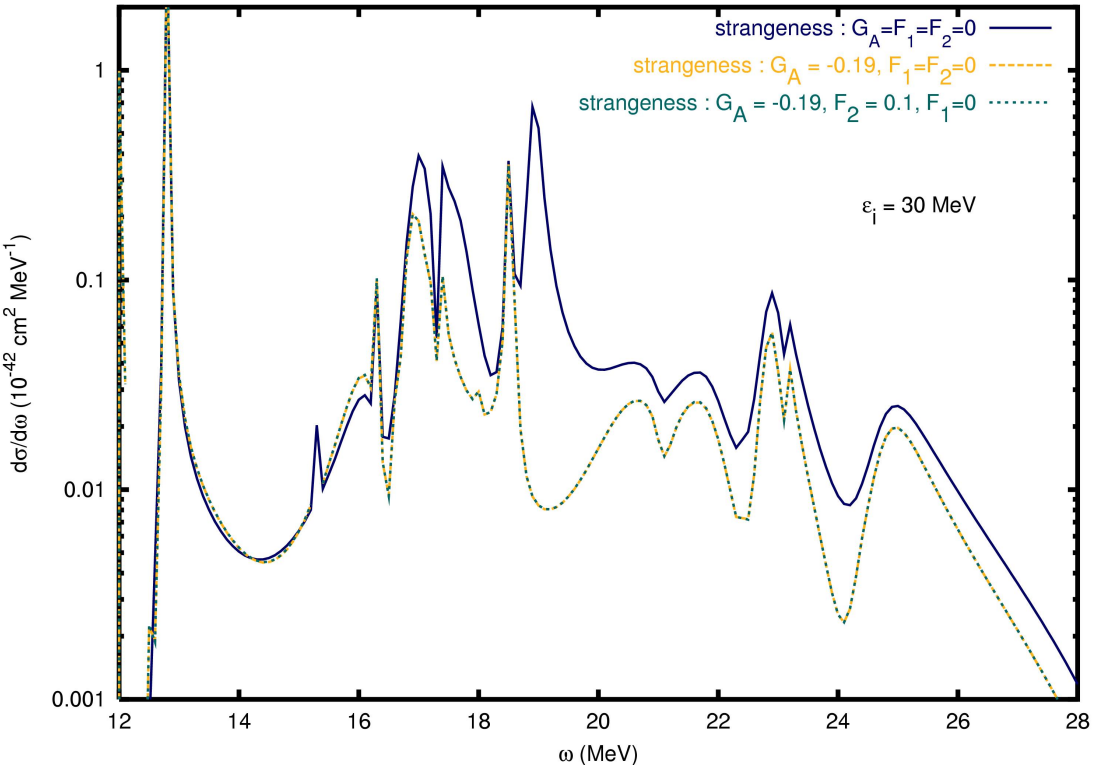

FIG. 2. Continuum Random Phase Approximation calculation for the influence of the strangeness on the cross section for the neutral-current interaction $^{16}\mathrm{O}(\nu,\nu)^{16}\mathrm{O}$'.

experiments. Recent work however shows [17, 18] that both effects are intertwined and a combined analysis of both electron and neutrino scattering data is a prerequisite for a thorough understanding of the influence of the strangeness content of the nucleon.

Another important issue in neutrino physics is that of oscillations. The recent experimental confirmation of neutrino oscillations sparked off an enormous experimental and theoretical interest in the oscillations properties of these particles. Several collaborations are working on the extension of the present knowledge about neutrino masses and mixing angles, so as to complete the picture about this non-standard neutrino behavior.

Oscillation experiments are essentially about counting neutrinos : the number of neutrinos of a certain flavour vanishing from the beam between source and target in disappearance experiments, or the number of neutrinos of a certain flavour appearing in the beam of an appearance experiment. The counting is done by detecting the reaction products of neutrino interactions with the target material. An accurate determination of all oscillation parameters requires data for inclusive neutrino cross sections with unprecedented precision.

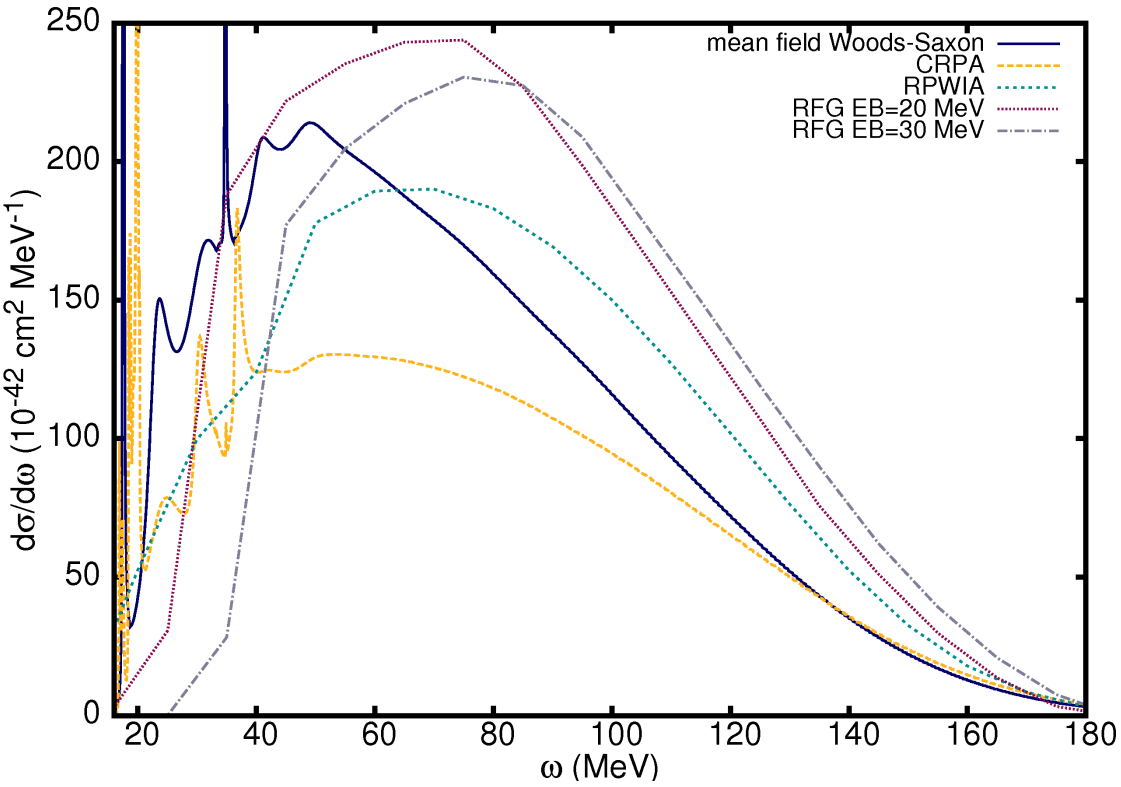

FIG. 3. Comparison between inclusive cross sections obtained within a relativistic Fermi gas calculation, a relativistic plane wave impulse approximation (RPWIA) approach, a mean-field calculation, and a calculation including CRPA correlations implemented using a Skyrme parametrization as residual interaction.

Although these experiments focus on neutrinos with energies of a few hundred MeV, the lack of monoenergetic neutrino beams implies that low-energy neutrinos do contribute to the signal in the detector. Whereas for scattering at higher energies are satisfactionary described using a Fermi gas model, for energies below 100 MeV cross sections are strongly influenced by nuclear structure effects and longrange correlations, as shown in Figure 3. Recent data suggests that the influence of low energy neutrinos is not negligible [19]. New neutrino-nucleus data at low energies would hence also contribute to the understanding of data in oscillation experiments.

Supernova neutrinos constitute another important example. They are the only particles that reach the outside world from a collapsing star core and hence the only messengers able to carry information about the processes driving the collapse and explosion. Moreover, their interactions with material in the star are important for the dynamics of the supernova

process and neutrinonucleosynthesis. Detecting neutrinos from a future galactic supernova might learn a lot about the processes going on in the center of the star and the dynamics of the supernova implosion and explosion, provided the interaction of supernova neutrinos with the material in a terrestrial detector is well understood. The detection of neutrinos learns about the flavour of the arriving neutrinos, the energy of the incoming particles (see Fig. 4), whether neutrinos or antineutrinos were emitted, they can provide directional information, information about the fate of the star and the mass and oscillation characteristics of the neutrinos [7].

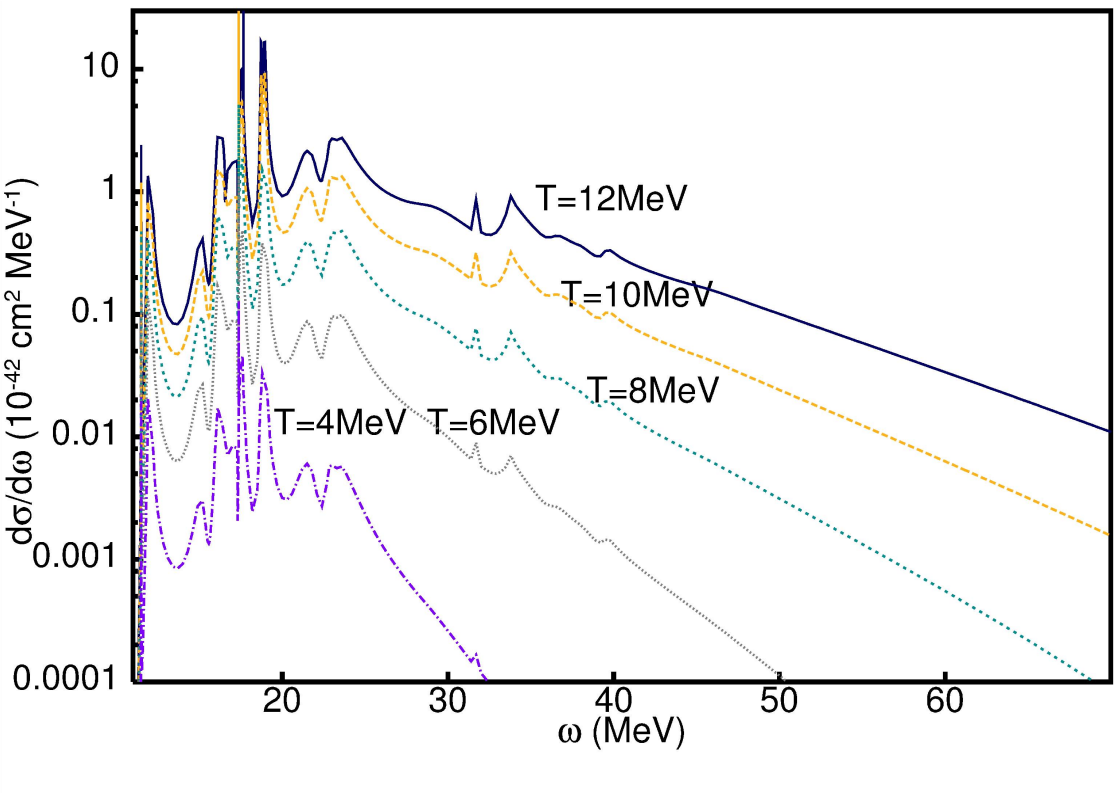

FIG. 4. Cross sections for neutral current scattering off ^{16}O, folded with different supernovaneutrino energy spectra.

Summarizing, detecting neutrinos and extracting the information they bring along, is complicated by the need for a thorough understanding of neutrino-nucleus interactions at these low energies. Detailed theoretical studies that are checked against experimental data, are therefore a prerequisite when one wants to use cross section measurements as a source of information about other processes these neutrinos are involved in.

III. COHERENT ELASTIC NEUTRINO-NUCLEUS SCATTERING AT THE ESS

In the coherent elastic neutral current process ν+A $\rightarrow$ ν+A, a neutrino interacts coherently with the nucleons in a nucleus via exchange of a Z boson [20, 21]. The coherence condition is satisfied so long as the momentum transfer $q \ll 1/R$, which for most medium A target nuclei holds for neutrino energies up to about 50 MeV. The cross-section can be calculated straightforwardly in the Standard Model, with small nuclear uncertainties, and is of the order of magnitude of 10^{-39} cm^2. In contrast to other neutrino interaction cross-sections in the few tens of MeV regime, this cross-section is huge: it exceeds that for inverse beta decay by two orders of magnitude. The coherent νA scattering process is interesting for several reasons: it is important in supernovae; it may be useful for supernova detection; and because the cross section is known with small uncertainties in the SM, a deviation from expectation could indicate new physics. Furthermore there may even be practical applications, such as nuclear reactor monitoring.

In spite of the large cross-section, this process has never been observed. The reason for the difficulty in measuring it is that the experimental signature is the recoil of the scattered nucleus, and recoil energies are tiny. For example, a 30 MeV neutrino interacting with an argon nucleus will cause recoils with maximum energy of less than 48 keV: such tiny energies are well below the detection thresholds of most traditional neutrino detectors. There are ongoing attempts to measure coherent elastic νA scattering at nuclear reactors [22, 23]. Reactors emit neutrinos in the few MeV range, and nuclear recoil energies are in the few keV range. Detectors sensitive to such low energies are very difficult to make large and clean, and such experiments face daunting backgrounds.

An alternate approach to coherent elastic νA detection is to employ a stopped pion source. Neutrinos are a natural by-product at a spallation neutron source [24]. When protons hit a target, copious pions are produced. Negative pions have a high probability of being captured by a nucleus, while positive pions stop and decay via $\pi^+ \rightarrow \mu^+ + \nu_\mu$. The muon daughters then also decay at rest via $\mu^+ \rightarrow e^+ + \nu_e + \bar{\nu}_\mu$. The neutrino spectrum from these weak decays is well known and is shown in Fig. 5. Stopped-pion neutrino sources at LANSCE and ISIS have previously been exploited for neutrino physics.

Stopped-pion neutrino energies are in the few tens of MeV range, leading to nuclear recoils in the few to few hundred keV range. In recent years, driven by the search for dark

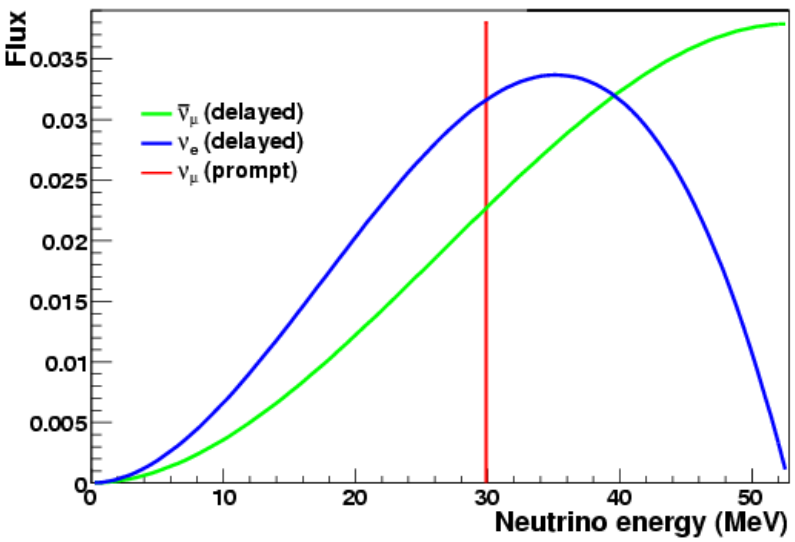

FIG. 5. Stopped pion neutrino spectrum.

matter WIMPS, a number of new technologies have been developed, with capabilities for measurement of nuclear recoils with thresholds in the few to few tens of keV range. These include solid state detectors, noble liquids (neon, argon and xenon) and warm liquid detectors. For coherent νA detection, a stopped pion neutrino source offers several advantages with respect to a reactor source of neutrinos. Although the flux tends to be lower, because the neutrino energies are higher, the nuclear recoil energies are correspondingly higher and easier to detect. Furthermore, if the beam is pulsed, the duty factor offers steady-state background rejection (and allows precise measurement of beam-unrelated background). In addition, three different flavors are available, allowing Standard Model tests complementary to those which could be done using monoflavor reactor $\bar{\nu}_e$.

An experiment to detect coherent elastic νA scattering, called CLEAR (Coherent Low Energy Nuclear(A) Recoils) has been proposed for the Spallation Neutron Source at Oak Ridge National Laboratory in Tennessee [25]. The SNS is pulsed at 60 Hz with about a 500 ns pulse width, so the monoenergetic ν_μ will be in time with the beam on that timescale, while the $\nu_e, \bar{\nu}_\mu$ follow on a 2.2 μs muon decay timescale.

The overall background rejection factor due to the pulsed beam is a few times 10^{-4}. The proposed experiment (shown in Figs. 7 and 8) comprises a single-phase noble liquid detector, which can be filled with either argon or neon, located inside a PMT-instrumented

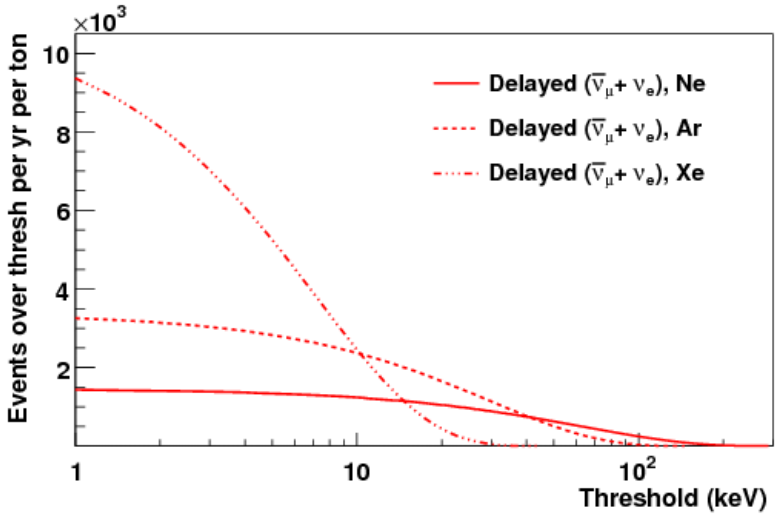

FIG. 6. Integral recoil spectrum for an SNS experiment, for different target materials.

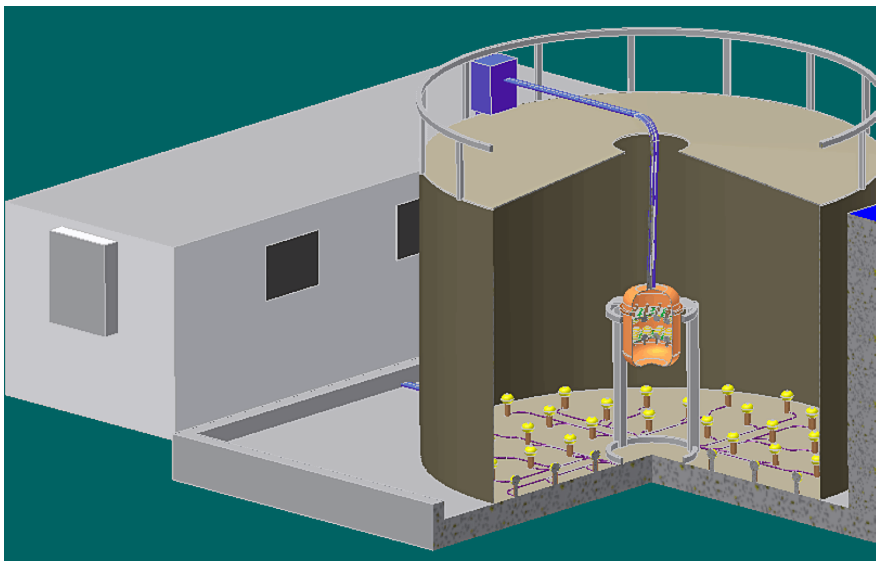

FIG. 7. CLEAR detector setup at the SNS.

water tank serving as shielding and cosmic ray veto. Pulse shape discrimination provides identification of nuclear recoils. The expected signal is about 1100 events per year in 456 kg of Ar (above 20 keV recoil energy), or about 450 events in 391 kg of Ne (above 30 keV recoil energy). Backgrounds include cosmic rays, radon, other radioactivity (including ^{39}Ar for the argon fill,) and beam-related neutrons (see Figs. 9 and 10). Beam-unrelated background can be well measured using beam-off data. A first-generation experiment could measure the νA scattering rate to 10-15%. Another possibly applicable detector technology is a Xe

two-phase TPC.

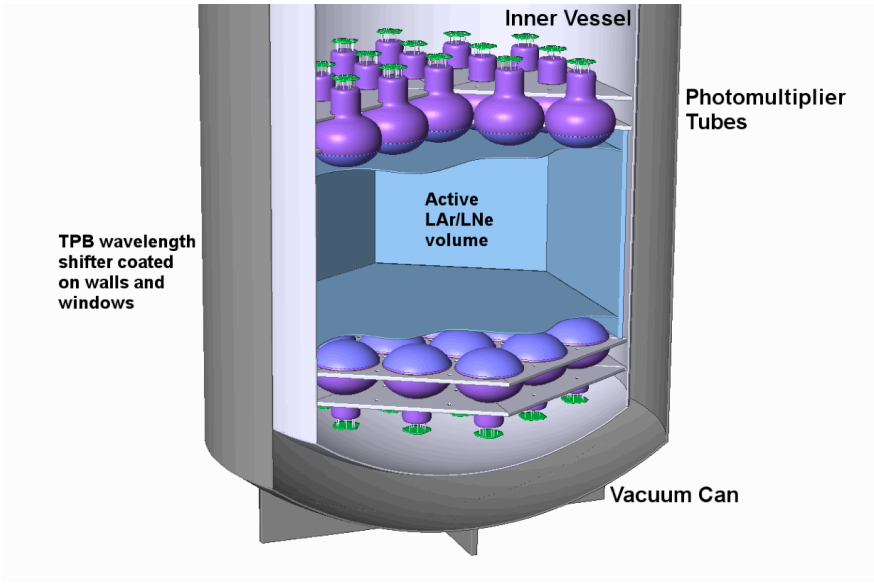

FIG. 8. CLEAR inner noble liquid detector.

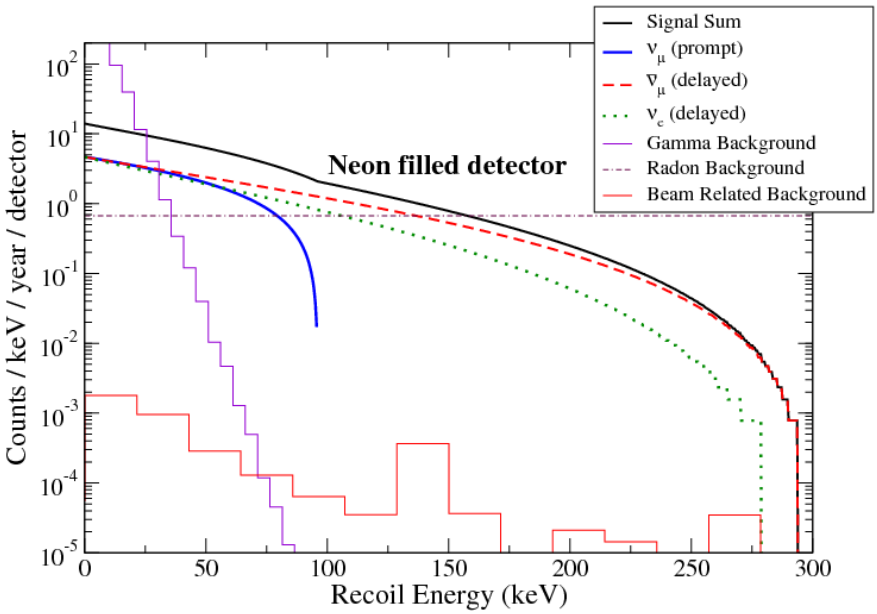

FIG. 9. Differential recoil spectrum for neon, with expected backgrounds.

A CLEAR-like coherent νA experiment could be done at any stopped pion source. The number of signal events scales linearly with detector mass and neutrino flux (which scales roughly with beam power) and as the inverse square of distance from the target. The 'wish list' for a neutrino source for such an experiment includes a high intensity and well-

understood neutrino flux, and narrow beam pulses for effective background rejection. Although the high intensity of the ESS neutrino source would be welcome, longer pulses would degrade its capabilities with respect to the SNS: the non-beam-related backgrounds scale with duty factor. However, additional background could potentially be mitigated by improving background rejection in other ways. For example, an underground site for the detector, more stringent radioactive background requirements, and the use of argon depleted of ^{39}Ar could conceivably win a few orders of magnitude of background rejection, making the ESS a competitive future possibility.

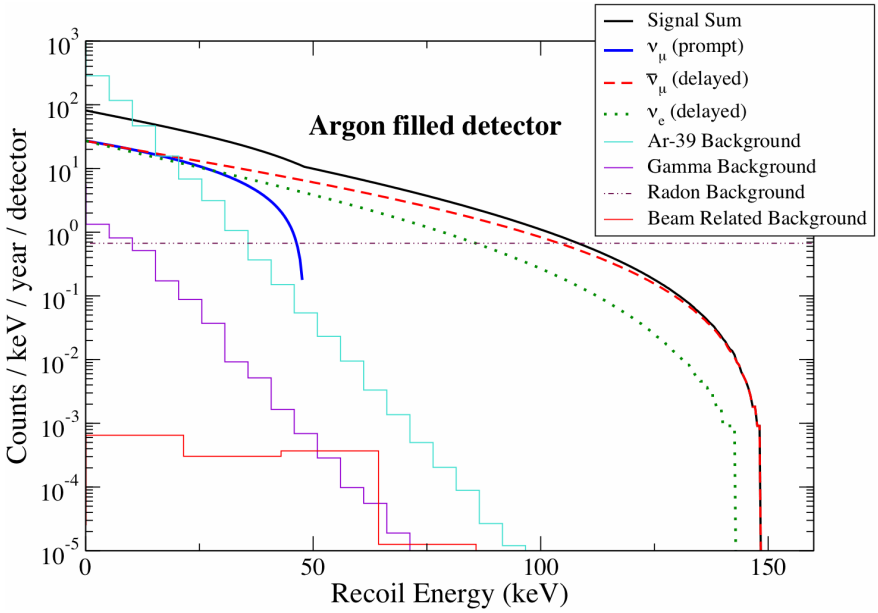

FIG. 10. Differential recoil spectrum for argon, with expected backgrounds (J. Nikkel).

IV. LOW ENERGY NEUTRINO SCATTERING MEASUREMENTS AT THE ESS

Spallation sources produce large amount of neutrinos from decay-at-rest muons and thus can be well adapted to accommodate state-of-the-art neutrino experiments. A neutrino program at ESS might include neutrino-nucleus cross section measurements relevant for neutrino and core-collapse supernova physics, electroweak tests and lepton-flavor violation searches.

Large amounts of neutrinos (and typically very few electron anti-neutrinos) are pro-

duced at spallation source facilities. KARMEN [26] and LSND [27] experiments at ISIS and LANSCE respectively already exploited spallation source neutrinos to carry out a neutrino oscillation program. The same experimental setups have also been used to perform measurements of neutrino scattering on carbon as well as electroweak tests (lepton flavor universality, Weinberg angle, and lepton-flavor violation searches) [28]. Detailed investigations of the neutrino physics program that can be performed at the future SNS facility can be found in [29] presenting also an in-depth study of possible backgrounds and of detectors' design. Here we describe the possibility of having an interesting neutrino program at the future ESS facility (if the tecnichal requirements can be met). The results are taken from [28].

The only alternative to the spallation source in producing controlled neutrino fluxes in the 100 MeV energy range could be a low energy beta-beam facility [30], based on the novel method of the beta-beams that exploits the beta-decay of boosted radioactive ions. Detailed investigations of the low energy beta-beam physics potential have pointed out a variety of interesting applications in nuclear physics, in the study of fundamental interactions and core-collapse supernova physics. Beta-beams have two main advantages compared to spallation sources: i) they produce collimated beams of both electron neutrinos and anti-neutrinos; ii) the average energy of the neutrino beams can be varied. On the other hand, spallation sources reach significantly larger neutrino production rates.

A. Measurements of neutrino-nucleus cross sections

Precise measurement of neutrino-nucleus cross sections is crucial for timely applications, which spread from the calibration of neutrino detectors to constraining neutrino-less double beta decay calculations. Neutrino detectors based on nuclei are used to observe the neutrinos from a future core-collapse supernova explosion as well as from the past explosions (the diffuse supernova neutrino background). Neutrino-nucleus cross sections on stable and radioactive nuclei are also necessary to understand stellar nucleosynthesis and, in particular, to unravel the site of the r-process one of the major open questions in nuclear astrophysics. The theoretical description of neutrino-nucleus cross sections in the low energy range is based on several complex models. Regardless the high degree of sophistication achieved, important discrepancies remain between the predicted neutrino-nucleus cross sections. The

realization of precise measurements of the neutrino scattering cross sections for an ensemble of nuclei would help to pin down differences among the models, enabling accurate and reliable description of the isospin and spin-isospin nuclear response.

To give an estimate of the expected rates at ESS we assume a neutrino flux at the source of 10^{15} electron neutrinos/s and a fully efficient 1 ton cubic detector. The expected neutrino event rates are shown in Table I, neglecting statistical and systematic errors coming from possible backgrounds, so that our numbers of events can be easily scaled, for any neutrino production rate and experiment running time.

Target nucleus	Events at 10 m	at 20 m
^{12}C	1470	384
^{16}O	998	261
^{40}Ar	8860	2310
^{56}Fe	9100	2330
^{100}Mo	17300	4420
^{208}Pb	34500	8820

TABLE III. Number of events for 10^{15} ν_e/s , in a year ($3 \cdot 10^7$ s), with a fully efficient 1 ton cubic detector at two distances from the neutrino source [28].

As can be seen from Table III convolved DAR cross sections as well as the event rates are lowest for carbon and oxygen nuclei. This is mainly due to the high reaction threshold but, for oxygen, also due to the closed shell structure. The highest event rates are obviously obtained for detectors based on heavy nuclei. One of the most important ingredients to pin down is the contribution of the forbidden transitions to the neutrino cross section. For a closed shell nucleus as oxygen, the forbidden 1^- and 2^- excitations dominate the cross section. Still oxygen is an exceptional case: the allowed (Gamow-Teller and Fermi) transitions accounts for less than 2% of the total cross section. In most cases allowed excitations are the dominant ones; while the forbidden ones are non-negligible. For example their contribution is at the level of 30% for ^{100}Mo and ^{208}Pb.

B. Measurement of the Weinberg angle

Neutrino detectors can also be used to study neutrino-electron scattering. The expected event rate per year is 230 (60) at 10 (20) meters from the source for electron-neutrino scattering, together with about 40 (10) at 10 (20) meters for muon-(anti)neutrino scattering on electrons. Although such events are much weaker compared to those on nuclei, they can be separated in the detector by identifying forward scattered events. If the systematic errors are kept sufficiently low, one can use this measurement to extract non-standard contributions to the weak interaction (e.g. flavor-changing neutral currents effects) and perform a precise measurement of the Weinberg angle at low momentum transfer. The current best value for electron-neutrino scattering on electrons is σ = 10.1 +/- 1.1 (stat) +/- 1.0 (sys) Eν_e 10^{-45} cm^2 obtained with a measurement based at a spallation source facility [31].

The time-structure of the beam pulse can be crucial for the accurate determination of the Weinberg angle at spallation sources. Indeed, positive pion decay produce neutrinos of different flavors, whose scattering on electrons have a very different reaction cross section dependence on the Weinberg angle, as can be seen in Figure 11. If however one disposes of a detector with a decent energy resolution the determination of the Weinberg angle can be improved even in the case of long pulses. To this aim one has to determine the size of the jump in the electron energy window at E_e = 29.7 MeV. In practice, this method can be realized by counting the number of events and fitting the electron energy distributions in two separate windows: one containing electron energies below 29.7 MeV, and the other comprising the events whose energies exceed 29.7 MeV. Although such a procedure increases the statistical error in each window by roughly a factor of 2, compared to the total cross section measurement, the jump height turns out to have a sensitivity to the Weinberg angle as large as S=2 (to be compared with S=0.5 for total cross section measurement). Therefore the impact of the increased statistical error in determining the Weinberg angle is compensated by the significant improvement of S [3].

The measurement made by the LSND collaboration have identified about 200 events as electron neutrino scattering using 167 tons of liquid scintillator at 17 meters from the target. If a 5 ton scintillator detector can be placed as close as 10 meters from the ESS source for example, one can expect in a running time of 1 year almost 5 times more events [28].

C. Search for Lepton Flavour Violation in neutrino scattering

If the amount of anti-neutrinos is as low as expected at the SNS facility, namely 10^{-5}, one could use this very pure source of neutrinos to search for rare processes such as the Lepton-Flavour-Violating decay $\mu^+ \to e^+ + \bar{\nu}_e + \nu_\mu$. This search has been performed, e.g. by the KARMEN Collaboration using 65 tons of scintillator at 17 meters from the source which has given the current best limit for the branching ratio of 0.9 10^{-3} [32]. This experiment requires a precise identification of the associated events, measuring the neutron through neutron capture on Gadolinium or on protons. We expect 11300 (2950) $\overline{\nu}_e - p$ scattering events in water at 10 (20) meters from the source, if we assume as many as 10^{15} $\overline{\nu}_e$/s are produced, these numbers must be scaled according to the suppression factor, that depends on the specific spallation source considered.

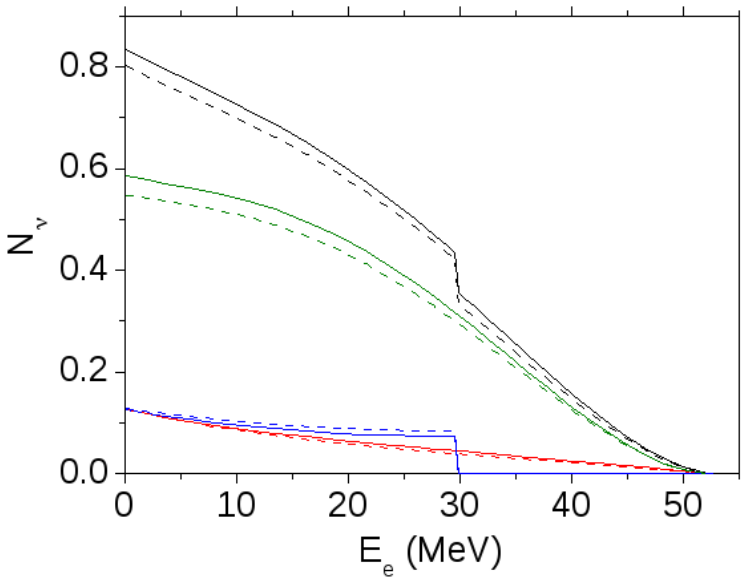

FIG. 11. Energy distribution of the neutrino-electron scattering events [28].

V. STATUS OF STERILE NEUTRINOS FROM OSCILLATION DATA

Motivated by the results from the MiniBooNE experiment we review the global neutrino oscillation fit to short-baseline neutrino data by adding one, two or three sterile neutrinos with eV-scale masses to the three Standard Model neutrinos. Four-neutrino oscillations of the (3+1) type, which have been only marginally allowed before MiniBooNE, become even more disfavored with the inclusion of this experiment. In the framework of so-called (3+2) five-neutrino mass schemes the MiniBooNE results can be nicely reconciled with the LSND appearance evidence thanks to the possibility of CP violation available in such oscillation schemes; however, the tension between appearance and disappearance experiments represents a serious problem in (3+2) schemes, so that these models are ultimately not viable. This tension remains also when a third sterile neutrino is added, and we do not find a significant improvement of the global fit in a (3+3) scheme.

A. Introduction

At the beginning of 2007 the first results from the MiniBooNE (MB) experiment [33] at Fermilab were presented on a search for $\nu_\mu \to \nu_e$ appearance with a baseline of 540 m and a mean neutrino energy of about 700 MeV. Since then, new measurements with improved statistics been periodically released [34–38]. The primary purpose of this experiment is to test the evidence of $\bar{\nu}_\mu \to \bar{\nu}_e$ transitions reported by the LSND experiment at Los Alamos [39] with a very similar L/E range. Reconciling the LSND signal with the other evidence for neutrino oscillations is a long-standing challenge for neutrino phenomenology, since the mass-squared differences required to explain the solar, atmospheric and LSND experimental results in terms of neutrino oscillations differ from one another by various orders of magnitude. Consequently, there is no consistent way to explain all these three signals invoking only oscillations among the three known neutrinos. Therefore, in order to explain the LSND anomaly one had to invoke an extension of the three-neutrino mixing scenario, introducing either a mechanism to generate at least a third mass-square difference, or a new form of flavor transition beyond oscillations. Following Refs. [40–42], below we will concentrate on the first possibility, starting from models with one extra sterile neutrino (Sec. V B) and then considering models with two and three sterile neutrino states (Sec. V C).

B. Four-neutrino mixing

In four-neutrino models, one extra sterile state is added to the three weakly interacting ones. The relation between the flavor and the mass eigenstates can be described in terms of a 4×4 unitary matrix U, which generalizes the usual 3×3 leptonic matrix of the Standard Model. There are six possible four-neutrino schemes that can accommodate the results from solar and atmospheric neutrino experiments and contain a third much larger Δm^2. They can be divided into two classes: (3+1) and (2+2). In the (3+1) schemes, there is a group of three close-by neutrino masses that is separated from the fourth one by the larger gap. In (2+2) schemes, there are two pairs of close masses separated by the large gap. While different schemes within the same class are presently indistinguishable, schemes belonging to different classes lead to very different phenomenological scenarios.

A characteristic feature of (2+2) schemes is that the extra sterile state cannot be simultaneously decoupled from *both* solar and atmospheric oscillations. To understand why, let us define $\eta_s = \sum_{i \in \mathrm{SOL}} |U_{si}|^2$ and $c_s = \sum_{j \in \mathrm{ATM}} |U_{sj}|^2$, where the sums in i and j run over mass eigenstates involved in solar and atmospheric neutrino oscillations, respectively. Clearly, the quantities η_s and c_s describe the fraction of sterile neutrino relevant for each class of experiment. Results from atmospheric and solar neutrino data imply that in both kind of experiments oscillation takes place mainly between active neutrinos. Specifically, from Fig. 46 of Ref. [43] we get $\eta_s \leq 0.31$ and $c_s \leq 0.36$ at the 3σ level. However, in (2+2) schemes unitarity implies $\eta_s + c_s = 1$. A statistical analysis using the *parameter goodness of fit* (PG) proposed in [44] gives $\chi^2_{\mathrm{PG}} = 30.7$ for 1 d.o.f., corresponding to a 5.5σ rejection ($\mathrm{PG} = 3 \times 10^{-8}$) of the (2+2) hypothesis. These models are therefore ruled out at a very high confidence level, and they will not be considered anymore.

On the other hand, (3+1) schemes are not affected by this problem. Although the experimental bounds on η_s and c_s quoted above still hold, the condition $\eta_s + c_s = 1$ no longer applies. For what concerns neutrino oscillations, in (3+1) models the mixing between the sterile neutrino and the three active ones can be reduced at will, and in particular it is possible to recover the usual three-neutrino scenario as a limiting case. However, as widely discussed in the literature (see, *e.g.*, Ref. [45] and references therein) these models are strongly disfavored as an explanation of LSND by the data from other short-baseline (SBL)

laboratory experiments. In the limit $\Delta m^2_{\rm LSND} \gg \Delta m^2_{\rm ATM} \gg \Delta m^2_{\rm SOL}$ the probability $P_{\nu_\mu \to \nu_e}$ which is relevant for LSND as well as for KARMEN [46], NOMAD [47] and MiniBooNE is driven by the large Δm^2_{41}, and is given by

$$P_{\nu_\mu \to \nu_e} = P_{\bar{\nu}_\mu \to \bar{\nu}_e} = 4\,|U_{e4}U_{\mu 4}|^2\,\sin^2\frac{\Delta m^2_{41} L}{4E}\,, \tag{1}$$

where L is the distance between source and detector. The LSND, KARMEN, NOMAD and MiniBooNE experiments give allowed regions in the (Δm^2_{41}, $|U_{e4}U_{\mu 4}|^2$) plane which can be directly obtained from the corresponding two-neutrino exclusion plots [33, 39, 46, 47]. At the light of the MiniBooNE result which is consistent with no oscillations above 475 MeV, practically all the LSND region is now excluded. In addition, further constraints on $|U_{e4}U_{\mu 4}|^2$ can be obtained by combining together the bounds on $|U_{e4}|$ and $|U_{\mu 4}|$ derived from reactor and accelerator experiments (mainly Bugey [48] and CDHS [49]) as well as solar and atmospheric data. The results of the global analysis presented in Ref. [40], which includes atmospheric and long-baseline data together with short-baseline experiments observing *no evidence* (NEV), yield $\chi^2_{\rm PG} = 24.7$ for 2 d.o.f., corresponding to a 4.6σ rejection (PG = 4×10^{-6}) of the (3+1) hypothesis. These results show that (3+1) schemes are now ruled out as a possible explanation of LSND [40]. In addition, it should be noted that the low-energy excess observed by MiniBooNE at $E_\nu \leq 475$ MeV cannot be explained in terms of oscillations with only one large mass-squared difference, thus adding another problem to these models in case this excess is confirmed to be a real signal.

C. Five-neutrino and six-neutrino mixing

Five-neutrino schemes of the (3+2) type are straight-forward extensions of (3+1) schemes. In addition to the cluster of the three neutrino mass states accounting for "solar" and "atmospheric" mass splittings now two states at the eV scale are added, with a small admixture of ν_e and ν_μ to account for the LSND signal. In the Appendix of Ref. [50] it was suggested that such models could somewhat relax the tension existing between short-baseline experiments and the LSND data. In Ref. [51] a complete analysis was performed, finding that indeed the disagreement between LSND and null-result experiments is reduced. Here we will reconsider this possibility at the light of the new MiniBooNE data. As explained in Refs. [33, 35, 37], MiniBooNE found no evidence of oscillations above 475 MeV, whereas below this energy an

unresolved excess of events is observed. Lacking any explanation in terms of backgrounds or systematical uncertainties, here we will follow Ref. [40] and present the results obtained using both the full energy range from 300 MeV to 3 GeV ("MB300") and for the restricted range from 475 MeV to 3 GeV ("MB475").

As for (3+1) models, in (3+2) schemes the *appearance* data (LSND, KARMEN, NOMAD, and MiniBooNE) can be described using the SBL approximation $\Delta m^2_{\rm SOL} \approx 0$ and $\Delta m^2_{\rm ATM} \approx 0$, in which case the relevant transition probability is given by

$$P_{\nu_\mu \to \nu_e} = 4\,|U_{e4}U_{\mu 4}|^2\,\sin^2\phi_{41} + 4\,|U_{e5}U_{\mu 5}|^2\,\sin^2\phi_{51} + 8\,|U_{e4}U_{\mu 4}|\,|U_{e5}U_{\mu 5}|\,\sin\phi_{41}\sin\phi_{51}\cos(\phi_{54}-\delta)\,, \quad (2)$$

with the definitions $\phi_{ij} \equiv \Delta m^2_{ij} L/4E$ and $\delta \equiv \arg(U^*_{e4}U_{\mu 4}U_{e5}U^*_{\mu 5})$. Eq. (2) holds for neutrinos (NOMAD and MB); for anti-neutrinos (LSND and KARMEN) one has to replace $\delta \to -\delta$. Note that Eq. (2) is invariant under the transformation $4 \leftrightarrow 5$ and $\delta \leftrightarrow -\delta$, and depends only on the combinations $|U_{e4}U_{\mu 4}|$ and $|U_{e5}U_{\mu 5}|$. An important observation is that non-trivial values of the complex phase δ lead to CP violation, and hence in (3+2) schemes much more flexibility is available to accommodate the results of LSND (anti-neutrinos) and MB (neutrinos). Indeed in this context MB data can be fitted very well while simultaneously explaining the LSND evidence. Furthermore, in this case also the low energy MB data can be explained, and therefore, in contrast to (3+1) schemes, (3+2) oscillations offer an appealing possibility to account for this excess. The global analysis presented in Ref. [41] finds an overall goodness-of-fit of 56%, showing that MB is in very good agreement with global SBL appearance data including LSND.

On the other hand, once *disappearance* data are included in the analysis, the quality of the fit decreases considerably. Indeed, even in (3+2) schemes short-baseline experiments pose stringent bounds on the mixing angles $|U_{ei}|$ and $|U_{\mu i}|$, in close analogy with (3+1) models described in Sec. V B. Since rather large values of $|U_{e4}U_{\mu 4}|$ and $|U_{e5}U_{\mu 5}|$ are needed to account for the negative result of MiniBooNE as well as the positive signal of LSND, one expects that reconciling appearance and disappearance data will be a problem also within (3+2) models. In order to quantify this disagreement in Ref. [40] the PG test was applied

to appearance versus disappearance data without MB, with MB475, and with MB300:

$$\text{APP vs DIS:} \quad \begin{cases} \chi^2_{\rm PG} = 17.5\,, & {\rm PG} = 1.5 \times 10^{-3} \quad \text{(no MB)}, \\ \chi^2_{\rm PG} = 17.2\,, & {\rm PG} = 1.8 \times 10^{-3} \quad \text{(MB475)}, \\ \chi^2_{\rm PG} = 25.1\,, & {\rm PG} = 4.8 \times 10^{-5} \quad \text{(MB300)}. \end{cases} \tag{3}$$

From these numbers it is clear that also in (3+2) schemes the tension between appearance and disappearance experiments is quite severe. If MB475 is used the result is very similar to the pre-MiniBooNE situation implying inconsistency at about 3.1σ, whereas in case of the full MB300 data the tension becomes significantly worse (about 4σ), since appearance data are more constraining because of the need to accommodate LSND as well as the MB excess at low energies. More recent analyses using newer data yield similar values, ${\rm PG} = 2.3 \times 10^{-4}$ for MB475 [42] and ${\rm PG} = 4 \times 10^{-5}$ for the entire MB data sample [41].

Finally, since there are three active neutrinos it seems natural to consider also the case of three sterile neutrinos. If all three additional neutrino states have masses in the eV range and mixings as relevant for the SBL experiments under consideration, such a model will certainly have severe difficulties to accommodate standard cosmology [52]. Besides this fact, the results of the search performed in Ref. [40] show that there is only a marginal improvement of the fit with respect to (3+2), to be compared with four additional parameters in the model. Hence, the conclusion is that here are no qualitatively new effects in the (3+3) scheme. The conflict between appearance and disappearance data remains a problem, and the additional freedom introduced by the new parameters does not relax significantly this tension.

D. Conclusions

In this talk we have reviewed the status of global fits to short-baseline neutrino oscillation data in the framework of (3+1), (3+2) and (3+3) oscillation models. Four-neutrino models are ruled out since (a) the don't allow to account for the low energy event excess in MB, (b) MiniBooNE result cannot be reconciled with LSND, and (c) there is severe tension between *appearance* and *disappearance* experiments. Five-neutrino models provide a nice way out for problems (a) and (b), but fail to resolve (c). Similarly, six-neutrino models do not offer qualitatively new effects with respect to (3+2). In all cases we find severe tension between

different sub-samples of the data, hence we conclude that at the light of present experimental results it is *not* possible to explain the LSND evidence in terms of sterile neutrinos.

E. Acknowledgments

This work is supported by Spanish MICINN grants FPA-2009-08958, FPA-2009-09017 and consolider-ingenio 2010 grant CSD-2008-0037, by Comunidad Autonoma de Madrid through the HEPHACOS project S2009/ESP-1473 and by EU grant EURONU.

---

[1] Ch. Volpe, contribution this conference

[2] A. Aguilar et al., Phys. Rev. **D64**, 112007 (2001).

[3] . Nakamura et al . (Particle Data Group), J. Phys. G **37**, 075021 (2010)

[4] J. Reichenbacher, scientific report no. 7093, FZKA-7093 (June 2005)

[5] G. Drexlin et al., NIM A **289** (1990) 490

[6] B. Armbruster et al., Phys. Rev. **D65**, (2002) 112001

[7] N. Jachowicz, G. C. McLaughlin, Phys.Rev.Lett. **96** (2006) 172301.

[8] C. Volpe, N. Auerbach, G. Colo, T. Suzuki, and N. Van Giai, Phys. Rev. C **62** (2000) 015501.

[9] E. Kolbe, K. Langanke, and P. Vogel, Nucl. Phys. **A652**, 1 (1999).

[10] N. Jachowicz, K. Heyde, J. Ryckebusch, and S. Rombouts, Phys. Rev. C **65**, 025501 (2002).

[11] K. Langanke, G. Martinez-Pinedo, Rev.Mod.Phys.**75**:819-862,2003.

[12] G. Drexlin et al., KARMEN Collaboration, Proceedings of Neutrino Workshop - Heidelberg 1987, p.147 ed. B. Povh and V. Klapdor, Springer Verlag ; Zeitnitz, KARMEN Collaboration, Prog. Part. Nucl. Phys. **32** (1994) 351.

[13] M. Albert et al., Phys. Rev. C **51** (1995) 1065.

[14] J. Kleinfeller et al., in Neutrino 96 eds. K. Enquist, H. Huitu and Maalampi, (World Scientific, Singapore, 1997)

[15] R. Imlay, Nucl. Phys. A629 (1998) 531c.

[16] J. P. Berge et al., Z. Phys. C **49**, 187 (1991).

[17] S.F. Pate, Phys. Rev. Lett. **92**, 082002 (2004).

[18] N. Jachowicz, P. Vancraeyveld, P. Lava, C. Praet, J. Ryckebusch, Phys.Rev.C**76**:055501,2007.

[19] MiniBoone Collaboration, Phys. Rev. Lett. **100**, 032301 (2008)

[20] D. Z. Freedman, D. N. Schramm, and D. L. Tubbs, Ann. Rev. Nucl. Part. Sci., **167** (1977).

[21] A. Drukier and L. Stodolsky, Phys. Rev. **D30**, 2295 (1984).

[22] J. I. Collar, J. Phys. Conf. Ser. **136**, 022009 (2008).

[23] H. Wong, Mod. Phys. Lett. **A23**, 1431 (2008).

[24] K. Scholberg, Phys. Rev. **D73**, 033005 (2006).

[25] K. Scholberg et al., arXiv:0910.1989 (2009).

[26] B.Armbruster et al. [KARMEN Collaboration], PRD **65** (2002) 112001 [arXiv:hep ex/0203021].

[27] C.Athanassopoulos et al [LSND Collaboration], Phys. Rev. Lett. **77** (1996) 3082 [arXiv:nucl-ex/9605003].

[28] R. Lazauskas and C. Volpe, J. Phys. G: Nucl. Part. Phys. **37** (2010) 125101, and references therein.

[29] F.T. Avignone and Yu.V. Efremenko, J. Phys. G **29** (2003) 2615.

[30] C. Volpe, Jour. Phys. G 30, L1 (2004) [hep-ph/0303222]; C. Volpe, "Beta-beams", Topical Review, J. Phys. G 34 (2007) R1-R44 [hep-ph/0605033].

[31] L.B.Auerbach et al. [LSND Collaboration], Phys. Rev. D **63** (2001) 112001 [arXiv:hep-ex/0101039].

[32] B. Armbruster et al. Phys. Rev. Lett. **90** (2003) 181804 [arXiv:hep-ex/0302017].

[33] A. A. Aguilar-Arevalo *et al.*[MiniBooNE Collaboration], Phys.Rev.Lett. **98** (2007) 231801. [arXiv:0704.1500].

[34] P. Adamson *et al.*[MiniBooNE and Minos Collaboration], Phys.Rev.Lett. **102** (2009) 211801 [arXiv:0809.2447].

[35] A. A. Aguilar-Arevalo *et al.*[MiniBooNE Collaboration], Phys.Rev.Lett. **102** (2009) 101802 [arXiv:0812.2243].

[36] A. A. Aguilar-Arevalo *et al.*[MiniBooNE Collaboration], Phys.Rev.Lett. **103** (2009) 061802 [arXiv:0903.2465].

[37] A. A. Aguilar-Arevalo *et al.*[MiniBooNE Collaboration], Phys.Rev.Lett. **103** (2009) 111801 [arXiv:0904.1958].

[38] A. A. Aguilar-Arevalo *et al.*[MiniBooNE Collaboration], [arXiv:1007.1150].

[39] A. Aguilar *et al.*[LSND Collaboration], Phys.Rev. D **64** (2001) 112007 [arXiv:hep-ex/0104049].

[40] M. Maltoni and T. Schwetz, Phys.Rev. D **76** (2007) 093005 [arXiv:0705.0107].

[41] G. Karagiorgi, Z. Djurcic, J. M. Conrad *et al.*, Phys.Rev. **D80** (2009) 073001 [arXiv:0906.1997].

[42] E. Akhmedov, T. Schwetz, arXiv:1007.4171.

[43] M. C. Gonzalez-Garcia, M. Maltoni, Phys.Rept. **460** (2008) 1-129. [arXiv:0704.1800].

[44] M. Maltoni and T. Schwetz, Phys.Rev. D **68** (2003) 033020 [arXiv:hep-ph/0304176].

[45] M. Maltoni *et al.*, Nucl.Phys. B **643** (2002) 321 [arXiv:hep-ph/0207157].

[46] B. Armbruster *et al.*[KARMEN Collaboration], Phys.Rev. D **65** (2002) 112001 [arXiv:hep-ex/0203021].

[47] P. Astier *et al.*[NOMAD Collaboration], Phys.Lett. B **570** (2003) 19 [arXiv:hep-ex/0306037].

[48] Y. Declais *et al.*, Nucl.Phys. B **434** (1995) 503.

[49] F. Dydak *et al.*, Phys.Lett. B **134** (1984) 281.

[50] O. L. G. Peres and A. Y. Smirnov, Nucl.Phys. B **599** (2001) 3 [arXiv:hep-ph/0011054].

[51] M. Sorel, J. M. Conrad and M. Shaevitz, Phys.Rev. D **70** (2004) 073004 [arXiv:hep-ph/0305255].

[52] S. Hannestad and G. G. Raffelt, JCAP **0611** (2006) 016 [arXiv:astro-ph/0607101].

Nuclear Physics Possibilities at ESS

P. Strasser,[1] René Reifarth,[2] Piet Van Duppen [a],[3] and Gabriél Martinez-Pinedo[4]

[1] *Muon Science Laboratory, Institute of Materials Structure Science, High Energy Accelerator Research Organization (KEK), Tsukuba, Ibaraki 305-0801, Japan*

[2] *GSI Helmholtzzentrum für Schwerionenforschung GmbH, Darmstadt, 64291, Germany J.W. Goethe Universität, Frankfurt a.M, D-60438, Germany*

[3] *Instituut voor Kern- en Stralingsfysica, K.U.Leuven, Belgium*

[4] *GSI Helmholtzzentrum für Schwerionenforschung, Planckstr. 1, 64291 Darmstadt, Germany*

The section on nuclear physics at ESS had five contributions covering possibillities at ESS for:

- Neutron-nucleus reaction studies using the neutron time-of-flight method
- Production of radioactive isotopes with an intense proton driver as is being studies in the Eurisol project, and at a smaller scale, in the ISOL@Myrrha project in Belgium
- Neutrino-nucleus interactions
- Muon-capture on radioactive nuclei.

Apart from the contribution on Eurisol the sections below cover the topics dicussed in the session. The prospects for combining these physics subjects under the ESS umbrella are discussed in the individual sections, but in general an important point is whether these studies can be combined in a parasitic mode or not, at what requirements these studies have for intensity and time-structure of the proton driver. As an example it seems clear that Eurisol will require too much proton beam for it to be combined with ESS, while e.g. studies of neutrino-nucleus interactions can be much easier accomodated under the ESS umbrella. As a consequence the prospects for muon-capture on exotic nuclei at ESS are not obvious.

[a] for the BriX collaboration

I. MUONIC RADIOACTIVE ATOMS

Muonic atom X-ray spectroscopy [1] has been successfully used for many years to determine the nuclear charge distribution. The most precise charge radii of nuclei have been obtained using this method, and they have been determined for almost all elements, but only for stable isotopes. New intense muon beams, with fluxes several orders of magnitude higher than at present muon facilities, would allow many novel experimental studies that were statistically not feasible until now. The investigation of the nuclear properties of unstable nuclei using muonic atom spectroscopy would become possible. This would be a unique tool to increase our knowledge of the nuclear structure far from stability, in particular, the nuclear charge distribution and the deformation properties of nuclei. It would usefully complement the knowledge obtained from electron scattering and laser spectroscopy, since in the past calibration data were used from muonic atom measurements with stable nuclei.

Initially, this project was strongly motivated by the recent advances of the radioactive isotope (RI) beam projects that are in operation, or were planned, at facilities where negative muon beams are also available. Presently, only TRIUMF with the ISAC project offers such a possibility, but with limited beam power. The E-arena in the J-PARC project was unfortunately abandoned. The RI Beam Factory project at RIKEN could be also of interest, provided intense negative muon beams can be produced there. Furthermore, the neutrino factory concept to produce unprecedented high flux of muons could benefit many muon related research topics, including the proposed study. The same proton driver beam could also be used simultaneously for the generation of RI beams. If realized, this would be a unique opportunity to combine massive amounts of muons with very intense RI beams. But the neutrino factory has yet to be approved and founded. However today it is a fact that the European Spallation Source (ESS) with its multi-MW proton driver beam will be soon the world's most powerful research facility for investigation with neutrons. ESS could also provide unique research opportunities for fundamental physics, in particular muonic radioactive atoms studies given that intense negative muon and RI beams can be generated. Identifying such opportunities now will allow considering them during the design update phase for a possible upgrade strategy.

We proposed the cold hydrogen film method [2] to expand muonic atom spectroscopy by utilizing nuclear beams, including, in the future, radioactive isotope beams, to produce

muonic radioactive atoms. The basic concept is to stop both muon and nuclear beams simultaneously in a solid hydrogen film, followed by the application of the direct muon transfer reaction to higher Z nuclei to form muonic radioactive atoms (see Fig. 1). This method will enable the study of unstable nuclei by the muonic X-ray method at facilities in which both intense negative muon and RI beams will be available.

An experimental program (μA*) to perform muonic atom spectroscopy with stable ions implanted in a solid hydrogen/deuterium film is in progress at the RIKEN-RAL muon facility to experimentally establish the feasibility of this method [3, 4]. Promising results were first obtained in pure solid D2 films with argon ions implanted non-uniformly, to study the muon transfer reaction and the diffusion process of dμ atoms. Then, a new surface ionization type ion source has been constructed and installed on the existing μA* apparatus at port 4 with the aim of using in the future radioactive isotopes. This type of ion source is capable of producing ions from alkali and alkaline-earth metals with high efficiency. At the moment, only stable beams will be produced. Very encouraging results were obtained from transfer experiments performed with isotopically separated strontium ions (^{88}Sr, ^{87}Sr, ^{86}Sr) implanted in pure solid deuterium films. Barium isotopes (^{138}Ba, ^{137}Ba) were also measured. This new surface ion source is also capable of producing ions from rare-earth elements with high efficiency. They seem ideal candidates for an experiment to study very high Z nuclei with deformation properties. For instance, samarium isotopes show very abrupt changes in their nuclear characteristics from spherical to highly deformed nuclei. ^{144}Sm is magic in neutrons (N=82) and display the characteristics of a stiff spherical nucleus which is very hard to excite, whereas ^{152}Sm and ^{154}Sm reveal low energy levels characteristic of highly deformed nuclei whose muonic X-ray spectra show a 2p hyperfine structure (h.f.s.). The latest measurements were performed with isotopically separated samarium ions. Figure 2 shows the delayed energy spectra measured by the Ge detector with 1-mm pure D2 and about 1 ppm of ^{148}Sm and ^{152}Sm ions implanted non-uniformly, respectively. The measured isotope shifts are consistent with that observed in previous experiments performed using enriched Sm isotopes [5, 6]. ^{148}Sm has still a spherical nucleus, while ^{152}Sm is clearly showing a 2p h.f.s. characteristic of a highly deformed nucleus. This experiment was performed using natural samarium oxide (Sm^2O^3) in the ion source, and only about 6×10^{16} ions of Sm ions in the target. In these measurements, the experimental precision is limited essentially for statistical reasons. The competition with other measurements that use enriched stable

isotopes in very large quantities is difficult. However, one advantage of this method is that the isotope separation can be performed during the implantation, and that high purity isotopes can be measured. The measurement is also free from the chemical substance of the element if it can be fully ionized. An experiment using long-lived radioactive isotopes is under consideration.

The present experiments are performed with a relatively large number of implanted ions because conventional negative muon beams have large sizes ($\sim$ 4 cm in diameter) and relatively low intensity at 27 MeV/c ($\sim$ 5000 μ^-/s). Future muon facilities with higher muon flux would require fewer implanted ions. If very narrow momentum spread negative muon beams could be produced, either by phase-space rotation or cooling, muons could be stopped in a much thinner region more efficiently, and the use of a magnetic confinement field around the target would constrain incoming muons within a small target area ($<$ 1 cm2). The ion beam could then be stopped precisely at the same position increasing the transfer yield. This would dramatically reduce the number of radioactive nuclei needed to be implanted in the solid hydrogen target.

The possibility to perform radioactive muonic atoms studies at the ESS will depend on whether an intense muon source and intense RI beams can be produced there. In its present design, muon beams could be produced at ESS but, due to the long-time structure and the relatively low duty factor of the primary proton beam, it would be difficult to make use of the full beam power and therefore the muon intensity would not exceed existing European muon facilities at PSI or ISIS. Therefore, it is strongly recommended that the option of a short-pulse using compressor rings to compress the proton pulse before being forwarded to a second target station, as it was considered in an earlier design, should be kept as a possible upgrade strategy. This short-pulse would be essential to most experiments using muons by making use of ESS multi-MW proton driver beam full potential. Experiment using long-lived radioactive isotopes could be then performed. However, to go to short-lived radioactive isotopes, RI beams would need to be produced on-site close to the muon source. At first a RI beam facility at ESS may be understood as a competition to existing or future facilities in Europe like the EURISOL project. But on the other hand, this could also be seen as a complementary project in a bigger nuclear physics framework.

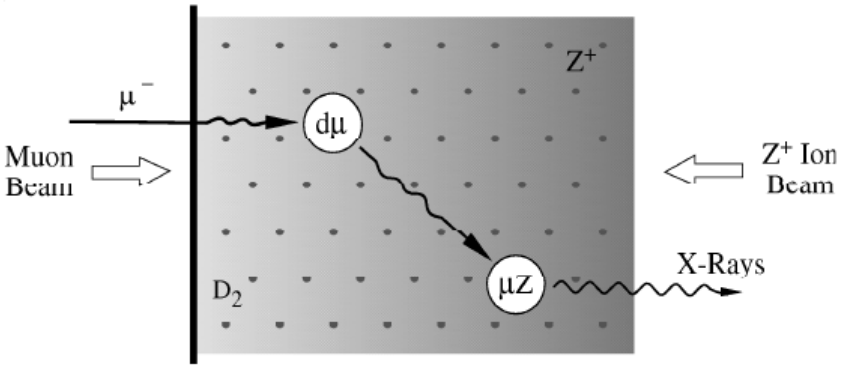

FIG. 1. Simplified scheme of muonic atom formation from implanted ions in a solid deuterium film.

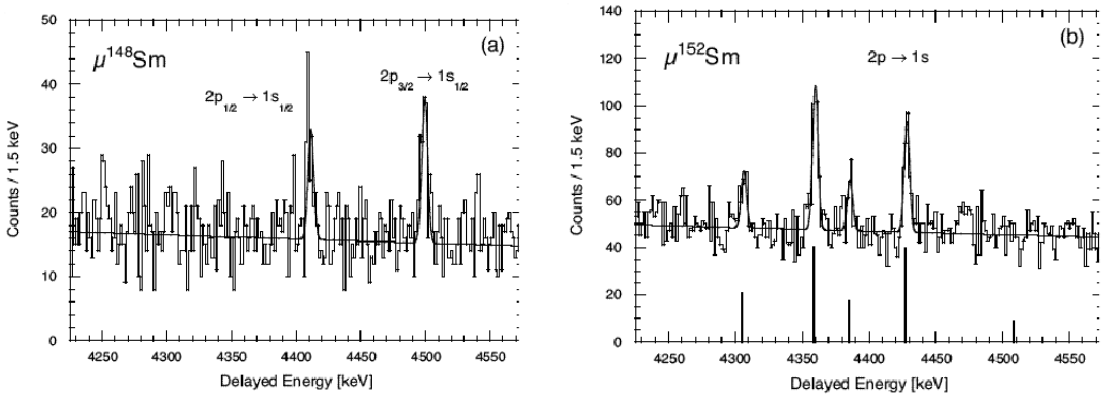

FIG. 2. Delayed energy spectrum of the 2p→1s muonic transitions in Samarium measured with 1-mm pure D2 and about 1 ppm of Sm ions implanted non-uniformly: (a) ^{148}Sm and (b) ^{152}Sm, respectively. Theoretical prediction shown underneath for ^{152}Sm [5, 6].

II. NUCLEAR ASTROPHYSICS USING N-TOF FACILITIES

A. The s process

Almost all of the heavy-element abundances beyond iron are produced via neutron capture reactions, about equally shared between the slow neutron capture nucleosynthesis (s process) and the rapid neutron capture nucleosynthesis (r process). Starting at the iron-peak seed, the s-process mass flow follows the neutron rich side of the valley of stability via a sequence of neutron captures and β--decays synthesizing the elements between iron and bismuth.

If different reaction rates are comparable, the s-process path branches and the branching ratio reflects the physical conditions in the interior of the star. Such nuclei are most inter-

esting, because they provide the tools to effectively constrain modern models of the stars where the nucleosynthesis occurs. As soon as the β-decay is significantly faster than the typically competing neutron capture, no branching will take place. Therefore experimental neutron capture data for the s process are only needed, if the respective neutron capture time under stellar conditions is similar or smaller than the β-decay decay time, which includes all stable isotopes. Depending on the actual neutron density during the s process, the "line of interest" is closer to or farther away from the valley of stability.

The modern picture of the main s-process component refers to the He shell burning phase in AGB stars [11]. Nuclei with masses between 90 and 209 are mainly produced during the main component. The highest neutron densities in this model occur during the ^{22}Ne(α,n) phase and are up to 10^{12} cm^{-3} with temperatures around kT = 30 keV. The other extreme can be found during the ^{13}C(α,n) phase where neutron densities as low as 10^{7} cm^{-3} and temperatures around kT = 5 keV are possible. Similarly to the main component, also the weak component referring to different evolutionary stages in massive stars has two phases [16, 17]. Mainly nuclei with masses between 56 and 90 are produced during the weak component. The first phase occurs during the helium core burning with neutron densities down to 10^{6} cm^{-3} and temperatures around kT = 25 keV. The second phase happens during the carbon shell burning with neutron densities up to 10^{12} cm^{-3} at temperatures around kT = 90 keV.

The left part of Figure 3 shows a summary of the neutron capture and β-decay times for radioactive isotopes on the neutron rich side of the valley of stability, under the condition that the neutron capture during the ^{13}C(α,n) occurs faster than the β-decay at stellar temperature. Obviously the vast majority of isotopes, where an experimental neutron capture cross section is desirable, have terrestrial β-decay half-lives of at least thousands of days. The right part Figure 1 shows the same as the left part, but for the higher neutron density and temperature. Now isotopes with half-lives down to a few days can be of interest for the s-process reaction network.

B. Neutron capture measurements

Only a handful of direct measurements on radioactive isotopes could be performed so far in the astrophysically interesting region of 1-200 keV. Most of those measurements are

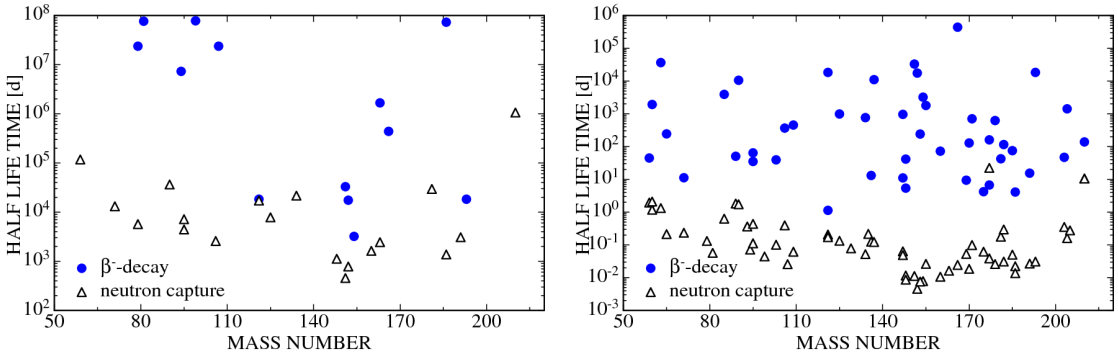

FIG. 3. Left: Half life times with respect to neutron capture (open triangles) for a neutron density of 10^7 cm^{-3} and terrestrial β-decay half life times (filled circles) for unstable isotopes on the s-process path as a function of mass number. Shown are only isotopes where the neutron capture is faster than the β -decay at kT = 5 keV. The neutron capture cross sections are taken from [8] and the half lives under stellar conditions from [15]. Right: Same as left, but for a neutron density of 10^{12} cm^{-3} and β-decays at kT = 30 keV.

activation measurements, which provide only integral information. The time-of-flight (TOF) method, which provides the desired differential cross sections, is much more generally applicable, but requires significantly bigger samples. With the neutron fluxes available so far, the TOF method is therefore restricted to very long-lived isotopes.

Improved experimental techniques, especially as far as the neutron source and sample preparation are concerned, are necessary to perform direct neutron capture measurements on such isotopes [12]. Though the activation method or accelerator mass spectroscopy of the reaction products could be applied in a limited number of cases, experimental facilities like DANCE at LANL (USA) [12], n-TOF at CERN (Switzerland) [7] and the upcoming projects like SARAF (Israel) and FRANZ at the Goethe University in Frankfurt (Germany) [13] are addressing the need for such measurements on the basis of the more universal method of detecting the prompt capture γ-rays, which is required for the application of the neutron time-of-flight (TOF) technique.

C. The potential of the ESS

The ESS has the potential of becoming a prime candidate for TOF measurements on radioactive nuclei for astrophysical purposes. The expected neutron fluxes are orders of magnitudes higher than currently available, which translates into a shorter half life of the possible isotopes under investigation [9]. The most important question to be addressed is the time structure of the proton pulse, in particular the length of the proton pulse and the repetition rate.

Since spallation sources are white sources, energy-dependent cross section measurements are based on the TOF technique. The range of energies that are accessible depends therefore strongly on the width of the proton pulse, since for any given time of flight at the sample position a range of neutron energies is present. The bigger the proton pulse, the wider the range of energies. A careful analysis reveals that measurements in the keV-region are not possible, if the width of the proton pulse is greater than approximately 1 µs, see Table I.

	En=1 MeV TOFn=1.5 µs	En=100 keV TOFn=4.6 µs	En=10 keV TOFn=15 µs	En=1 eV TOFn=1.5 ms
ΔTOF	ΔEn	ΔEn	ΔEn	ΔEn
5 ns	7 keV	0.2 keV	7 eV	10 µeV
0.7 µs	1.6 MeV	32 keV	1 keV	1 meV
1 ms	n/a	n/a	n/a	5 eV

TABLE I. The table shows the neutron-energy resolution during a TOF measurement as a function of proton-pulse width (1. column) and neutron energy (column 2-4). The astrophysically most important neutron energies are in column 2 and 3. The long-pulse solution of the ESS (ΔTOF=1 ms) would not allow TOF measurements for astrophysics, while it would be possible with a short-pulse solution (ΔTOF=0.7 µs)

Similarly, the repetition rate of the proton beam has to be below approximately 100 Hz. The reason for this limit is the fact that the slowest neutrons from the preceding pulse have to be able to pass through the sample before the new neutrons with high energies arrive. This effect is called wrap-around.

III. ISOL@MYRRHA: AN ON-LINE ISOTOPE SEPARATOR COUPLED TO THE MYRRHA PROTON ACCELERATOR

The MYRRHA project at SCK-CEN (Mol, Belgium), that has recently received green light from the Belgian government, consists of a proton accelerator with a proton energy of 600 MeV and a design intensity of 4 mA, coupled to a liquid Lead-Bismuth Eutectic (LBE) spallation neutron source. The spallation target is located in the center of a subcritical reactor core with a fast-neutron spectrum and cooled with liquid lead-bismuth. Apart from the experimental and irradiation possibilities in the subcritical reactor, e.g., for waste transmutation, the MYRRHA proton accelerator on its own can be used as a supply of proton beams for a number of experiments. In order to explore new research opportunities offered by the accelerator, a pre-study was initiated within the framework of the "Belgian Research Initiative on eXotic nuclei" (BriX) network of the Interuniversity Attraction Poles Programme of the Belgian State. This study is investigating unique possibilities for fundamental research using high-intensity proton beams.

An interesting approach for fundamental research using the 600-MeV proton accelerator is the installation of an Isotope Separator On-Line (ISOL) system to produce intense low-energy Radioactive Ion Beams available for experiments requiring very long beam times. Because of the strong similarities of the driver accelerator parameters, the so-called Isol@myrrha will follow closely the RIB production schemes that are developed and successfully used at the ISOLDE-CERN and TRIUMF facilities. It will be equipped with ruggedized target-ion source systems that allow the use of a selection of target materials, including actinide targets, that can withstand the proton beam power. Two types of ion sources are foreseen: hot cavity surface ion sources directly coupled to the high temperature target container that would allow at the same time the implementation of resonant laser ion ionization (RILIS) and a simple low-charge state electron resonance ion source (ECRIS) coupled to the target container with a cold transfer line for gaseous beam production. By using a part (between 100-200 µA) of the 600 MeV proton beam Isol@myrrha will produce a wide spectrum of intense and pure radioactive Q=1+ ion beams at 50 keV energies. The rationale behind the limited choice of simplified and ruggedized target-ion source systems for Isol@myrrha is that the facility should deliver RIB for experiments needing very long beam times up to a few months. In order to make effective use of the precious beam time,

the parallel multi-users aspect of Isol@myrrha will be a key issue in the feasibility study.

The radioactive beams from ISOL@MYRRHA will be used for experimental campaigns involving measurements, which

- need very high statistics;
- need many time-consuming systematic measurements;
- hunt for very rare events;
- and/or have an inherent limited detection efficiency.

This approach would complement other European RIB initiatives, as is illustrated in Figure 4, where a comparison is given between typical experiments at high-intensity RIB facilities with ˜one-week beam times (in blue) and typical experiments at an high-intensity RIB facility with ˜few-months beam times (in red). Such measurements requiring high-intensity beams and long beam times are an important source of information for quasi all fields in science making use of RIB's, ranging from fundamental-interaction measurements with extremely high precision over systematic measurements for condensed-matter physics and production of radio-isotopes.

A report outlining the different technical and physics aspects of the ISOL@MYRRHA project can be downloaded [17]. The time line of the MYRRHA project has now been fixed and it is envisaged that the MYRRHA proton accelerator should be operational by 2020 and the full project (including the coupling to the reactor core) is envisaged to go on-line by 2023.

With the availability of the proton driver of the ESS project, it might be interesting to consider an ISOL@ESS project to produce intense and pure radioactive ion beams for experiments and applications in the field of fundamental interaction studies, nuclear physics, atomic physics, condensed matter research and biomedicine.

IV. NEUTRINO-NUCLEUS REACTIONS AT THE ESS

Neutrino-nucleus reactions are important in many astrophysical environments. These include the collapse of massive stars and the subsequent explosive nucleosynthesis. During the collapse neutrino-nucleus reactions are important for the thermalization of neutrinos and for the determination of the emitted neutrino spectra at bounce with important implications for future supernova neutrino detection. During the explosion neutrino interactions determine

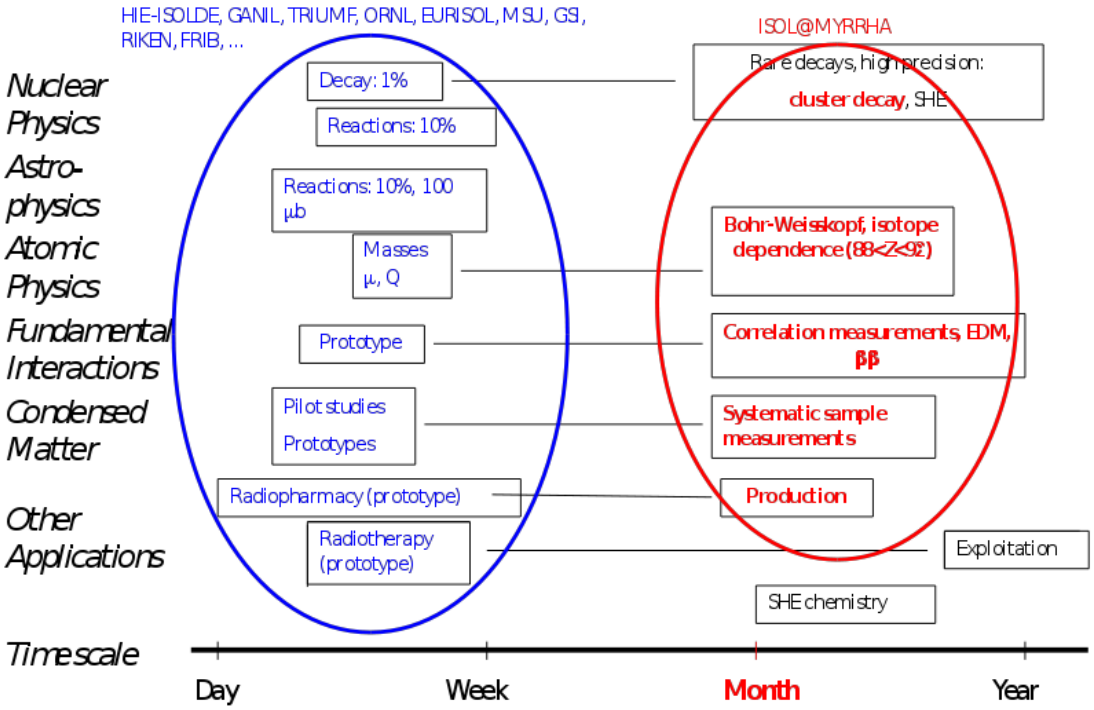

FIG. 4. A comparison between typical experiments at high-intensity RIB facilities with ˜one week beam times (in blue) and typical complementary experiments at the high-intensity ISOL@MYRRHA facility with ˜few-months beam times (in red).

whether the ejected matter is proton or neutron rich and the subsequent nucleosynthesis. In all these cases neutrinos have energies of a few tens of MeV. The European Spallation Source (ESS) will produce large amount of neutrinos from muon decay at rest with very similar energies. The ESS constitutes an ideal place to measure for the first time many of the relevant neutrino-nucleus cross sections.

A. Inelastic neutrino-nucleus reactions

Massive stars end their lives as type II supernovae, triggered by a collapse of their central iron core [18]. As the collapse proceeds and the density increases neutrino interactions with matter become increasingly important and require a careful treatment, which is usually done within Boltzmann transport theory [19, 20]. Here elastic neutrino-nucleus and inelastic neutrino-electron scattering have been identified as the sources for neutrino trapping (which occurs at densities around a few 10^{11} g/cm^3) and neutrino thermalization, respec-

tively. Recently inelastic neutrino-nucleus scattering has been included for the first time in supernova simulations, as another mode of energy exchange between neutrinos and matter. The relevant cross sections have been calculated based on large-scale shell model calculations for the allowed GT transitions and within the random phase approximation for forbidden transitions [21], taking special care of finite temperature effects [22]. At low and modest neutrino energies Eν the cross sections are dominated by GT0 contributions for which the shell model has been validated by detailed comparison to precision M1 data derived from electron scattering on spherical nuclei which are mainly due to the same isovector response [23].

Although inelastic neutrino-nucleus scattering contributes to the thermalization of neutrinos with the core matter, the inclusion of this process has no significant effect on the collapse trajectories. However, it increases noticeably the opacity for high-energy neutrinos in the ν_e neutrino burst just after the bounce. As these neutrinos excite the nuclei, they are down-scattered in energy, in this way significantly reducing the high-energy tail of the spectrum of emitted supernova neutrinos [24]. This makes the detection of supernova neutrinos by earthbound detectors more difficult, as the neutrino detection cross section scales with E_ν^2.

B. Neutrinos and Explosive Nucleosynthesis

Core-collapse supernovae are the birth places of neutron stars. During the explosion, around 10^{53} erg, corresponding to the binding energy of the neutron star, are emitted in all neutrino species from a thermal surface denoted as neutrinosphere. These neutrinos produce an outflow of baryonic matter known as the neutrino-driven wind. Recent hydrodynamical studies of core-collapse supernovae have shown that the bulk of neutrino-heated ejecta during the early phases (first seconds) of the supernova explosion is proton-rich [19].

The early proton-rich ejecta constitutes the astrophysical site for the νp-process that has been recently suggested as a mechanism for the production of light-p nuclei [25]. The νp operates in proton-rich environments with high neutrino and antineutrino fluxes. Initially the ejected matter is very hot and constituted of free nucleons. The competition of neutrino captures on neutrons and antineutrino captures on protons drives the matter proton-rich as both neutrino types have rather similar luminosities and the average antineutrino energy is not large enough compared to the neutrino energy to compensate for the difference in

reaction Q-values. Upon reaching cooler regions, i.e. with increasing distance from the neutron star surface, the nucleons assemble in nuclei and, without further neutrino reactions, the proton-rich matter freezes out with a significant production of N=Z nuclei like ^{56}Ni and ^{64}Ge and some free protons left. However, antineutrino captures on these protons ensure a significant presence of free neutrons which can be captured on the N=Z nuclei via (n,p) and (n,γ) reactions allowing for matter flow beyond ^{56}Ni and ^{64}Ge which otherwise with their long halflives against proton capture and beta decay could not be overcome during the dynamical timescale of supernova nucleosynthesis (a few seconds).

Matter ejected at later times is expected to become neutron-rich and allow for the occurrence of an r-process. Several studies have shown that neutrino-nucleus interactions can have a large impact in r-process nucleosynthesis (see [26]).

When neutrinos, produced in the hot supernova core, pass through the outer shells of the star, they can induce nuclear reactions and in this way contribute to the element synthesis (the ν-process [27]). For example, the nuclides ^{11}B and ^{19}F are produced by (ν,ν'n) and (ν,ν'p) reactions on the quite abundant nuclei ^{12}C and ^{20}Ne. These reactions are dominantly induced by ν_μ and ν_τ neutrinos and their antiparticles (combined called ν_x neutrinos), which have larger average energies (about 20 MeV) than electron neutrinos and anti-neutrinos. As found in detailed stellar evolution studies [28, 29] the rare odd-odd nuclides ^{138}La and ^{180}Ta are mainly made by the charged-current reaction ^{138}Ba(ν_e,e^-)^{138}La and ^{180}Hf(ν_e,e^-)^{180}Ta. Hence, the ν-process is potentially sensitive to the spectra and luminosity of ν_e and ν_x neutrinos, which are the neutrino types not observed from SN1987a, and requires high quality neutrino-nucleus cross sections.

Finally, neutrinos are detected on Earth by their interaction with nuclei present in the detector material. Here again reliable neutrino-nucleus cross sections are necessary to fully exploit a future supernova neutrino detection. This is necessary not only to improve our understanding of the explosion mechanism but also for disentangling purely nuclear effects from oscillation effects due to the propagation of neutrinos through the stellar mantle, enabling us to learn about neutrino properties including the mass hierarchy and mixing angles.

C. Neutrinos at ESS

Neutrino production at spallation sources have been studied in great detail (see for example [30]). The dominating neutrino production channel is $\pi^+ \rightarrow \mu^+ + \nu_\mu$ ($t_{1/2}$ = 26ns) followed by $\mu^+ \rightarrow e^+ + \nu_e + \bar{\nu}_\mu$ ($t_{1/2} = 2.2\mu$s). $\nu\mu$ are almost monoenergetic with an energy of around 30 MeV and $\bar{\nu}_\mu$ and ν_e have a continuous spectrum with averages energies around 30 MeV, These energies are similar to the ones expected in core-collapse supernovae, making the ESS a unique facility for the study of neutrino-nucleus cross sections at the energies relevant for supernova physics.

Based in the detailed study of [30] and considering that at the ESS will have 2 ms pulses of 2.5 GeV protons with a power of 5 MW (1.2×10^{16} protons/s), we expect 3.1×10^{15} neutrinos of each flavor (ν_μ, $\bar{\nu}_\mu$, and ν_e). Due to the long pulse structure, it will not be possible to distinguish between neutrinos produced form π^+ decay and neutrinos produced from μ^+ decay. This is certainly a drawback for neutrino oscillation studies. However, it will still allow for a rich program of neutrino-nucleus cross sections measurements. Here the priority is to place a detector as close as possible to the neutrino source.

As discussed above neutrino interactions with ^{12}C are responsible for the production of ^{11}B in neutrino-nucleosynthesis. Some of the relevant cross sections have been already measured by the LSND and KARMEN collaborations. Consequently, it provides a way of testing the neutrino detector and to monitor the neutrino flux for other experiments. Neutrino reactions with ^{16}O are also important for neutrino nucleosynthesis studies. In addition, neutral current cross sections for ^{16}O(ν,ν' pγ) and ^{16}O(ν,ν' nγ) are important for the detection of supernova neutrinos in water Cherenkov detectors [31] and may constrain the strange-quark content of the nucleon [32].

The reaction ν_e +d$\rightarrow$ e^- +p+p can be considered as the inverse of the reaction p+p$\rightarrow e^+$ +d+ ν_e that is the main reaction of the pp-chain responsible for hydrogen burning in stars less massive than 1.2 solar masses. Both reactions above have been computed by effective field theory approaches [33] and are believed to be known with an accuracy of a few percent. Updating the estimate of [30] to the ESS neutrino flux and assuming a one ton detector of D^2O at a distance of 10m, one can expect that the neutrino cross section will be measured with an statistical accuracy $< 1\%$ in one year. This measurement will prove our understanding of electroweak processes on light nuclei.

Neutrino inelastic scattering in iron group nuclei has been shown to play an important role in shaping the spectra of neutrinos emitted during the early times of the supernova explosion [23]. Currently only the charge current ν_e absorption cross section on ^{56}Fe has been measured by the KARMEN collaboration [34]. The ESS will allow for a full program of neutrino measurements on iron group elements of particular relevant for supernova dynamics and nucleosynthesis.

Reference [30] provides an extensive list of neutrino reactions that can be measured in an spallation facility.

---

[1] L. Schaller, Z. Phys. **C56** (1992) S48.

[2] P. Strasser et al., Hyp. Interact. **119** (1999) 317.

[3] P. Strasser et al., AIP Conf. Proc. **793**, 242 (2005).

[4] P. Strasser et al., Hyp. Interact. **193** (2009) 121.

[5] D. Hitlin et al., Phys. Rev. **C1** (1970) 1184.

[6] R.J. Powers et al., Nucl. Phys. **A316** (1979) 295.

[7] U. Abbondanno, et al., Phys. Rev. Lett. **93(16)** (2004) 161103.

[8] Z.Y. Bao et al., Atomic Data Nucl. Data Tables **76** (2000) 70.

[9] A. Couture and R. Reifarth. Atomic Data and Nuclear Data Tables **93(5)** (2007) 807.

[10] M. Heil et al. Progress in Particle and Nuclear Physics **59(1)** (2007) 174.

[11] M. Lugaro et al., Ap. J. **586** (2003) 1305.

[12] R. Reifarth et al., NIM A **531** (2004) 528.

[13] R: Reifarth et al., Publications of the Astronomical Society of Australia **26(3)** (2009) 255.

[14] R. Reifarth, et al., NIM A **524** (2004). 215.

[15] K. Takahashi and K. Yokoi, Atomic Data Nucl. Data Tables **36** (1987) 375.

[16] C. Travaglio et al., Astrophysical Journal **601(2)** (2004) 864.

[17] "ISOL@MYRRHA: An On-Line Isotope Separator coupled to the MYRRHA proton accelerator": iks32.fys.kuleuven.be/wiki/brix/index.php/Main_Page

[18] H.-T. Janka, K. Langanke, A. Marek, G. Martínez-Pinedo, B. Müller, Phys. Repts. **442** (2007) 38.

[19] R. Buras, M. Rampp, H.-T. Janka, K. Kifonidis, Astron.&Astrophys., **447** (2006) 1049.

[20] M. Liebendörfer et al., Astrophys. J. Suppl. **150** (2004) 263.

[21] A. Juodagalvis et al., Nucl. Phys. **A747** (2005) 87.

[22] J.M. Sampaio et al., Phys. Lett. **B529** (2002) 19.

[23] K.Langanke et al, Phys. Rev. Lett. **93** (2004) 202501.

[24] K. Langanke, et al., Phys. Rev. Lett. **100** (2008) 011101.

[25] C. Fröhlich, et al., Phys. Rev. Lett. **96** (2006) 142502.

[26] K. Langanke, G. Martínez-Pinedo, Rev. Mod. Phys. **75** (2003) 819.

[27] S.E. Woosley, D. H. Hartmann, R.D. Hoffman, W.C. Haxton, Astrophys.J. **356** (1990) 272.

[28] A. Byelikov et al., Phys. Rev. Lett. **98** (2007) 082501. C60

[29] A. Heger et al., Phys. Lett. **B606** (2005) 258.

[30] F.T. Avignone and Y.V. Efremenko, J. Phys. G: Nucl. Part. Phys. **29** (2003) 2615.

[31] K. Langanke, P. Vogel, and E. Kolbe, Phys. Rev. Lett. **76** (1996) 2629.

[32] E. Kolbe, K. Langanke, F.-K. Thielemann, Eur. Phys. J. **A3** (1998) 389.

[33] K. Kubodera, Prog. Part. Nucl. Phys. **64** (2010) (2) 417.

[34] E. Kolbe, K. Langanke, G. Martínez-Pinedo, Phys. Rev. (1999) 052801.

Muon Physics Possibilities at ESS

K. Jungmann,[1] Y. Kuno,[2] J.S. Lord,[3] E. Morenzoni,[4]
K. Nagamine,[5] and C.J.G. Onderwater[1]

[1]*Kernfysisch Versneller Instituut, University of Groningen, Groningen, The Netherlands*

[2]*Department of Physics, Osaka University, Osaka, Japan*

[3]*ISIS, Rutherford Appleton Laboratory, HSIC, Didcot, United Kingdom*

[4]*Paul Scherrer Institute, Villigen, Switzerland*

[5]*KEK, Tsukuba, Japan and RIKEN, Tokyo, Japan and University of California, Riverside, USA*

I. INTRODUCTION

Muon physics has contributed significantly to progress in fundamental particle-, atomic-, condensed matter, and bio-physics, has produced most precise values for fundamental constants, has provided tests conservation laws at the highest precision levels, and has lead to applications e.g. in tomography of containers and mountains. The European Spallation Source Scandinavia in Lund will be based on a multi-MW proton driver machine in the 2.5 GeV energy range. This opens opportunities to produce muons at large quantities either from a dedicated target station onto which the full beam or part of it will be directed or by thin targets inserted into the primary proton beam line [1, 2]. Because muons live only 2.2 μs the time structure of the beam is important for sensitive muon experiments in both condensed matter and particle physics.

II. THE MUON

The muon has unique and significant properties [3] which make it invaluable for a broad spectrum of scientific applications [4] to study either the muon itself as a fundamental particle or its behavior in matter.

A. Muon mass, life time, interaction, production and decay

The muon is the charge lepton of the second particle generation, with the negative muon (μ^-) being the particle and the positive muon (μ^+) being the antiparticle. The muons ($\mu^\pm$) have an electric charge of $\pm 1 q_e$, the charge of the electron (e). They have spin 1/2 and a mass $m_\mu = 106$ MeV/c^2 which is 1/9 proton mass and 207 electron masses. Muons have a magnetic moment (μ_μ) which is 3.2 times larger than that of the proton. The muons have a lifetime $\tau_\mu = 2.2\ \mu s$ (in vacuum). At the present level of our knowledge muons behave as a structure-less (point-like) particles. They interact mostly electromagnetically with surrounding atoms and molecules in matter. They are sensitive to weak interactions and they are insensitive to the strong interaction. Efficient muon production at an accelerator begins with the production of charged pions ($\pi^\pm$) from a high energy proton (p) beam on a (fixed, low Z, typically carbon) target according

$$p + \text{nucleus} \rightarrow \pi^\pm + \text{new nucleus} + \text{by-products}. \tag{1}$$

Muons appear in the weak interaction pion-to-muon decay according

$$\pi^+ \rightarrow \mu^+ + \nu_\mu \ \text{ and } \ \pi^- \rightarrow \mu^- + \bar{\nu}_\mu. \tag{2}$$

Muon beams can be produced with a "thin" pion production target inserted into the main beam of a proton beam facility (see Table I) such as a spallation source, where a fraction of order a few % of the protons are used to generate pions. Also dedicated target station onto which the full beam of protons or a split offpart of it is directed. Secondary beams of muons are achieved by efficient ion optical collection of the muons from pion decay [1] [2].

Due to maximum parity violation in weak interaction the muons from pion decay at rest via this two body channel are 100 % polarized. Muons decay mostly via the weak interaction

$$\mu^+ \rightarrow e^+ + \bar{\nu}_\mu + \nu_e \ \text{ and } \ \mu^- \rightarrow e^- + \nu_\mu + \bar{\nu}_e. \tag{3}$$

[1] Because muons are charged particles, it is possible to improve drastically beam properties of the accelerator produced muons. Two distinguished examples are muon micro-beam [5] and slow positive muons [6, 7]. As explained later, with the help of intense ESS proton beam of both long pulse and short pulse will be powerfully applied to produce these advanced muon beams.

[2] The high intensity proton beam with a unique time structure at ESS has the capability to produce muons by installing relevant muon beam instrumentation in front of neutron producing targets, with minimum interference. Successful co-existence of neutron and muon facilities has been proven and is a regular standard at ISIS-RAL [8], PSI and J-PARC [9].

Parameter	ISIS TS1	PSI	TRIUMF	J-PARC	ESS-Long Pulse	ESS-Short Pulse	ESS-Special [a]
Proton energy	800 MeV	590 MeV	500 MeV	3000 MeV	1000 MeV	1000 MeV	1000 MeV
Pulse length	2*100 ns	Cont	Cont	2*600 ns	2 ms	2*600 ns	25 ns
Repetition rate	40 Hz	Cont	Cont	25 Hz	16.7 Hz	50 Hz	33 kHz
Mean current	180 μA	2.3 mA	0.14 mA	0.33 mA	5 mA	5 mA	125 μA
Mean power	144 kW	1.77 MW	0.07 MW	1 MW	5 MW	5 MW	125 kW
Mean Power chopped to $\leq 2\mu s$ every $\geq 30\mu s$	144 kW	(118 kW)	(4.7 kW)	1 MW	333 kW	5 MW	125 kW
Mean Power chopped to $\leq$ 100ns $\geq 30\mu s$	72 kW	(5.9 kW)	(240 W)	167 kW	16.6 kW	416 kW	125 kW
Mean Power chopped to $\leq$ 25ns $\geq 30\mu s$	1 kW	(1.5 kW)	(60 W)	42 kW	(4.2 kW)	104 kW	125 kW

[a] see section III H.

TABLE I. Beam parameters of some present and proposed muon sources. Note, the number of produced pions and muons is to good approximation proportional to the beam power devoted to their production. The possibilities for ESS compare very favorably for ESS in various scenarios.

For an ensemble of muons the decay electrons (positrons) are predominantly emitted against (in) the direction of the muon spin because of parity violation and hence they signal the muon spin at the time of the decay. Other decay modes are below 1 %. Rare or according to presently known conservation laws forbidden decay modes could signal New Physics beyond the Standard Model.

1. Muon penetration capability through thick materials with energy increase

Because of the predominant electromagnetic interactions, the absence of nuclear interactions and the 207 times heavier mass than the electron, mean ranges of beyond 1 m in water, 30 cm in carbon and 10 cm in iron are possible with the highest energy muons available directly from a 1000 MeV proton source. High-energy cosmic-ray muons are able to

penetrate rather thick materials such as volcanic mountains [4, 10].

III. CONDENSED MATTER RESEARCH WITH MUONS

A. The method of μSR

The technique of μSR, i.e. muon spin relaxation, muon spin rotation or muon spin resonance, implants spin polarized positive muons in a sample, where they interact with their surroundings via their charge and magnetic moment. The asymmetrically emitted decay positrons which are related to the muons spin at the moment of decay are counted. Because the e^+ energy extends up to 53 MeV, the direction of the μ^+ spin can be known in each event of the muon decay by measuring the emission direction of the high-energy e^+ using detectors placed outside of the target material under investigation. The evolution of the average spin over a few muon lifetimes is measured. With suitable theoretical models, and usually measurements in different external magnetic fields, we can calculate the magnitude and frequency spectrum of static and dynamic microscopic magnetic fields experienced by the muon.

The mechanisms for spin relaxation are the same as detected in nuclear magnetic resonance (NMR) or electron paramagnetic resonance (EPR). Because of the rather large muon magnetic moment and the unique μs time window for the dynamics of the surrounding local fields, one can easily detect a static and dynamical mG field in the atomic-level microscopic space. Also, the μSR method can be applied to amorphous or crystalline materials, at any temperatures, and under zero external magnetic field.

The technique of μSR has applications in a wide range of condensed matter science such as magnetism (including molecular and frustrated magnetic materials), superconductivity, semiconductors, chemistry (especially radical chemistry and reactions, where the muon picks up an electron to form muonium (the bound state of a positive muon and an electron, chemically like atomic hydrogen), molecular dynamics and ionic conductivity [11,12,13]. Negative muons form a tightly bound state around a nucleus, emitting characteristic X-rays in the process. Their lifetime is reduced by the possibility of capture by the nucleus. The behavior of the two muon species in matter may be summarized as:

A μ^+ behaves like a light proton, a μ^- behaves like a heavy electron.

B. μSR Instrumentation

A typical μSR instrument has the ability to apply magnetic fields to a sample, either parallel or perpendicular to the initial spin, and vary the sample temperature. Other sample environments such as electric fields, RF magnetic fields or illumination may be added depending on the experiment.

The simplest muon experiment is integral counting. A continuous beam of muons enters the sample and we measure the time-average polarization via the decay positrons. A high flux can be used, with a sufficiently segmented detector array, and the time structure is not important. Usually some parameter such as magnetic field is varied allowing resonances to be plotted.

Time-differential muon spin relaxation or rotation uses either a detector for incoming muons, or a well defined pulse structure with pulses shorter than the muon lifetime spaced at over 10 muon lifetimes apart. The time interval between muon arrival and decay is recorded in histograms, one per detector. The evolution of polarization after the pulse is obtained.

Finally pulsed excitation techniques first implant muons in the sample in a steady state, perhaps with a holding longitudinal magnetic field, then apply a stimulus such as RF magnetic field or light. The response of the muon spin to this is measured. For example a "90 degree" RF pulse can rotate the muon polarization into the transverse direction, giving a signal equivalent to the "free induction decay" in NMR. This can overcome the frequency limit due to a finite muon pulse width, or dephasing by muon site changes shortly after implantation [14, 15].

C. Muon states in matter; diamagnetic μ^+, muonium and μ^--atom

Most scientific applications of muons, except radiography, use muons stopped in matter. Once muons enter matter they take after a short slowing-down process the following states during most of their life-times: μ^+ as diamagnetic μ^+ in most metals and Muonium (Mu), the hydrogen-like bound state of a μ^+ and an e^- in semiconductors and insulators. μ^- as a small and tight muonic atom.

D. Excitation and electron introduction before stopping

When the μ^+ spin probe is applied to soft matter objects such as conducting polymers, proteins etc., it is able to explore new aspects of the functions of the materials, because of the "active" nature of energetic charged particle probes. During the slowing-down process after injection and prior to formation of a chemical bonding at the stopping site, the μ^+ can excite a magnetic triplet state in the stopping molecules, providing a probing-capability of the molecular-level behavior of a macromolecule which has a non-magnetic ground state (excitation of magnetic molecular state) [16]. In most of soft matter like macroscopic bio-molecules, the μ^+ takes on an electronic state of muonium during its slowing-down process by accompanying the electron, which takes a characteristic motion in the stopping macromolecule. Thus, electron transfer phenomena can most sensitively be monitored. In addition to conducting polymers, biological electron transfer in heme-proteins and DNA has been studied (electron introduction for biological electron transfer) [17]. In semiconductors the slowing-down muon loses some of its energy by exciting electrons across the gap, and the resulting excess conduction electrons and holes may interact with the same muon once it stops.

E. Thin layers and surfaces

The "conventional" μSR technique [18, 19] makes direct use of muons impinging on the sample with $> 3-4$ MeV energy. The stopping range of surface muons in a solid varies from 0.1 mm to 1 mm with a straggling of about 20 % of the mean value. Up to recently this has limited the μSR investigations to bulk properties of matter and to samples, which can be grown with sufficient thickness. The development at PSI of a beam of a low energy (LE) beam of fully polarized μ^+ with tunable energies between 0.5 and 30keV enables now investigations of near-surface regions, thin films, interfaces and multi-layers up to depths of 300 nm and of samples which can be grown only as thin films [20]. Such LE muons are obtained by moderation of a secondary muon beam in layer of frozen inert gases such as Ar or Ne [21] or by photoinization of muonium atoms [20]. The actual LE-μ^+ flux obtained from 1.9×10^8 surface muons with a momentum spread of ~ 9 % are 11000 epithermal muons/s at a frozen gas moderator source and about 4500 LE-muons/s at the sample (with a s-Ar moderator) on a beam spot with typical 10^{-20} mm FWHM. Using a longer muon production target and

a s-Ne moderator the rate at the sample can be raised to more than 10^4 LE-muons per s. This extends greatly the use of μSR to new objects of investigations and provides a novel magnetic/spin probe for thin films, multilayers, buried layers and surface regions, the study of whose properties has become in recent years one of the most active areas of research in condensed matter and material science [22]. One of the most powerful features of LE-μSR is that it can measure magnetic field profiles on a scale of few nm and it is therefore sensitive to the magnetic or superconducting state of near surface regions. An example is the absolute model independent determination of the characteristic length of superconductors such as penetration depth [23]. Its dependence on temperature, doping, orientation, or B-field contains information about the superconducting order parameter and gap symmetry and is of central importance for any theory of unconventional superconductivity. Multilayers or heterostructures display an immense wealth of physical phenomena as a consequence of the reciprocal influence of materials with different electronic properties. Here the ability to selectively probe the different layers has been recently used to probe the spin polarization of current-injected electrons in the active layer of an operational organic spin valve structure [24]. This measurement allows to determining the temperature dependence of the spin diffusion length. Relating this microscopic quantity to macroscopic parameters such as the magneto-resistance allows to reveal the role of the various mechanisms that limit the spin coherence in fully functional and realistic devices.

F. Suggestion for continuous muons with ESS long pulse; DC micro-beam

The muon sources presently operating are either continuous (PSI, TRIUMF) or pulsed, with pulse length much less than the muon lifetime (ISIS, J-PARC). As the pulse length on the ESS long pulse target station will be much greater than the muon lifetime, the source has to be treated as continuous, but with a low duty cycle (on for 1-2ms every 60ms). It would be best used for integral counting methods such as level crossing resonance, where a high flux of muons can be used. More detectors would be needed than on a true continuous beam with the same time-averaged flux, but this is not a problem with modern technology. Time-differential experiments using a muon counter are possible provided the flux is reduced to prevent pile-up (more than one muon in the sample at once, so the decay positrons may be mixed up). Collimation would give a narrow beam with low flux to measure very small

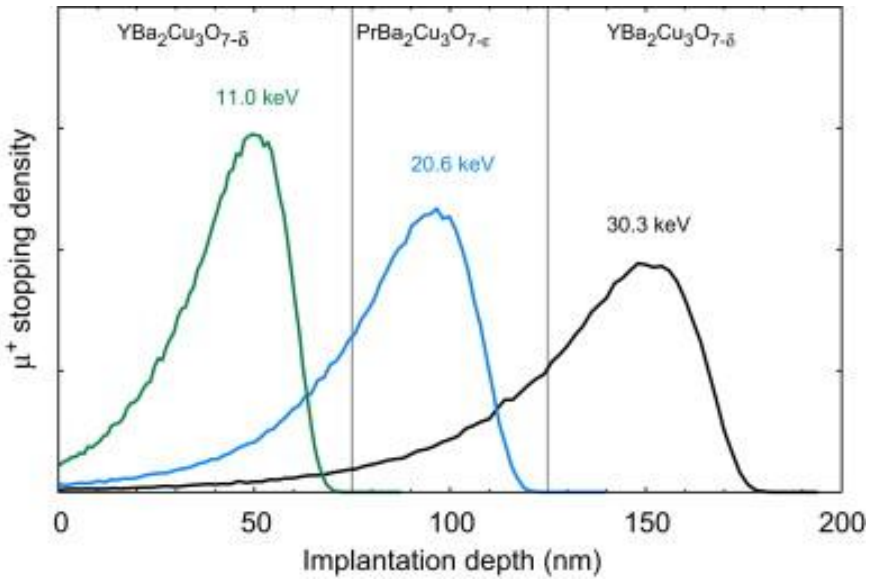

FIG. 1. Example of low energy muon stopping profiles in a $YBa_2Cu_3O_7$ (75nm) – $PrBa_2Cu_3O_7$ (50nm) – $YBa_2Cu_3O_7$ (75nm) heterostructure, showing the layer by layer sensitivity.

samples, and an instrument could be optimised for this. Cryogenic moderation can be used to obtain very low energy muons for surface and thin film studies, again the efficiency of the process may reduce the rate to no more than one muon in the sample at once. However the overall data rate for any time differential measurement is severely limited because of the low duty cycle, it could be greater than the present low energy muon source but a factor of 30 below most time differential instruments. Using a muon beam kicker, it would be possible to chop the long pulse to produce a train of muon pulses of lengths between 100ns and 2s, spaced sufficiently to measure muon relaxation from each (perhaps 20-30s). Pulses of up to the muon lifetime could be used for pulsed (RF) excitation or slow relaxation rates and would give a data rate of about twice the ISIS double-pulse beam. Pulses exceeding the muon lifetime are not so useful since most of the muons have decayed before relaxation measurement can begin. Short pulses could be tuned to increase the frequency response at the expense of rate, perhaps matching or exceeding that of the ISIS source although the rate will be about a factor of 4 lower for an equivalent pulse length. The beam could be switched between several time differential instruments operating in this mode with an integral instrument using all the remaining muons. Optical excitation of the muons may be difficult since a flash-lamp or laser will not be able to recharge and fire again many times within the 2ms pulse train.

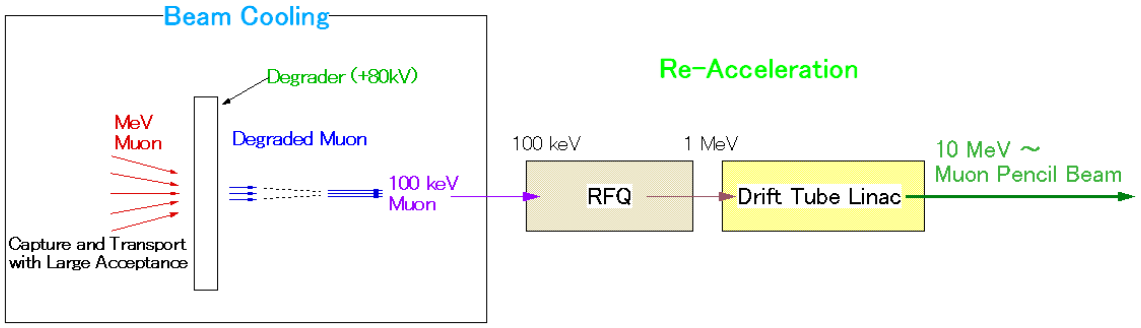

FIG. 2. Schematic diagram for muon micro-beam generation using large-acceptance muon capture, a muon degrader and muon acceleration linac.

The muon micro-beam, which should be best suited for the ESS long pulse can be generated by a scenario given in Fig. 2 [17]. Muons at MeV energy which are produced by the accelerator proton beam are collected with beam collection optics with large solid-angle acceptance. Muons at several 10 keV will be obtained through an energy degrader; these muons are captured, bunched and accelerated by an RFQ and DTL accelerators to produce a narrow and straight 10MeV muon beam with minimum energy spread. The scenario basically follows the principle of conservation of phase-space volume in the acceleration of the degraded particles. Design studies [17] show this muon micro-beam will be a 10 MeV straight beam, with a narrow spatial size (<1 mm diameter), narrow energy width (a few 0.1 %) and a high luminosity of $10^9/(\mathrm{cm}^2\mathrm{s})$. This would allow the full beam to be deposited into a sample as small as 1 mm diameter and 100 micron thick with 10,000 times more intensity than any other muon source in the world. Because of the unique time-structure and mm-size of the ESS proton beam, the intense and high-quality Muon Micro-Beam can be implemented most effectively.

At ESS Long Pulse, the 1.334 GeV, 3.75 mA proton beam is available with a time structure of 16 2/3 Hz repetition rate and 2.0 ms width. Strong and low-duty RF fields of the RFQ and DTL accelerators necessary for the production of the muon micro-beam can nicely be matched to the time structure of this ESS proton beam (see Fig. 3). The use of the existing continuous proton beam facilities like PSI or TRIUMF is not suitable for this purpose, where a substantial loss of muons would be inevitable. This instrumentation could

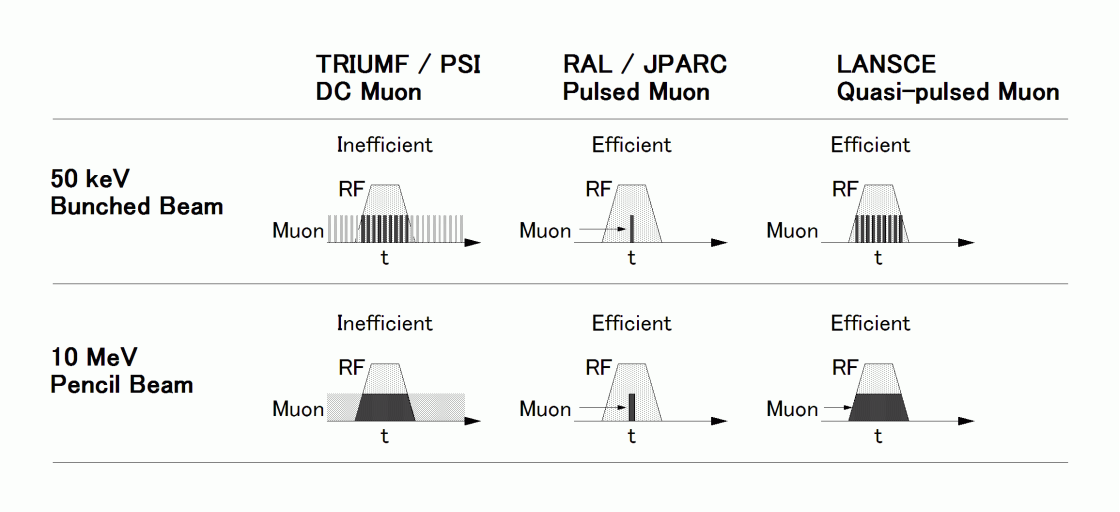

FIG. 3. Comparison of beam time structure between the world-wide muon facilities in order to be used to produce the proposed 10 MeV uon micro-beam. The efficient use of the ESS proton beam can be seen.

also be installed at pulsed muon facilities at intense proton synchrotron like RAL-ISIS in the UK or J-PARC in Japan to create a pulsed micro-beam facility. However, since those proton beams will have diameters of a few cm at the production target, a muon micro-beam produced there might have lower quality and intensity compared to the one presently proposed for ESS.

The materials science research by muon spin rotation/relaxation/resonance (μSR) spectroscopy and the muon catalyzed fusion (CF) research will be advanced by the availability of the proposed muon micro-beam:

(i) Characterization of functional and complex materials under high pressure beyond 10 GPa

The muon micro-beam can be delivered through a small (less than mm) window and stopped inside a material placed under a very high pressure environment like a diamond anvil cell. Currently high-pressure μSR studies are done below 1 GPa.

(ii) Characterization of single crystal samples of exotic materials

The micro-beam size can allow efficient examination of samples as small as 1 mm diameter and 100 micron thick – this is a size more compatible with newly grown complex materials which are typically grown either as films or in very small single

crystals. This is in contrast to current muon beam sources where the flux is spread over > 1 cm diameter.

(iii) Characterization of biological materials inside various environments

The micro-beam can be stopped in any small scattering limited (mm-size) spot at a depth up to 10 cm from the surface of a live-substance to probe molecular level magnetic properties. New life science application will be opened. Brain function research is a promising example with a capability of probing oxy-hemoglobin through triplet-state excitation [16].

(iv) Realization of break-even in muon catalyzed fusion

Since both positive and negative muon micro-beams can be obtained simultaneously, in addition to materials research, the beams can be used for studies of nuclear fusion catalyzed by negative muons in pressurized D-T mixtures in order to investigate a break-even condition [25].

G. Suggestion for pulsed muons with ESS short pulse; Pulsed slow muon

The short pulse solution would be ideal for techniques such as RF resonance, optical excitation using a laser or low energy muon production by laser ionization. For RF or other pulsed excitation measurements, the muons are allowed to accumulate in the sample in a holding longitudinal magnetic field, then the pulse is applied and the response (for example a free induction decay of the transverse polarisation) is observed. A repetition rate of 50Hz is well matched to most laser systems.

With the short proton pulse scenario at ESS (1.4 s width) a pulsed muon beam can be generated as initiated at KEK [26] and developed at RAL-ISIS and J-PARC. At ESS, the strongest pulsed slow positive muons can be realized by employing laser ionization of thermal muonium [7]. As shown in Fig. 4, a saw-tooth RF of transporting electric field is able to realize a sharp (ns) and narrow (sub-mm) beam spot at a μSR sample position.

There are several important subjects to be investigated by using the produced intense slow positive muons:

(i) Fundamental physics

Since the highest peak-intensity and low-duty pulsed positive muon with the highest

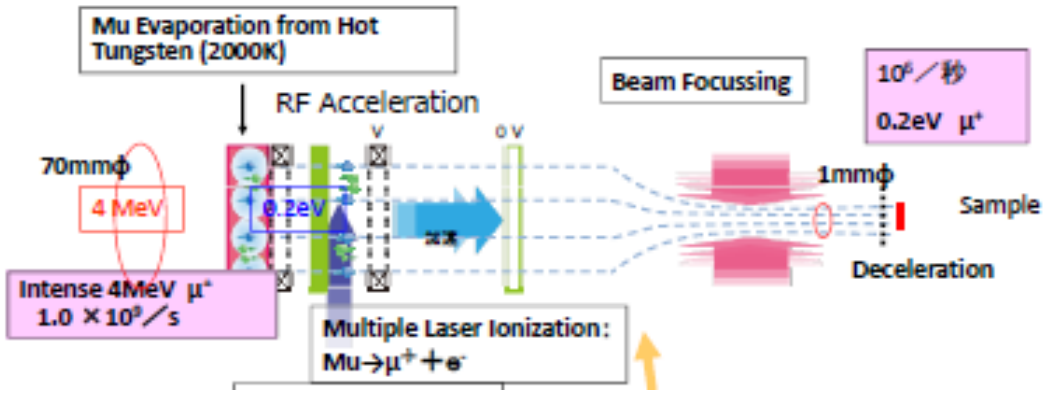

FIG. 4. Schematic layout of ultra-slow muon production by laser resonant ionization of thermal muonium from hot tungsten. For ESS short pulse, multiple lasers to cover 1.4 s and RF acceleration will be employed.

luminosity and the narrowest beam divergence will be produced, various fundamental physics applications will be opened. A distinguished example is a next phase g-2 experiment with a compact storage ring as proposed to J-PARC [27] (see sect. IV C 1).

(ii) Spintronics material development by detection of conduction electron spin polarization in semiconductors.

There is no method to detect conduction electron spin polarization (CESP) in popular semiconductors like Si, Ge or graphite, since optical methods cannot be applied due to a small spin-orbit force and indirect gap. The use of spin polarized μ^+ and/or μ^- with spin exchange collision between bound electron with CE provide a unique solution. Recently a feasibility study was successfully conducted on n-type GaAs [28]. By employing intense slow muons at ESS, depth-profile measurements can be conducted for a wide-range of semiconductor device candidates for industrial application.

(iii) Hunting for non-linear muon phenomena of interacting muons

The produced slow positive muons will mark the highest tempo-spatial density so that muons may have a chance to interact with each other. Some significant exotic phenomena may take place. Typical examples are muon-paired diffusion in metal at low temperature and the formation of muonium molecules and many more.

With short pulses it is also possible to perform standard pulsed time-differential measurements. The length of the pulse limits the maximum precession frequency or fastest

relaxation rates that can be measured but for some experiments this may be acceptable. Some improvement in frequency range can be obtained by chopping the muon beam, either to one of the two pulses or into shorter portions, though the data rate will be reduced. With the pulse length matching the ISIS source the data rate is still likely to be 6 times that of ISIS. Chopping need not waste muons but can divide them between several instruments.

H. Other options

If we have freedom to use the accelerator as we like, other options can be envisaged. During the 58ms between long pulses, switch the proton beam away from the neutron target and to a separate muon target and beam stop. Instead of a long pulse put only a short pulse (a few RF "bunches") of protons every 20-40us. This will give a pulsed muon source with pulse length largely limited by the pion lifetime of 26ns (for surface muons) or the linac RF frequency (for higher energy decay muons). This source could have twice the flux of the ISIS single pulse beam with 4 times the frequency range though since the beam need not be preserved for use in a neutron target, a thicker muon target would give further flux increases. The count rate on the detectors would be much reduced compared to a 50Hz pulsed machine, so they need not be divided into as many independent channels. It would also be possible to collimate the beam to reduce the flux to 1 muon per bunch on average and use a muon counter to give very high timing resolution, roughly matching the data rate of a conventional time-differential instrument but with lower background counts. Cryogenic moderation could be used to produce low energy muons, although the rate would be low. In this case the trigger detector could optionally be removed to improve the energy resolution while still giving a useful frequency range. This pulsed source would be suitable for RF resonance but the high repetition rate may cause problems for laser excitation or laser production of low energy muons.

I. Conclusions for condensed matter muon research

ESS with long pulses will provide the strongest continuous muon-micro beam useful for μSR condensed matter studies under high pressure, advanced muon catalyzed fusion research towards a realization of break-even, etc. The long pulse muon source has a few applications

for which its high flux gives an advantage over present sources, and most present experiments can be performed though they may have lower count rates than regularly achieved elsewhere. Given the same overall protons per pulse, it is better for muons (or at least no worse) if the pulse is longer, while for neutrons a shorter pulse may be preferred. ESS with short pulses will provide the strongest pulsed slow μ^+ beam useful for materials research for spintronics devices, fundamental physics like muon g-2 and hunting for non-linear effect of muons in condensed mater etc. The short pulse muons source opens thereby new possibilities for condensed matter research and provides positive muon sources which enable novel particle physics experiments. Typical muon condensed matter experiments use a few days of beam time and the experimental team will use other measurement techniques on the same samples in order to give a complete picture. Muons at ESS should form part of the user facility, sharing support with the neutron instruments. At other facilities such as ISIS we find there is a large overlap both in the user communities and the technical support.

IV. PARTICLE PHYSICS WITH MUONS

Particle physics with muons includes searches for rare decay modes of the muon, precise measurements of its parameters such as its lifetime, its magnetic anomaly and a sensitive search for a permanent electric dipole moment as well as measurements of fundamental constants such as the muon mass, the fine structure constant α_{QED} or the muon magnetic moment. This research is carried out either with free muons, muonium or muonic atoms [1, 2]. It requires dedicated high precision experimental setups to cope with systematic uncertainties and significant beam time to acquire sufficient statistics.

A. Rare muon decays: Charged Lepton Flavor Violation

After the firm establishment of the neutrino mixing by neutrino oscillation experiments and the precise measurements of the quark mixing by B factories, mixing of charged leptons only remains yet unobserved. It is considered that searches for charged lepton mixing, which violates lepton flavor, would be important to obtain some clues of new physics beyond the Standard Model [29]. In the Standard Model (SM), if the neutrino mixing is included, this charged lepton flavor violation (cLFV) could occur in principle through loop diagrams

with neutrino mixing. However, the contribution is suppressed by (m/mW)4, which yields only very small branching ratio probability of the order of $O(10^{-54})$. Therefore, cLFV has a very wide window of searching for new physics beyond the neutrino mixing in the SM. Various theoretical models which predict sizable magnitudes of their branching ratios exist. Among them, most-well-motivated models are supersymmetric (SUSY) extension of the Standard Model, such as SUSY-GUT or SUSY-Seesaw models. For such theoretical models, cLFV would occur through the slepton mixing which arises from renormalization group equation (RGE) from the Planck scale. The predicted branching ratios are just a few orders of magnitude lower than the present experimental limits. Therefore, future experiments would have a robust potential for discovery. Among the charged leptons, the muons is the most promising, because the number of muons available for measurements is large, and will be much larger with the highly intense proton machines which are being constructed and planned.

1. Experimental searches for charged Lepton Flavor Violation

Two typical examples of cLFV processes with muons, namely $\mu^+ \to e^+\gamma$ and $\mu^- N \to eN$, are discussed to elucidate the complexity of this research.

(i) $\mu^+ \to e^+\gamma$ decay

The event signature of $\mu^+ \to e^+ \gamma$ decay at rest is that a positron and a photon are moving back-to-back in coincidence with their energies equal to a half that of the muon mass ($m_\mu/2 = 52.5$ MeV). The present experimental upper limit for $\mu^+ \to e^+ \gamma$ is 1.2×10^{-11}, which was obtained by the MEGA experiment at Los Alamos National Laboratory (LANL) in the US. A new experiment at PSI called MEG, which aims to achieve a single event sensitivity of 2×10^{-13} was built. An improvement factor in a $\mu^+ \to e^+ \gamma$ sensitivity will be expected to utilize a continuous muon beam of 100 % duty factor at PSI. Physics data taking has already started in 2008, obtaining a preliminary result from the 2008 data of BR($\mu \to e\gamma$) $< 2.8 \times 10^{-11}$.

(ii) $\mu^- N \to eN$ conversion in a muonic atom

When negative muons are stopped in matter and captured by atoms, they form muonic atoms and cascade down to their 1s ground state. The muons in the 1s state either

decay in a muonic orbit or are captured by the nucleus by emitting a neutrino (nuclear muon capture). When an electron is emitted instead of a neutrino, the process occurs as μ^- + N(A,Z) → e +N(A,Z) and is called a "$\mu^- e$ conversion". This process is lepton-flavor violating and is a coherent process which enhances the rate by a factor equal to the number of nucleons over the normal nuclear muon capture. The experimental signature of $\mu^- e$ conversion is a single mono-energetic electron whose energy is about the muon mass of about 106 MeV/c^2 with the muonic binding energy subtracted. The previous search for $\mu^- N \to eN$ conversion was performed by the SINDRUM II collaboration at PSI. They set an upper limit of BR($\mu^- + Au \to e + Au$) $< 7 \times 10^{-13}$.

B. Future experimental prospects

Considering its marked importance to physics, it is highly desirable to consider a nextgeneration experiment to search for cLFV with muons. There are three muon cLFV processes to be considered; namely, $\mu^+ \to e^+\gamma$, $\mu \to eee$ decays and $\mu^- N \to eN$ conversion.

Process	Backgrounds	Beam Requirement	Issue
$\mu^+ \to e^+\gamma$	accidentals	continuous beam	detector resolutions
$\mu \to eee$	accidentals	continuous beam	detector resolutions
$\mu^- N \to eN$	beam-associated	pulsed beam	beam qualities
$\mu^+ e^- \to \mu^- e^+$	accidentals	pulsed beam	muonium production

TABLE II. A list of major backgrounds, beam requirement and issues for various charged Lepton Flavor Violation processes with muons.

The three muon LFV processes have different experimental issues that need to be solved to realize improved experimental sensitivities. They are summarized in Table II. The processes of $\mu^+ \to e^+\gamma$ and $\mu \to eee$ decays are limited by accidental backgrounds. If the incident muon beam rate is increased by a factor N, background suppression has to be improved by a factor of N^2. To achieve this, the detector resolutions have to be significantly improved, which is in general very challenging. In particular, improving the photon energy resolution for $\mu^+ \to e^+\gamma$ is difficult. On the other hand, for $\mu^- N \to eN$ conversion, there are no accidental background events, and thus an experiment with higher rates can be performed.

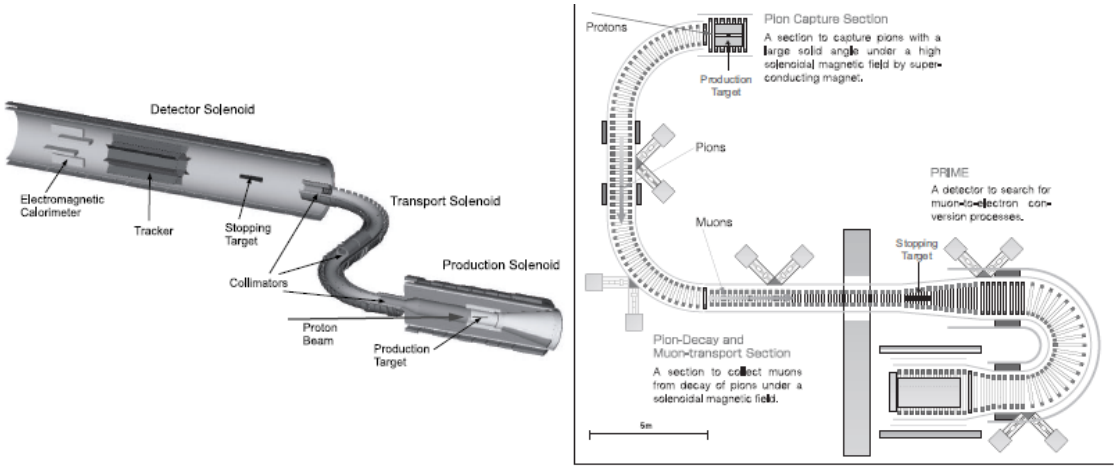

FIG. 5. Schematic layout of the Mu2e experiment at FNAL (left) and the COMET experiment at J-PARC (right).

If a new muon source with a higher beam intensity and a better beam quality for suppressing beam-associated background events can be constructed, measurements of higher sensitivity can be performed.

Furthermore, it is known that there are more physics processes contributing to $\mu^- N \to eN$ conversion and a $\mu \to eee$ decay than a $\mu^+ \to e^+\gamma$ decay. Namely, the dipole interaction of photon-mediation can contribute to all the three processes, but the box diagrams and four-fermion contact interaction can contribute to only $\mu^- N \to eN$ conversion and $\mu \to eee$ decay. In summary, in consideration of the experimental and theoretical aspects, a search for $\mu^- N \to eN$ conversion would be a natural next choice to accomplish significant improvements in future. There are two proposed experiments of searching for $\mu^- N \to eN$ conversion in a muonic atom at sensitivity of better than 10^{-16}. One in the US is the Mu2e experiment [30], and the other in Japan is the COMET experiment [31] (see Fig. 5).

1. PRISM

Future $\mu^- e$ conversion experiments in the ESS era need a dedicated muon beam which meets specific beamrequirements:

(i) High beam intensity

To achieve a high sensitivity, a highly intense muon beam of more than 10^{12} muons/s

is needed. It can be achieved with high-field pion capture by superconducting magnets surrounding the proton target.

(ii) Proton beam pulsing

To reduce beam-related prompt backgrounds, a proton beam should be pulsed and detection should be performed during the beam pulses.

(iii) High purity

To eliminate pions which is one of the critical background, a long muon beam line where pions decay out is needed. One method of having more than 100 meter flight length is to use a muon storage ring.

(iv) Narrow Energy Spread

To eliminate electrons from muon decays in orbit, good energy resolution of electron detection is critically important. To achieve this, a thin muon stopping target and a muon beam of narrow energy spread are needed.

PRISM is a proposed highly intense muon source dedicated to a e conversion experiment [30]. The schematic layout of PRISM is shown in Fig. 6. PRISM stands for "Phase Rotated Intense Slow Muon source". The muon intensity aimed is more than about 10^{12} muons/sec with multi MW proton beam power which would be available such as at ESS. The central momentum is about 68 MeV/c. Narrow energy spread of < 3 % is achieved by a phase rotation method which is a technique to accelerate slow muons and decelerate fast muons by high rf fields. Phase rotation is performed in a muon storage ring to save a number of rf cavities. As another benefit, pions in a beam are stored in the ring and decay away. Their expected survival rate is less than 10^{20}. As a muon storage ring, a fixed field alternating gradient (FFAG) synchrotron ring is chosen, which is called the PRISM-FFAG ring. With the use of a muon beam from PRISM, a search for μe conversion with a single event sensitivity of 3×10^{-19} can be performed.

2. Requirements for proton beams

The requirements for a proton beam to carry out the PRISM/PRIME experiment are: (a) The proton beam should have a narrow beam pulse whose width is about 10 ns in FWHM

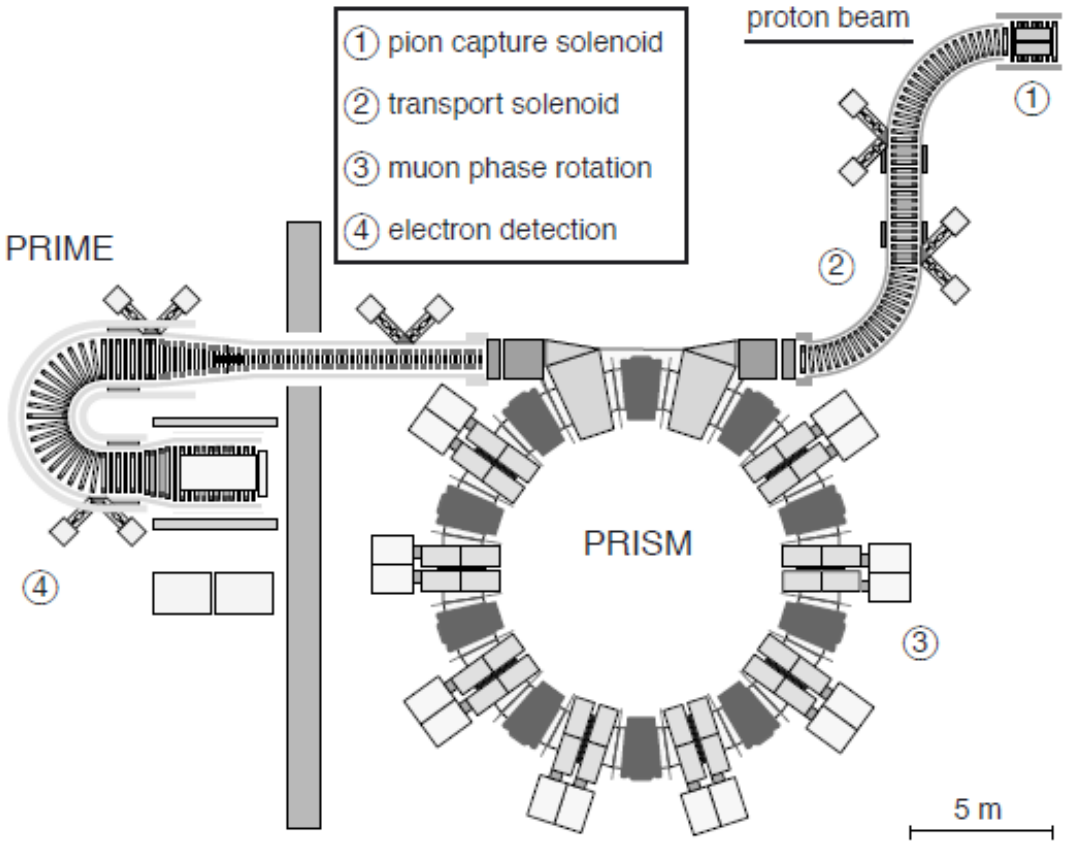

FIG. 6. Schematic layout of the PRISM/PRIME detector.

for phase rotation. (b) The repetition of pulsed proton beams should be about 100 Hz to 1000 Hz, which corresponds to that of the kicker magnets to inject and extract a muon beam from the PRISM FFAG. Multi MW proton beam power at the ESS would provide a great opportunity to carry out this kind of the PRISM/PRIME experiment. And in the case of the ESS, an additional buncher ring to manipulate a beam time structure might be necessary to handle such a proton time structure. Hopefully, the second target station might be necessary.

3. Conclusions for rare decays

Muon particle physics has attracted much attention in science. Various particle physics topics need different requirements on a proton beam, in particular time structure and beam energy, as shown in Table III. In particular, the search for cLFV with muons has large potential to obtain hints for new physics beyond the Standard Model. The physics of cLFV

has received glowing

	Time Structure	Width	Beam Energy
$\mu^+ \to e^+\gamma$	CW		2.5 GeV
$\mu \to eee$	CW		2.5 GeV
$\mu^- N \to eN$ (PRISM)	pulsed (1kHz)	10 ns	2.5 GeV
$\mu^+ e^- \to \mu^- e^+$	pulsed (100kHz)		2.5 GeV
muon g-2	pulsed ($<$ 1kHz)	100 ns	10 - 25 GeV
Muon g-2 (cold)	pulsed (100kHz)	10 ns	2.5 GeV
Muon edm	pulsed (1Hz)		2.5 GeV

TABLE III. Proton beam requirements on time structure and energy for various muon particle physics topics.

attention from both theorists and experimentalists. Ultimate searches for $\mu^- N \to eN$ conversion at a single event sensitivity of 3×10^{-19} can be considered at ESS. Here, high intensity proton accelerator would play a crucial role, since these searches would not be achieved without high intensity proton accelerators of multi MW beam power, such as the ESS. These attempts would offer extraordinary opportunities for exploring new phenomena which would otherwise be directly inaccessible at future high energy colliders.

C. Precision Measurements of Fundamental Constants

Precision experiments have been carried out at almost all places where muons, in particular surface muons were available. The experiments which could be carried out to date are all statistics limited and all could be improved at a facility delivering significantly more muons than presently available.

1. Possible experiments

(i) Muon magnetic anomaly.

The deviation of the magnetic g-factor of the muon from the Dirac value 2 is known as the muon magnetic anomaly. It has been measured in 4 consecutive experiments,

3 at CERN and the latest one [33] at the Brookhaven National Laboratory (BNL). The latest experiment took place in a 14 m diameter dedicated magnetic storage ring with very homogeneous field. Muons at 3.1 GeV/c^2 momentum were used. The final experimental result has an accuracy of 0.5 ppm and differs at present from the Standard Model theory value by 3.2 standard deviations [34]. Whether this is an indication of new physics, a statistical fluctuation or an error in theory or experiment remains to be seen. Therefore a new experiment using the refurbished BNL is being started at FERMILAB at present. A novel idea uses cold muons from 15 a laser source and a small magnet [27]. Such an approach promises systematic uncertainties which are significantly different from the FERMILAB straightforward approach. The low energy experiment could be accommodated also at ESS provided a surface muon beam of high intensity would be provided as an input to the muonium photo-ionization source.

(ii) Muon permanent electric dipole moment

A permanent electric dipole moment (edm) of a fundamental particle violates both parity and time reversal symmetry. With CPT as unbroken symmetry it also violates the CP symmetry. Therefore known sources of CP-violation such as which give rise to CP violating effects in, e.g. kaons and B-mesons, induce tiny edms for fundamental particles. They are several orders of magnitude below present experimental limits. On the other hand, several speculative models beyond the Standard Model, such as supersymmetry, predict edms just below established limits. For the muon this could be within the reach of an experiment which could be carried out at ESS using polarized muons stored in a small magnetic storage ring using a novel idea which enables searches for edms in free charged particles [35, 36]: A charged particle circling in a magnetic storage experiences in its rest frame a radial motional electric field. This can be orders of magnitude beyond what is technically possible between electrodes in a laboratory [37]. Owing to this motional field the muon spin would precess out of the plane of orbit, which could be detected by time evolution of the count rate ratio of electron counters on both sides of the orbital plane. The experiment would require either very short pulses or one muon at a time and significant running to acquire sufficient statistics. One year of running in a parasitic mode to the main ESS activities could reach the sensitivity to confirm or reject the models with the highest predicted

edm values.

(iii) Muon lifetime

The best determination of the Fermi coupling constant in weak interaction comes from a precise measurement of the muon mass and its lifetime. A measurement the muon lifetime with unprecedented accuracy has been very recently reported from PSI. The experiment exploited single positive muons stopped in a sold target and recorded their decay positrons. A precision of 1 ppm was reached [38].

(iv) Muonium spectroscopy

Muonium atoms ($\mu^+ + e^-$) for recent atomic spectroscopy experiments have been produced either with close to 100 % efficiency by stopping μ^+ in Kr gas or with a few % efficiency from a SiO_2 powder converter in vacuum. Zeeman transitions between magnetic sublevels of the ground state could be measured with microwave spectroscopy at 1.7 T field [39], from which the magnetic moment and the zero field hyperfine splitting could be extracted. The latter gave the best value for α_{QED} was extracted for a bound state. For muonium atoms in vacuum the 1S-2S energy difference could be determined with precision laser two-photon spectroscopy [40], from which the charge quantization for muons end electrons was confirmed. With α_{QED} from a single trapped electron and relying on the correctness of QED calculations for the HFS splitting one can alternatively extract the best value for the muon mass. Such spectroscopy experiments could be significantly improved at ESS provided pulsed beams of typically 1 μs pulse width and interpulse distances of > 20 μs could be provided.

2. Conclusions for precision experiments

Since all precision experiments are presently statistics limited, a muon source of high flux would offer unique possibilities for improvement of most important parameters. To first order a total of typically 10^{15} muons delivered in suited pulses would make new experiments worthwhile provided there is a strong commitment by ESS concerning the availability of suited beams and by the experimental teams concerning setting up dedicated state of the art equipment without systematic limitations.

D. Radioactive Muonic Atoms

ESS can deliver both ample amounts of muons and at the same time short lived radioactive atoms at the same site. This would enable, e.g., muonic x-ray spectroscopy in order to determine nuclear properties of rare and short lived nuclei. Initial research towards this goal has been successfully started at the RIKEN-RAL facility of ISIS by combining muons and trace alkaline-earth and rare-earth isotopes implanted in solid D2 [41]. Whereas at that facility one is limited to stable or long lived radioactive species, ESS could open the field for short lived isotopes due to the availability of both crucial ingredients, the muons and the radioactive nuclei, on one site. For such research the short-pulse version of ESS would be essential to fully exploit the potential of a multi-MW proton driver beam [3].

V. MUONS AT ESS – AN ENRICHMENT FOR SCIENCE

Muon physics could significantly be boosted at ESS with new muon secondary beams derived from the main proton driver beam of the spallation source. The options include a thin target in the primary proton beam line. Here the muons are produced parasitically and have the time structure of the neutron source. Alternative options are to kick a fraction of the beam onto a dedicated target. Here the time structure can be modified depending on the kicker time shape. Muons at ESS would significantly enrich the spectrum of material research possibilities at one location. This would be in the tradition of materials research where typically several suited methods are employed to investigate condensed matter phenomena. Particular for condensed matter muon science novel methods would be enabled which could significantly widen the possibilities. Muons at high rates from a multi-MW proton driver at ESS could open new dimensions for particle physics, both for searches for rare decays and for the determination of fundamental constants. To carry out these physics programs, additional investment, such as a buncher ring and the second target station, might be needed. However, the physics motivation of muon particle physics programs that can be performed at ESS are very competitive to the LHC, and have a high discovery potential for new physics of Nobel-prize winning quality. It will depend on the dedication of the ESS facility and the respective user communities whether the exciting possibilities in muon physics will be

[3] This subject is covered in more detail in the Nuclear Physics article of this volume.

realized. It would be a pity if such great opportunities at the ESS were missed.

---

[1] A. Bandyopadhyay et al., Rep. Prog. Phys. **72** (2009) 106201

[2] J. Äystö et al., hep-ph/0109217

[3] C. Amsler et al. (Particle Data Group), Phys. Lett. **B667** (2008) 1

[4] K. Nagamine, Introductory Muon Science, Cambridge Univ. Press (2003)

[5] H. Miyadera, A. Jason and K. Nagamine, contribution to Particle Accelerator Conference (Albuquerque, 2007)

[6] E. Morenzoni et al., Phys. Rev. Lett. **72** (1994) 2793

[7] K. Nagamine et al., Phys. Rev. Lett. **74** (1995) 4811; P. Bakule et al, Nucl. Instr. and Meth. B **266** (2008) 335

[8] T. Matsuzaki et al,, Nuclear Instruments A **465** (2001) 365

[9] Y. Miyake et al., Physica **B404** (2009) 957

[10] K. Nagamine, et al., Nucl.Instr. Meas. A **356** (1995) 585

[11] R.H. Heffner and K. Nagamine eds. Special Issue on μSR: muon spin rotation, relaxation or resonance, Journal of Physics: Condensed Matter **16** (2004), S4403

[12] S.F.J. Cox, J Phys C: Solid State Phys. **20** (1987) 3187

[13] S.J. Blundell, Contemporary Physics **40** (1999) 175

[14] S.P. Cottrell, S.F.J. Cox, J.S. Lord and C.A. Scott, Appl. Magn. Reson. **15** (1998) 469

[15] A.D. Hillier, S.P. Cottrell, P.J.C. King, G.H. Eaton and M.A. Clarke-Gayther, Physica B **326** (2003) 275

[16] K. Nagamine, et al., Proc. Japanese. Academy., Ser. B **83** (2007) 120

[17] K. Nagamine and E. Torikai, J. Phys. Condensed Matter **16** (2004) S4797

[18] A. Schenck, Muon Spin Rotation Spectroscopy: Principles and Applications in Solid StatePhysics, Adam Hilger, Bristol, 1985

[19] S. J. Blundell, Contemporary Physics **40** (1999) 175

[20] P. Bakule, E. Morenzoni, Contemporary Physics **45** (2004) 203

[21] T. Prokscha et al., Nucl. Instr. Meth. A **595** (2008) 317

[22] E. Morenzoni, Physica B **404** (2009) 577 and references therein

[23] T.J. Jackson et al., Phys. Rev. Lett. **84** (2000) 4958

[24] A.J. Drew et al., Nature Materials **8** (2009) 109

[25] K. Nagamine, "Muon Catalyzed Fusion", Chapter 11 of Landolt-Brnstein New Series, EnergyTechnologie, ed. K. Heinloth, (2005) Springer-Verlag, 555

[26] K. Nagamine, Hyperfine Interactions **8** (1981) 787

[27] N. Saito et al. Letter of Intent to J-PARC (2010)

[28] K. Yokoyama et al., Physica B **404** (2009) 856

[29] Y. Kuno and Y. Okada, Rev. Mod. Phys. **73**, 151 (2001); see also M. Raidal et al., Europ. Phys. Jour. C **57** (2008) 13

[30] R.M. Carry et al. (Mu2e collaboration), Proposal to Search for $\mu^- N \to eN$ with a Single Event Sensitivity Below 1016, FNAL proposal (2008).

[31] Y. Kuno et al. (COMET collaboration), J-PARC 50 GeV Proton Synchrotron Proposal P21 "A Experimental Search for Lepton Flavor Violating $\mu^- N \to eN$ Conversion at a sensitivity of 1016 with A Slow-Extracted Bunched Proton Beam", unpublished, 2007. See `http://j-parc.jp/NuclPart/pac 0801/pdf/Kuno.pdf`

[32] Y. Kuno et al. (PRISM collaboration), J-PARC 50 GeV Proton Synchrotron LOI P20 "An Experimental Search for a $\mu N \to eN$ Conversion at Sensitivity of the Order of 10^{-18} with a Highly Intense Muon Source: PRISM", unpublished, 2006. See `http://jparc.jp/NuclPart/pac0606/pdf/p20-Kuno.pdf`

[33] G.W. Bennett, et al., (Muon (g 2) Collaboration), Phys. Rev. D **73**, (2006) 072003

[34] M. Davier, et al., Eur. Phys. J. C **66** (2010) 127136

[35] F.J.M. Farley et al., Phys. Rev. Lett. **93** (2004) 052001

[36] G.W. Bennett et al. (Muon (g-2) Collaboration), Phys. Rev. D **80** (2009) 052008

[37] A. Adelmann et al., arXiv:hep-ex/0606034

[38] D.B. Chitwood et al., Phys. Rev. Lett. **99** (2007) 032001; D.W. Hertzog priv. com.

[39] W. Liu et al, Phys. Rev. Lett. **82** (1999) 711

[40] V. Meyer et al.,Phys.Rev.Lett. **84** (2000) 1136

[41] P. Strasser et al., Hyp. Interact. **193** (2009) 121

Medical Opportunities at ESS

U. Köster[1] and K.J. Peach[2]

[1]*Institut Laue-Langevin, BP 156, 6, rue Jules Horowitz, 38042 Grenoble Cedex 9, France*

[2]*Particle Therapy Cancer Research Institute* [a]*, University of Oxford,*

Denys Wilkinson building, Keble Road, Oxford, OX1 3RH, UK

Medical applications of neutrons are reviewed. These include radionuclide production for medical diagnosis, imaging and internal radioisotope therapy, and the use of neutrons to treat certain forms of cancer, either directly as a form of high Linear Energy Transfer (LET) radiation or indirectly through Boron Neutron Capture Therapy (BNCT). Opportunities to implement such applications at the upcoming European Spallation Source (ESS) are discussed.

I. INTRODUCTION

80 years after the discovery of the neutron, neutrons have today important applications in a great variety of disciplines, there-under also medical applications. Neutrons can be employed in different ways for medicine and health "technology":

- Direct use of fast neutron beams for external radiotherapy. This form of hadron therapy can be considered as alternative to usual radiation therapy with X-ray[1] or gamma ray sources.
- Use of thermal or epithermal neutron beams for neutron capture therapy, a binary treatment combining features of external and internal radiation therapy.
- Use of neutrons for production of radioisotopes that are in turn employed for diagnostics and therapy in nuclear medicine.
- Use of neutron scattering or neutron radiography techniques to address questions relevant for medical applications.

[a] Part of the James Martin 21st Century School

[1] In the medical field the designation "X-ray" covers also MeV photons produced via Bremsstrahlung of MeV electrons. Most external beam radiotherapy is today performed with such MeV photons.

The first two points are discussed in section III. The last subject is vast, ranging from protein crystallography to strain analysis of hip joints, and goes beyond the scope of the present article. These aspects will not be addressed here, but an overview can be found in [1]. In section II we will discuss current production and use of radioisotopes for nuclear medicine applications in high-flux reactors and possible synergies of future radioisotope production with the accelerators and targets used in spallation neutron sources, and in particular at the European Spallation Source ESS.

II. RADIONUCLIDE PRODUCTION

Various radioisotopes differ by their properties, such as half-life, decay radiation and (bio-) chemical behaviour. The properties and applications of some important examples will be discussed in the following. We distinguish between "established" isotopes that are commercially available in good and certified quality and usually in any required quantity. A second class are "emerging" isotopes that often have superior nuclear properties for certain applications, but that are not yet available in the same quantity and/or quality as the "established" ones. Finally there are "R&D isotopes" which have some very promising properties but which are yet very scarcely used, often because they are just not available in the required quantity and/or quality. Some of these R&D isotopes could also be produced at spallation neutron sources, laying the base for wide-spread applications in nuclear medicine.

The radioisotopes for diagnostic or therapeutic nuclear medicine applications are usually produced by nuclear reactions. The required projectiles are typically either neutrons (from high flux reactors) or charged particles (from small or medium-sized cyclotrons or other accelerators). At present the total number of applications in nuclear medicine is dominated by far by reactor-produced isotopes over accelerator-produced isotopes.

A. Diagnostics

Diagnostic procedures in nuclear medicine are based on radiotracers emitting gamma rays or positrons. The in-vivo distribution of the radiotracer is imaged in 2D or 3D, either by detection of single gamma rays in a gamma camera or SPECT (single photon emission computer tomography) or the coincident detection of two 511 keV gamma rays after positron

annihilation in PET (positron emission tomography). Moreover radioisotopes are used as tracers in biochemical research, e.g. in-vitro.

1. $^{99}Mo/^{99m}Tc$:

The presently most important radioisotope for nuclear medicine studies is ^{99m}Tc. Its 140 keV γ-ray is ideal for SPECT imaging. With a relatively short half-life of 6 h and the quasi-absence of beta particles the radiation dose to the patient is low. ^{99m}Tc is conveniently eluted in "non-carrier-added" quality (i.e. with very high specific activity) from simple and reliable ^{99}Mo ($T_{1/2}$ = 66 h) generators that can be used for about one week. Various technetium compounds have been developed for a multitude of nuclear medicine applications. The combination of these advantages explains why ^{99m}Tc is used in about 80% of all nuclear medicine studies. 28 million applications employing ^{99m}Tc are performed per year. Every week about 3000 TBq (80 kCi) of ^{99}Mo have to be produced to load the ^{99}Mo/^{99m}Tc generators that are shipped to the users (mainly hospitals or radiopharmacies). At present the world supply of ^{99}Mo is entirely produced with neutron induced reactions in irradiation reactors. Two different reactions may serve this purpose, namely fission or neutron capture.

The fission cross-section of ^{235}U for thermal neutrons is 586 barn. In 6.1% of all fission events mass 99 isobars are emitted that decay rapidly to ^{99}Mo. Hence, the partial cross section for producing ^{99}Mo from ^{235}U irradiation is 36 barn. Also other, stable, molybdenum isotopes (95, 97, 98,^{100}Mo) are produced in fission. When irradiating a ^{235}U target for 7 days and letting short-lived isotopes decay for one day, then 11% of the remaining fission-produced molybdenum nuclei are ^{99}Mo and no radioactive Mo isotopes other than ^{99}Mo are present. The uranium target is dissolved and a series of chemical separations are performed to extract the Mo fraction. The resulting so-called "fission-moly" with high specific activity is adsorbed on an acid alumina column that serves as chromatographic generator for elution of ^{99m}Tc with saline solution.

Alternatively to fission, ^{99}Mo can also be produced by neutron capture on ^{98}Mo. However, the thermal neutron capture cross section is particularly low for ^{98}Mo, only 0.13 barn. Hence, even after long irradiation of highly enriched ^{98}Mo targets, the ratio of ^{99}Mo to stable Mo will only reach $4{\cdot}10^{-6}$ in a thermal neutron flux of $1{\cdot}10^{14}$ n/(cm^2 s), for natural Mo targets only $1{\cdot}10^{-6}$. The so produced ^{99}Mo has low specific activity and more complex generator

types are needed to handle the large amount of stable molybdenum without affecting the quality of the final product ^{99m}Tc.

Irradiation in still higher neutron flux densities (10^{15} n/(cm^2 s)) or in epithermal neutron spectra produces higher specific activities, but only a limited number of such irradiation positions are available world-wide. Neutron capture is therefore only used for local or regional production of ^{99}Mo while the far dominant quantity is provided by neutron-induced fission of (highly enriched) ^{235}U targets. In the last decades five nuclear reactors (NRU Chalk River, Canada; HFR Petten, The Netherlands; BR2 Mol, Belgium; OSIRIS Saclay, France and SAFARI Pelindaba, South Africa) used to supply about 95% of the world needs of ^{99}Mo.

Recently extended shutdowns of the two major suppliers (NRU and HFR) that previously used to cover over two thirds of the world supply have lead to a serious ^{99}Mo/^{99m}Tc supply crisis [2, 3]. This has triggered many discussions and initiatives on alternative ^{99}Mo production in existing and future facilities. A straightforward solution is the backfitting of existing reactors with irradiation positions for ^{235}U targets. A neutron flux of few 10^{14} n/(cm^2 s) is best suited for fission production of ^{99}Mo from ^{235}U targets. Such irradiation positions are in principle available at many research reactors. However, irradiation of massive fission targets requires a dedicated forced cooling system. Moreover, handling of (highly enriched) ^{235}U targets requires special licensing and monitoring. It is obviously most natural to implement such production at reactors that are already running with fuel elements of this type and that are perfectly equipped with sensitive instrumentation, e.g. to detect any traces of released fission products. Therefore it makes no sense to use for this purpose the neutron flux of a spallation neutron source that has usually no fissile materials on site.

In addition to the traditional "fission-moly" producers in Europe (HFR, BR2 and OSIRIS), recently the MARIA reactor in Świerk-Otwock, Poland and the LVR-15 reactor in Řež, Czech Republic, demonstrated a small-scale production of ^{99}Mo. A dedicated irradiation position is being installed in the FRM2 in Garching, Bavaria and expected to start large-scale production in 2014 [4]. Also the new RJH in Cadarache, France will be equipped with positions for large-scale fission-moly production to replace after 2015 the production at OSIRIS.

Initially processing of the irradiated targets will be performed in the existing radiochemical facilities (Covidien Petten, The Netherlands and IRE Fleurus, Belgium). However,

^{99}Mo/^{99m}Tc represent only 17% of the total activity and 5% of the gamma dose rate of an irradiated fission target (after 7 days of irradiation and 1 day of decay). Therefore in the longer run a local processing of the irradiated targets (in Garching and Cadarache respectively) would make sense since it avoids regular long-distance shipping of active targets in heavy containers. This change would also present an opportunity to convert the process from highly enriched uranium (HEU) targets to low enriched uranium (LEU) targets to address non-proliferation issues.

The combination of additional production at FRM2 and RJH with continuing production at HFR (eventually replaced by the planned PALLAS reactor) and BR2 (eventually replaced by the planned MYRRHA accelerator-driven subcritical system) plus possible smaller suppliers will assure a secure long-term supply of ^{99}Mo/^{99m}Tc in Europe.

High-flux reactors on different continents (SAFARI, OPAL in Australia, RA-3 in Argentina, etc.) provide a national or regional supply of ^{99}Mo and can contribute small amounts to the world market.

The situation is dramatically different in North America. The US consume about half of the world needs of ^{99}Mo but did not produce any ^{99}Mo since two decades. Instead they used to import "cheap" ^{99}Mo from Canada and Europe[2] [5]. A sustainable solution for North America has still to be found and important investments into new production facilities are needed.

2. Other imaging isotopes

^{99m}Tc is quite unique as a neutron-rich isotope for diagnostics. Generally neutron-rich isotopes will emit in their decay also betas which would cause an unnecessarily high dose to the patient. Therefore they are less used for diagnostic purposes. An exception is ^{133}Xe that has a very short biological half-life (rapidly exhaled) and can therefore be used for lung imaging. Also ^{133}Xe is produced by neutron induced fission of ^{235}U.

Neutron-deficient isotopes decay either by positron emission, which can be used for PET imaging, or by electron capture. When the latter is accompanied by emission of gamma

[2] One cannot help but think of the world market of hydrocarbon fuels: if a finite resource is traded over longer time at prices that do not take into account all indirect costs (depreciation and replacement costs of the irradiation reactors in the case of ^{99}Mo and environmental costs related to hydrocarbon fuel exploitation respectively) eventually leads to a situation that is not sustainable!

rays or X-rays of suitable energy it can serve for SPECT imaging. The majority of neutron-deficient isotopes used in nuclear medicine is produced in charged particle induced reactions (mainly (p,n)) at dedicated compact cyclotrons. More than 600 such cyclotrons exist world-wide. They are often based at hospitals or close-by, assuring a decentralized supply of these imaging isotopes (^{18}F, ^{11}C, ^{13}N, ^{15}O, etc.).

Certain radioisotopes however are produced in (p,xn) reactions at higher energies that cannot be supplied by low-energy cyclotrons.

^{82}Sr/^{82}Rb

The short-lived 75 s ^{82}Rb beta+ emitter is continuously eluted from ^{82}Sr/^{82}Rb generators and used for PET imaging of heart and brain with low radiation dose to the patient. It can replace myocardial SPECT imaging with ^{99m}Tc [6]. The trend to more PET imaging and the present ^{99}Mo/^{99m}Tc supply crisis lead to an increased demand for ^{82}Sr/^{82}Rb generators. Usually ^{82}Sr ($T_{1/2}$=25 d) is produced in ^{85}Rb(p,4n)^{82}Sr reactions, but only few accelerators exist world-wide that provide sufficiently intense beams of energetic protons ($>$ 60 MeV) for this purpose.

^{68}Ge/^{68}Ga

Downstream of ^{82}Sr production targets the protons are still sufficiently energetic to produce ^{68}Ge in ^{69}Ga(p,2n) reactions. The long-lived ($T_{1/2}$=270 d) isotope ^{68}Ge is loaded onto generators from which the 68 min PET isotope ^{68}Ga is conveniently eluted [7]. As trivalent element gallium behaves often similarly to other trivalent elements used for therapy (see below).

^{44}Sc

Another trivalent isotope for PET imaging is ^{44}Sc. In the decay of ^{44}Sc also gamma rays of 1157 keV energy are emitted in coincidence with the positrons. A suitable detection system could use the triple coincidences between two 511 keV annihilation gammas and the 1157 keV gamma for a triangulation, hence improving the position resolution ("point of event" instead of "line of event") [8]. ^{44}Sc can be produced by ^{44}Ca(p,n) reactions but is more conveniently provided from a ^{44}Ti generator. The very long-lived ^{44}Ti ($T_{1/2}$=60 years) is usually produced by long irradiations via ^{45}Sc(p,2n) reactions on rare and costly scandium targets. ^{44}Ti is also produced by spallation of heavier targets, such as Ti, V, Cr, etc. ^{44}Ti could therefore also be produced cheaply and efficiently by machining those mechanical parts of a high energy proton accelerator that are anyhow exposed to high beam

doses (collimators, beam dump, etc.) of a suitable material and foresee a way to (remotely) remove the irradiated parts after sufficient time (years) to extract the ^{44}Ti radiochemically. Such a "parasitic" mode of radioisotope harvesting does not disturb in any way the main users of the facility.

B. Therapy

Endoradiotherapy is based on bringing radioactive emitters inside the human body for localized irradiations, either as brachytherapy or targeted radioisotope therapy.

1. Brachytherapy

In brachytherapy sealed sources of emitters of beta-radiation or low-energy gamma rays are temporarily or permanently introduced to locally irradiate tumours or other tissues. Typically radioisotopes such as ^{32}P, ^{103}Pd, ^{125}I or ^{192}Ir with half-lives of several weeks are used. They are mainly produced by neutron capture in high flux reactors. These radioisotopes are usually bound or enclosed in a solid matrix.

Alternatively the radioisotopes can be used as liquid solution that is injected into a previously positioned balloon then removed after some minutes of irradiation.

Several percent of the European population suffer from stenosis, the constriction of blood vessels. Stenosis is often treated by balloon dilatation (angioplasty), but a restenosis (repeated clogging up) may occur. In coronary arteries it may eventually lead to an infarctus and in extremities (legs) it may lead to a severe damage eventually requiring amputation. Restenosis can be prevented by intravascular brachytherapy where short-term irradiation of the vascular cells prevents their hyperproliferation [9]. An isotope particularly useful for intravascular brachytherapy is ^{188}Re ($T_{1/2}$=17 h). To limit the duration of irradiation during which the blood vessel is blocked by the inflated balloon, the activity and hence the concentration of ^{188}Re in the liquid needs to be quite high. Such ^{188}Re solutions are conveniently eluted from compact ^{188}W/^{188}Re generators requiring ^{188}W ($T_{1/2}$=69 d) with very high specific activity. The tungsten isotope ^{188}W is produced by double-neutron-capture on enriched ^{186}W targets. The neutron flux has to be high if the intermediate ^{187}W, which has a half-life of only 23.7 h, is to have a chance of capturing another neutron to produce

^{188}W instead of decaying. The specific activity of the produced ^{188}W goes therefore with the square of the neutron flux. Only three reactors worldwide provide a thermal neutron flux in excess of 10^{15} n/(cm^2 s) and can produce ^{188}W with very high specific activity (>100 GBq/g): the SM3 reactor in Dimitrovgrad, Russia; HFIR in Oak Ridge, US and the RHF of ILL in Grenoble, France.

All other reactors have significantly lower neutron fluxes (and/or length of the reactor cycle respectively) and cannot reach the required specific activity. Even the future European spallation source ESS with a nominal neutron flux of $3.1{\cdot}10^{14}$ n./(cm^2 s) [10] would not be competitive if no special measures are taken to locally enhance the flux ("flux trap").

2. Targeted radioisotope therapy

Over 40% of all cancers are detected when they are already metastasized. The chances for a cure are much lower since the usual methods for local tumour control (surgery, external radiotherapy or brachytherapy) cannot eliminate all metastases. Instead a systemic treatment is required for non-localized cancers, i.e. when already multiple metastases have been created, and for cancer types that are intrinsically non-local, e.g. leukemia. The usual systemic treatment is chemotherapy using cytotoxic substances. Specificity is usually limited and severe side effects occur. Alternatively targeted systemic therapies can be employed. Usually a bioconjugate is used that shows a high affinity and selectivity to bind to peptide receptors or antigens that are overexpressed on certain cancer cells with respect to normal cells. Ideally this bioconjugate should not only be capable of finding the cancer cells but should also destroy them or at least hinder their multiplication. However, this job profile "find the bad guy and eliminate him" is so challenging that only few such "special agents" have been found yet for specific applications.

Using instead a bioconjugate that is "only" capable of finding cancer cells without necessarily showing own cytotoxicity and combining this bioconjugate with a suitable radioisotope such as a (low-energy) electron or alpha emitter, allows irradiating and destroying selectively the cancer cells. Depending on the nature of the bioconjugate, these therapies are called Peptide Receptor Radio Therapy (PRRT) when peptides are used as bioconjugates [11] or radioimmunotherapy (RIT), when antibodies are used as bioconjugates [12]. Bioconjugates could also be antibody-fragments, nanoparticles, microparticles, etc.

For cancer cells having only a limited number of selective binding sites, an increase of the concentration of the bioconjugates may lead to blocking of these sites and, hence, to a reduction in selectivity. Therefore the radioisotopes for labeling of the bioconjugates should often have a high specific activity to minimize injection of bioconjugates labeled with stable isotopes that do not show radiotherapeutic efficiency.

Other radioisotope therapies make use of selective metabolic uptake and enrichment. Here the specific activity is less decisive.

^{131}I is still the most commonly used isotope for radioisotope therapy, see Figure 1: in form as iodide for treatment of certain thyroid problems exploiting the natural iodine metabolism in thyroid cells, as MIBG (meta-iodobenzylguanidine) for treatment of glioblastoma (again preferential metabolic uptake) or coupled to an antibody for treatment of lymphoma (e.g. Bexxar). Like ^{99}Mo also ^{131}I ($T_{1/2}$= 8 days). is mainly produced by thermal neutron-induced fission of (highly enriched) ^{235}U targets.

Unfortunately the beta decay of ^{131}I is accompanied by emission of higher-energy gamma rays that leads to increased whole-body radiation burden for the patient and to radiation protection issues for the hospital personal and the patient's relatives. Therefore often an isolation of the patient is required. For applications where the biochemical properties of iodine are not essential, i.e. when bound to a bioconjugate, other radioisotopes are preferred.

Various methods exist to couple efficiently most trivalent elements with bioconjugates such as peptides or antibodies. One trivalent therapy isotope is the pure beta emitter ^{90}Y ($T_{1/2}$= 2.7 days). ^{90}Y is presently used for RIT (e.g. Zevalin) on lymphoma and PRRT on inoperable neuroendocrine tumours (i.e. cancerous hormone-producing cellstumour). Compared to traditional treatment (chemotherapy) the results indicate higher remission rates for the patients (disappearance of the tumour), improved survival rates and quality-of-life, and fewer side effects. Also ^{90}Y is produced as fission product, but not in dedicated irradiations. It is "milked" from ^{90}Sr/^{90}Y generators where the long-lived ^{90}Sr can be extracted in the waste processing of power reactors.

Recent preclinical and clinical studies with PRRT showed that for small and medium-sized metastases even better results can be obtained when replacing ^{90}Y with ^{177}Lu; for larger metastases a combination of ^{177}Lu and ^{90}Y is indicated [13]. ^{177}Lu can be produced easily by irradiating ^{176}Lu targets. However, ^{177}Lu with higher quality (higher specific activity and absence of contamination with long-lived $^{177\mathrm{m}}$Lu [14]) is obtained in an indirect way where

^{176}Yb targets are irradiated. ^{177}Yb is formed upon neutron capture and decays rapidly to ^{177}Lu, but not to ^{177m}Lu. Lutetium is then chemically separated from the ytterbium target, providing ^{177}Lu of "non-carrier-added" quality. The only drawback of the indirect method using a ^{176}Yb target is the much smaller cross-section (2.4 barn versus 2100 barn); this means that a high neutron flux is required to produce significant ^{177}Lu activity from the highly enriched ^{176}Yb material. Due to the chemical separation, the quality (specific activity) of the final product does not depend much on the neutron flux at the irradiation position. However, highly enriched ^{176}Yb targets are very costly and an economically viable production of ^{177}Lu requires neutron fluxes of several 10^{14} n/(cm^2 s).

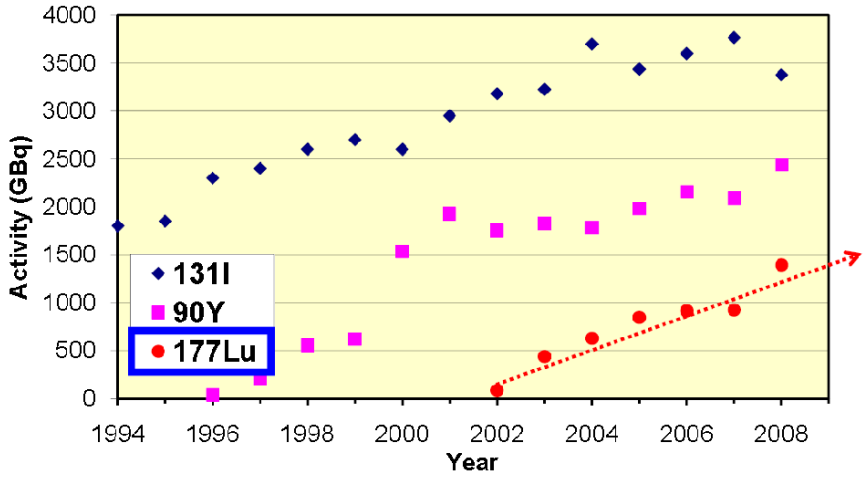

FIG. 1. Annual use of radioisotopes for systemic radiotherapy in Switzerland[a]. The overall use of radioisotopes is rising, but the use of "emerging" isotopes like ^{177}Lu is rising disproportionately.

[a] Switzerland is shown as example since detailed national statistics on the use of radioisotopes are available. Moreover, the nuclear medicine group of the University Hospital Basel is among the groups driving the development of PRRT and RIT in Europe. Hence with some delay a similar development can be expected for other European countries.

The tumour uptake of bioconjugates varies considerably from one patient to another. This leads to an important variation in dose delivered to the tumour if the same activity (or activity per body mass or activity per body surface) was administered. Ideally a personalized dosimetry should be performed by first injecting a small quantity of the bioconjugate in question, marked by an imaging isotope (preferentially β^+ emitter for PET). Thus the tumour uptake can be quantitatively determined and the injected activity of the

therapy isotope can be adapted accordingly. To assure representative in-vivo behaviour of the imaging agent the PET tracer should be ideally an isotope of the same element as the therapy isotope, or, at least of a chemically very similar element such as neighbouring lanthanides. Thus so-called "matched pairs" of diagnostic and therapy isotopes of the same element are of particular interest. An example is ^{44}Sc (see above) and ^{47}Sc. The latter has 3.4 days half-life and short-range beta emission. ^{47}Sc has excellent properties for therapy, but its large-scale production is not straightforward. It can be produced by ^{47}Ti(n,p) reactions with fast neutrons (few MeV) but high flux densities are required for an efficient production [15].

The previously mentioned advantage of ^{177}Lu over ^{90}Y is due to its shorter-range beta radiation. If new bioconjugates are found that are more and more selective and can find individual cancer cells, then they should be combined with therapy isotopes having even shorter-range radiation to maximize damage to the cancer cell and minimize collateral damage. Decay alphas have typically some ten micrometer range, commensurate with the diameter of a single cancer cell. Moreover, their energy is deposited with high LET leading to enhanced probability for double strand breaks, see below. Unfortunately there exist only few alpha emitters with properties suitable for therapy applications. A very promising isotope is ^{149}Tb. It has 4.1 hours half-life and 17% of its decays proceed via emission of an alpha particle with 25 μm range, i.e. just a typical diameter of a cancer cell. As a lanthanide element it can be coupled to most bioconjugates with the established techniques known from ^{177}Lu or ^{90}Y. A pre-clinical trial with ^{149}Tb coupled to the monoclonal antibody rituximab showed impressive results in curing lymphoma [16]. In addition to alphas, ^{149}Tb has also a branch of beta+ emission. Thus the tumour uptake can be monitored by PET imaging. Alternatively the longer-lived isotope ^{152}Tb ($T_{1/2}$=17.5 h) can be used for PET imaging prior to treatment [17]. ^{155}Tb ($T_{1/2}$ = 5.3 days) can be used for SPECT imaging. Terbium is a unique element providing four isotopes with favorable properties for nuclear medicine applications. The forth isotope, ^{161}Tb, is a therapy isotope with properties similar to ^{177}Lu, but in addition a strong emission of low energy Auger and conversion electrons. Such low energy electrons have a very short range, of one cell diameter or less. In the latter case the radioisotope must be internalized into a cancer cell and be brought close to the cell's nucleus to cause damage to the DNA and destroy the cell. Coupled to a bioconjugate that is selectively internalized into cancer cells it can enhance the ratio for dose equivalent delivered

to the tumour cell with respect to normal cells. This should result in an improved tumour treatment with even less side effects [18]. Interesting pure Auger electron emitters for this purpose are e.g. ^{71}Ge or ^{165}Er, see Figure 2.

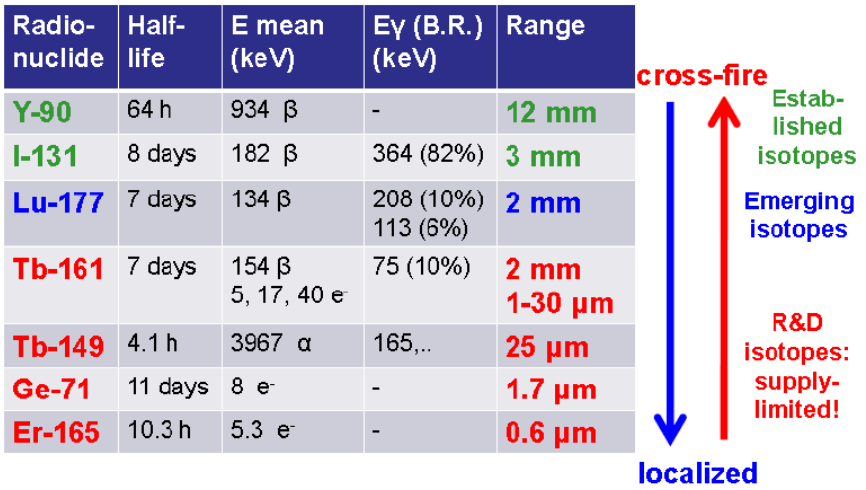

FIG. 2. Comparison of some radionuclides used for therapy. Modern, better targeted, bioconjugates should be combined with adequate radioisotopes that emit shorter-range radiation.

Despite their very promising properties most of these examples (^{149,152,155}Tb, ^{165}Er) are not yet available for clinical trials since the production with conventional methods (compact cyclotrons) is difficult or impossible. However, these isotopes are well produced by high-energy ($\approx$ GeV) spallation of a heavy metal target, e.g. tantalum, see Figure 3. Advanced methods exist to extract and separate the produced isotopes from the irradiated target. At the ISOLDE facility at CERN even very short-lived isotopes (half-lives of milliseconds to seconds) are extracted by the isotope separation on-line (ISOL) technique [20]. For the mentioned longer-lived isotopes the ISOL method is even more efficient. It can also be employed off-line, i.e. alternately irradiating cold targets, then heating them to release the isotopes in question. Today intense high-energy proton beams are only available at few facilities such as particle physics laboratories and spallation neutron sources. If a small part of the primary beam could be branched off for such a purpose, sufficient activity could be produced to treat many thousand patients per year.

Some of the isotopes (e.g. ^{149}Tb) have a relatively short half-life, making shipping over large distances inefficient. Sometimes the future perspectives of very promising therapies requiring few large-scale installations are criticized with the argument that a longer travel

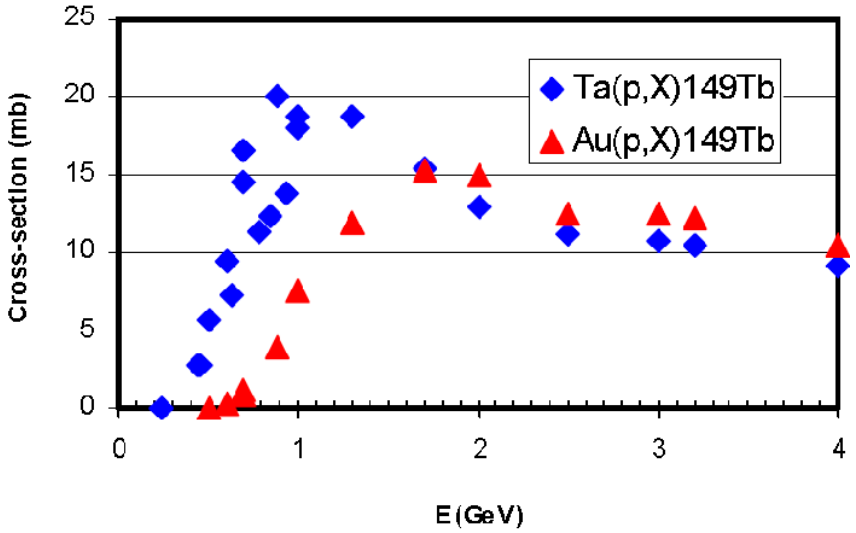

FIG. 3. Cross-sections for spallation production of ^{149}Tb from Ta or Au (as surrogate for Hg) targets. Experimental data [19] from different groups are shown.

to the treatment place is unacceptable for most patients. Today new therapies are indeed often restricted to patients that have already undergone various other therapies and are in a very advanced stage making travel to a remote treatment place difficult or impossible. Once it has been demonstrated that new high-LET therapies such as α-RIT, α-PRRT or hadron therapy with carbon ions show a better ratio of benefit to side effects for the patients it will be applied as therapy at earlier stages of the illness when the patients are in much better shape and could travel more easily to few centralized treatment centers per continent. Note that not so long ago the standard therapy for tuberculosis required an extended stay in the mountains [21].

C. Conclusion and Outlook

Nuclear medicine could not work without radioisotopes produced by neutron-induced reactions. An adequate supply of such isotopes is essential for this discipline. This is not only true for the "workhorse" ^{99}Mo/^{99m}Tc, but even more for emerging and R&D isotopes that have superior decay properties for certain diagnostic and therapy applications.

For radioisotope production the decisive parameter of a neutron facility is the time-averaged flux, not the peak flux. Therefore pulsed facilities have no advantage over continuous facilities. Hence, even next generation spallation neutron sources will not be able to

replace high-flux reactors in this field. However, if at a spallation neutron source also the proton beam from the driver accelerator is employed for isotope production, then complementary radioisotopes with favourable properties can be provided.

The lead times for the development of new pharmaceuticals exceed one decade and the same is true for radiopharmaceuticals. Thus, even if a new future facility could provide the "ideal isotope" it could not enter large-scale clinical practice immediately. "New" isotopes can only proof their superiority in (pre-)clinical studies and in clinical practice if they are provided regularly and with good quality. In the US, DOE is supplying a certain number of R&D isotopes, even if not all are available in the desired quantity [22]. In Europe some groups are experimenting with such R&D isotopes which are provided by bilateral arrangements from the few facilities capable of producing them. Development of new radiopharmaceuticals with "better" isotopes would be far more efficient if an adequate and simple supply of promising R&D isotopes was assured in Europe by the creation of a "distributed" user facility where the reactors and accelerators that are best suited for production of innovative isotopes would provide these for R&D purposes to the interested users. Obviously, while scientists are used to travel to their user facility, radioisotopes have to travel to their "mail-out-users". A European user facility would help to solve the important issues related to logistics and transport more efficiently and consistently.

The model of user facilities that proofed to be so successful for neutron scattering would certainly help promoting radioisotopes with superior properties in nuclear medicine clinical practice and eventually result in better treatment of cancer and other serious illnesses.

III. MEDICAL APPLICATIONS AT A NEUTRON SOURCE

In this section, "medical applications" is interpreted as "directly treating patients". After a short review of the incidence of cancer, and of the main treatment modalities, the two current therapies using (Fast [>1 MeV] Neutron Therapy neutrons and Boron Capture Neutron Therapy or BNCT) are reviewed.

A. Cancer and radiotherapy

Cancer occurs in about one third of the population in the advanced industrial countries, with two-thirds of cases involving people over the age of 65. As the number of people over that age increases through improvements in general health, so the number of cases of cancer is likely to increase. While some cancers are associated with specific risks (for example, the relationship between smoking and lung cancer) and thus the probability of having such a cancer can be reduced by mitigating those risk factors through lifestyle choices, some cancers are unavoidable. Although there have been great advances in understanding, in particular, genetic influences on the incidence of certain cancers, for the foreseeable future methods for treating cancer will still be required.

According to a report [23] by the UK Royal College of Radiologists in 2003 "Radiotherapy remains a mainstay in the treatment of cancer. Comparison of the contribution towards cure by the major cancer treatment modalities shows that of those cured, 49% are cured by surgery, 40% by radiotherapy and 11% by chemotherapy". In this, radiotherapy refers mainly to conventional irradiation using MV X-rays. More than half of patients with cancer will receive radiotherapy at some point during their treatment. Improvements in imaging (CT scans, MRI, PET) have yielded much better location of the tumour, and with this have come many improvements in radiotherapy, including Intensity Modulated Radio Therapy (IMRT) and stereotactic radiotherapy, which achieve remarkable conformance to the tumour shape, leading in general to an increased local tumour control probability (TCP) with decreased normal tissue complication probability (NTCP). Conventional radiotherapy continues to improve.

Wilson [24] proposed in 1947 that protons might be useful as an alternative to X-rays in the treatment of cancer, and over the past 50 years or so more than 50,000 patients have been treated. Until 1990, patients were treated in physics laboratories, using accelerators than were designed, built and operated for scientific experiments, but over the past 20 years new facilities have been built, either attached to hospitals or as purpose-built facilities. There are now more than 30 hospital-based proton and carbon ion centres world-wide, with more planned. It is estimated that one proton centres is needed for every 10 million people, with about one third of that number also capable of delivering carbon ion therapy (suitable for treating, for example, some tumours that are resistant to conventional radiation). The

depth-dose curves are compared for MV X-rays, electrons, protons and neutrons are shown in Figure 4. Note that the neutron depth dose curve depends strongly on energy, so that this is indicative of the main feature of neutron irradiation. Higher energy neutrons, e.g. produced by 66 MeV protons on beryllium targets, are deeply penetrating, similar to 8 MV X-rays. On the other hand, neutrons of few MeV, e.g. produced by fission, have a much steeper drop of dose [25], similar to MeV gamma rays.

In principle, since the depth-dose curve is similar for neutrons and X-rays, the same strategies should work in delivering a lethal dose to the tumour while protecting the organs at risk and limiting the dose to normal tissue.

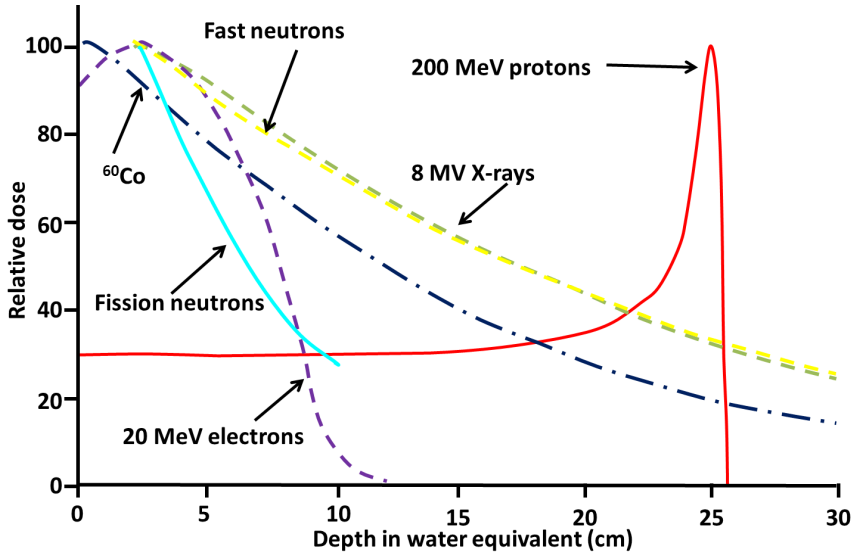

FIG. 4. The depth-dose curve for fast (yellow dotted curve) and fission (light blue solid curve) neutrons compared with MV X-rays and protons.

There are two key concepts in radiotherapy – the Relative Biological Effectiveness (RBE) and the Linear Energy Transfer (LET). The RBE is defined as the ratio of the dose required to achieve a given effect (cell survival probability for example) from a reference radiation (usually MV X-rays) to that of the alternative radiation source (see Figure 5). Note that RBE is not a constant, and depends on many factors, including total physical dose, cell type and position in the cell cycle. The reference radiation is these days usually taken as MV X-rays, and the RBE for protons is around 1.1. The RBE for heavier ions such as carbon is usually taken to be in the range 3-5, and for neutrons the RBE is variable, increasing significantly at low physical doses (see below). Therapeutic doses are often quoted in Gray

Equivalent (GyE), defined as the product of the physical dose and the RBE.

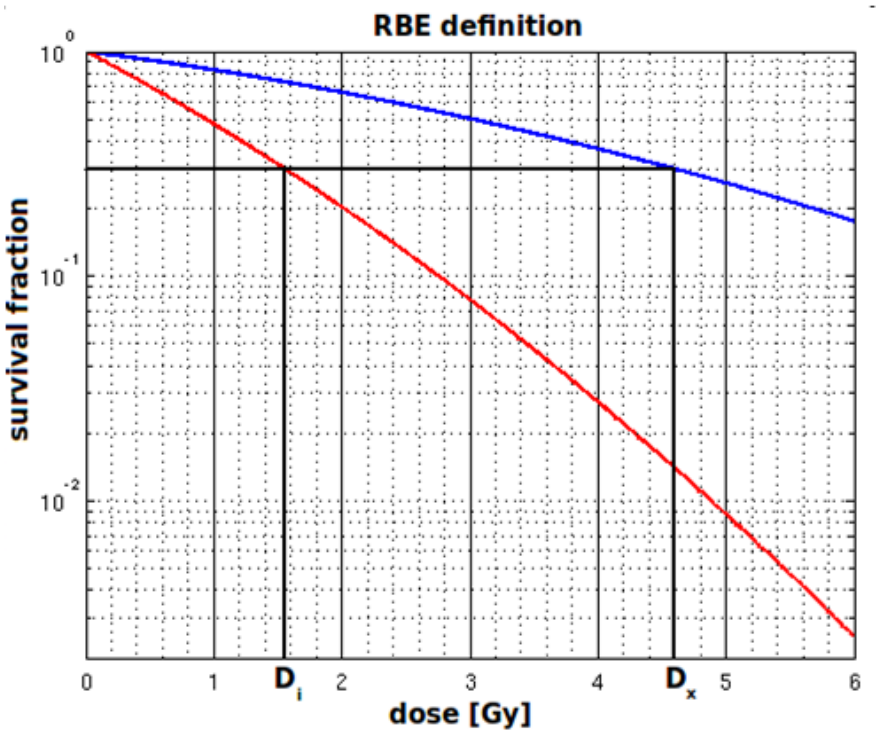

FIG. 5. Definition of RBE. The upper curve is the survival fraction as a function of the physical dose for the reference radiation (MV X-rays) and the lower curve is the survival fraction as a function of the physical dose for the test radiation. The RBE is then the ratio Dx/D1 (∼3 in this example).

The LET is defined as the energy transferred from the radiation source to the tissue per unit length, and is often expressed in keV/micron. This is clearly an important and relevant quantity for X-rays, where only a proportion of the incident energy is deposited in tissue, and this also applies to neutrons. However, for charged particles such as protons or carbon ions, where all of the incident energy is deposited in tissue (see below), the LET is related to the energy loss (dE/dx) by the particle per unit length, as expressed in the Bethe-Bloch equation. Note that the LET is not equal to dE/dx but is somewhat less, because the LET is concerned with the energy deposited in the cell, and some energy is lost through (for example) delta rays. It is convenient to split ionising radiations into low and high LET. Electrons, X-rays and protons are typically low LET radiation sources, whereas light ions (alphas, carbon ions) and neutrons have high LET. As an illustration, 1 Gy corresponds to about 1000 electron tracks, leading to 20-40 double strand breaks in the DNA chain, distributed more or less uniformly among the chromosomes, whereas the same 1 Gy dose,

leading to the same number of double strand breaks, corresponds to about 2 alpha particles, with the damage concentrated in a few chromosomes.

These two quantities are combined in Figure 6, which compares the deposition of dose as a function of depth in tissue for 8 MV X-rays and protons. The X-ray profile rises sharply reaching a peak at about 3 cm below the surface of the skin and then falls off more or less exponentially. By irradiating the tumour from many different directions, a significantly higher dose can be deposited in the tumour while keeping the dose to normal tissue and the vital organs sufficiently low that the body's normal mechanisms can repair the damage, although there are still likely to be some toxic reactions and there is always a risk of secondary tumours developing later. With protons, by selecting the energies correctly, more dose is deposited in the tumour than in normal tissue, even from a single direction, because of the characteristic "Bragg peak" where the rate of energy loss increases dramatically ($\sim 1/v^2$) as the charged particle comes to the end of its range.

One particular application of proton therapy is for the small number of rare childhood cancers. The advantage of proton therapy over alternative treatments is that a very much smaller volume of normal tissue is irradiated, thus reducing the probability of secondary tumours developing later in life, avoiding damaging the vital organs in the abdomen and thorax, and minimising disfigurement due to uneven growth of irradiated healthy tissue.

Radiation therapy is an important weapon in the treatment of many localised cancers. Modern radiotherapy, because of the improvements in imaging and earlier diagnosis, is increasingly sophisticated leading to better outcomes (increased local tumour control with reduced normal tissue toxicity) but, as always, there is room for further improvement and innovation.

1. Fast Neutron Therapy

Fast neutrons, like MV X-rays, pass through the body but, unlike X-rays, undergo nuclear interactions and produce high LET radiation damage. By irradiating from several different directions, a large amount of damage can be inflicted on the tumour while keeping the dose to normal tissue sufficiently low that repair can be effective. Fast neutron therapy is available in a few places, and has been shown (see for example [26]) to be effective in the treatment of certain tumours.

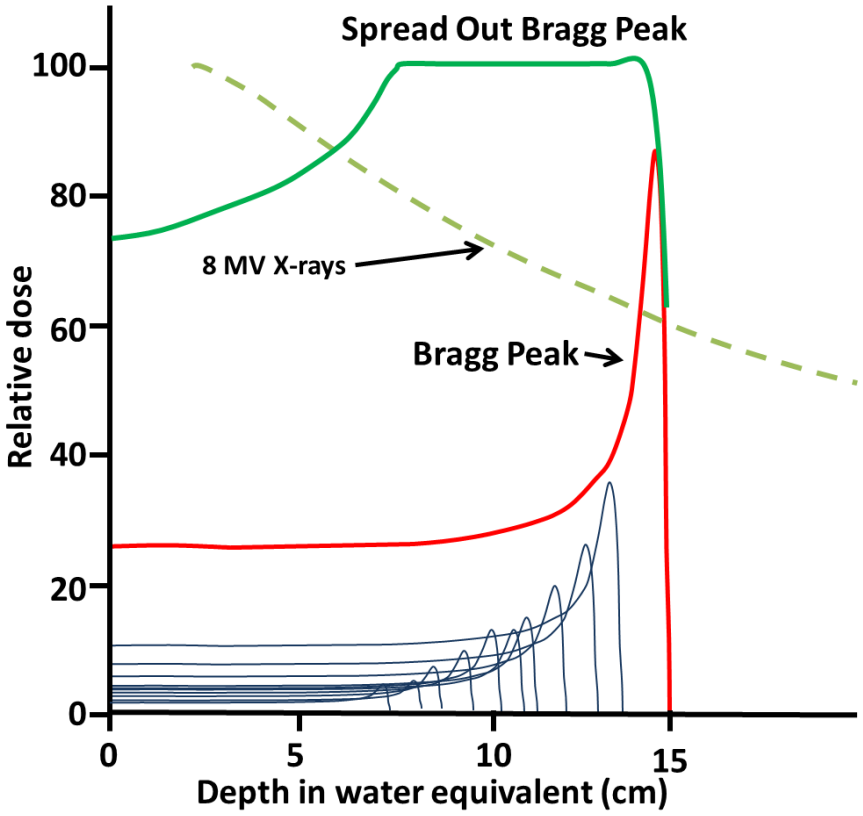

FIG. 6. The relative dose deposited as a function of depth in tissue (or water equivalent) for ^{10}MV X-rays and protons. The "Bragg Peak" (red) is the depth-dose profile for protons of a single energy. In order to cover the tumour, the proton energy is varied as shown (blue) in order to achieve a uniform dose (green) throughout the tumour – the Spread Out Bragg Peak (SOBP).

The clinical experience comes from several sources. Early results (see [27]) from the Hammersmith Hospital compared neutrons and X-rays with encouraging results, and at the University of Washington patients with salivary gland cancers were given a neutron boost, again with good results. A randomised control trial [28] reported increased local tumour control (70% neutrons against 58% X-rays) and ten-year survival rates (46% neutrons against 29% X-rays) for locally advanced prostate cancer. Work in Edinburgh (see [27]) on deep-seated tumours (e.g. bladder) gave disappointing results with no gain in tumour control and significant normal tissue toxicity and late malignancies. At Clatterbridge near Liverpool (see [27]), using higher energy neutrons from a 64 MeV cyclotron, no advantage was seen in tumour control with increased side effects and higher metastatic rates. Nevertheless, other centres report better results, with good control for example for prostate cancer (see

Figure 7).

The depth dose curve of fission neutrons in the MeV range is very distinct from that of high energy neutrons (tens of MeV) discussed previously. Due to the rapid drop of dose they are suited to treat shallow tumours close to the surface, sparing deep seated organs behind the tumour. Such cases are e.g. salivary gland tumours, malignant melanoma, chest wall recurrences of metastatic breast tumour or other unresectable tumours on the surface [4].

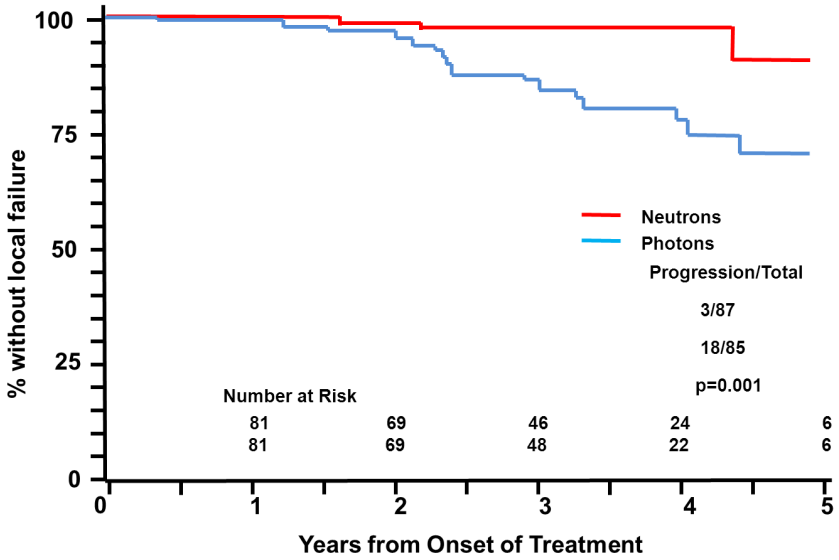

FIG. 7. Local tumour control for prostate cancer, neutrons compared with X-rays (after Wambersie et al, NEUDOS-2009, iTHEMBA, South Africa).

One of the problems with neutrons is that the RBE for fast neutrons varies with dose, as shown in Figure 8. Alike other high-LET radiation such as heavy ions, at low doses, neutrons are relatively more damaging. This effect has to be accounted for in a dedicated treatment planning.

2. Boron Neutron Capture Therapy (BNCT)

BNCT uses a binary approach in which two agents that are separately non-toxic (or little toxic) when combined in the tumour become toxic and are thus able to inflict fatal damage to the cancer cells while limiting damage to healthy tissue. In BNCT, a stable isotope (^{10}B) which has a high neutron capture cross section followed by breakup to charged particles is attached to a suitable molecule and ingested and selectively absorbed by the more rapidly

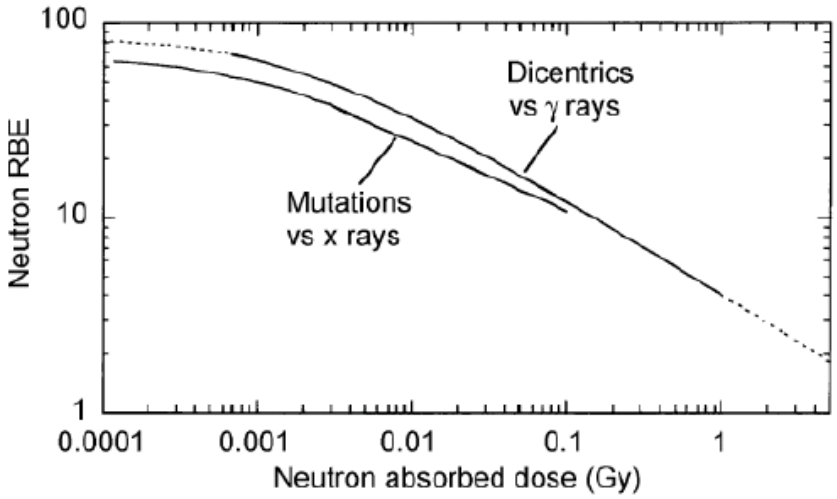

FIG. 8. The relative biological effectiveness (RBE) of neutrons for the induction of dicentric chromosomes (upper curves) and for mutations in Tradescantia (lower curves) as a function of the neutron-absorbed dose (lower panel). Dotted sections of the curves are extrapolations beyond the actual data. The chromosome data refer to ^{60}Co γ rays and 0.39 MeV neutrons; the mutation data refer to 0.43 MeV neutrons and 250 kV x rays. From ICRP 92: "Relative Biological Effectiveness (RBE), Quality Factor (Q), and Radiation Weighting Factor (wR)".

growing cancer cells. Second, the tumour site is irradiated with thermal or epithermal neutrons from a reactor or produced by an accelerator, triggering the reaction. The breakup fragments have low energy and are thus highly ionising and therefore very damaging. It was first proposed by Locher [29] in 1936, and early experiments using boric acid and related compounds were carried out at Brookhaven in the 1950s, but with disappointing results [30]. There has been renewed interest since the mid-1990s with the development of more sophisticated boron-containing compounds such as sodium borocaptate ($Na_2B_{12}H_{11}SH$ – BSH) or boronophenylalanine ($C_9H_{12}O_4BN$ – BPA). In the case of Boron, the relevant reaction is ^{10}B(n,α)^{7}Li, which has an effective nuclear cross-section of 3840 b and a Q-value of 2.79 MeV, producing mainly a 1.47 MeV α particle and a 0.84 MeV ^{7}Li nucleus, along with some γ-radiation. At these energies, the local energy deposition rate or LET (Linear Energy Transfer) is very high and therefore very damaging; the sum of the ranges of the two daughter products is about 12μm, or of the order of the size of a cell. The damage is thus very high and quite local. This also clearly has good normal tissue sparing properties, although there is a low dose due to the gamma radiation. While the toxicity of the boron-

loaded compounds for normal tissue is low, the neutron fluence has a non-negligible toxicity for normal tissue, e.g. due to ^{14}N(n,p) reactions on nitrogen that is omnipresent in human cells, in particular in amino acids.

BNCT is available at a small number of centres world-wide. A report [31] in 2008 included ∼350 patients who had been treated with BNCT, mainly brain and head-and-neck. It has also been used for high-grade gliomas, and specifically glioblastoma multiforme, which are highly resistant to most alternative forms of therapy. A course of treatment requires neutron flux densities $>10^9$ n./(cm^2 s) if individual treatment times are not to be unreasonably long ($<$ hour), but even so takes several sessions, although this is quite short relative to most conventional radiotherapy. The main source of neutrons is from reactors, but accelerator driven sources are being investigated, making the therapy more likely to be available in hospitals. Epithermal neutrons from accelerator-driven neutron sources would be required for deeper-seated tumours.

A review in 2005 [32] concluded: "Critical issues that must be addressed include the need for more selective and effective boron delivery agents, the development of methods to provide semi-quantitative estimates of tumour boron content before treatment, improvements in clinical implementation of BNCT, and a need for randomized clinical trials with an unequivocal demonstration of therapeutic efficacy. If these issues are adequately addressed, then BNCT could move forward as a treatment modality." While there has been more work in the interim, with significant new information, BNCT is not yet a standard treatment modality, and further trials are required to assess its clinical effectiveness and to measure the associated normal tissue complication probabilities.

IV. CONCLUSIONS FOR ESS

A. Thermal neutron irradiation position

The installation of an in-pile irradiation position with very high thermal neutron flux is definitively of high interest for the production of radioisotopes. It would be worthwhile to study if a "flux trap" (surrounded by neutron reflectors) could be used to enhance the locally available neutron flux sufficiently without affecting too much neighbouring beam tubes. Maybe a position that is geometrically not useable for extraction of neutron beams

could serve for such irradiations.

A flux above $1 \cdot 10^{15}$ n./(cm^2 s) would be extremely beneficial since it would enable production of certain radioisotopes with very high specific activities. Only three reactors world-wide have irradiation positions that reach such a flux: SM-3 in Dimitrovgrad, HFIR in Oak Ridge and ILL in Grenoble.

A flux above $4{\cdot}10^{14}$ n./(cm^2 s) would provide much needed backup capacity for production of innovative radioisotopes in Europe. Within EU only the high-flux reactors of ILL, BR2 in Mol, RJH in Cadarache (under construction) and Pallas (planned in the Netherlands) have positions with such high flux.

A position with lower flux (1–3 $\cdot 10^{14}$ n./(cm^2 s)) is still very useful for production of a variety of isotopes. For shorter-lived isotopes ESS could even become a principal source serving the regional market in Northern Europe.

Note that for certain isotopes a somewhat lower thermal neutron flux is acceptable if a strong epithermal flux component is present.

B. Fast neutron irradiation position

A second, separate, irradiation position with an intense fast neutron flux ($>1{\cdot}10^{14}$ n./(cm^2 s)), ideally with a strong component between 2 and 15 MeV and few thermal neutrons, would allow complementary production of other important radioisotopes and isomers by reactions such as (n,p), (n,2n), (n,n') or (n,α).

C. High energy proton irradiation position

Facilities providing intense beams of high energy (> 70 MeV) protons are even more scarce than neutron facilities capable of providing high neutron fluxes. Some injector accelerators for presently operating spallation neutron sources (LAMPF, PSI) or other high energy proton facilities (BNL) are providing already today important radioisotopes for nuclear medicine. The demand for such isotopes is rising and additional production capacity will be needed in future. It should be studied if part of the driver beam of ESS could be branched off with an intermediate energy for isotope production.

Some of the most promising radioisotopes for nuclear medicine can be produced by spal-

lation with protons > 1 GeV. Due to the multitude of radioisotopes produced in the same target, the quest for monoisotopic products will often require that the chemical separation has to be complemented by mass separation. The latter can be performed either on-line (ISOL) or off-line, e.g. by repeated cycles of irradiating and heating ISOL-type targets. For this purpose compact targets are preferred that are not necessarily compatible with primary beam currents in the mA range. A separated beamline should be foreseen to which a less intense proton beam ($\leq$ 0.1 mA on average) can be delivered.

A very straightforward additional use of high-energy protons can be made by machining the collimators that intercept part of the proton beam from titanium or vanadium. Spallation-produced ^{44}Ti will accumulate in these materials and can be retrieved after several years of irradiation and after decay of shorter-lived activities. ^{44}Ti ($T_{1/2}$=60 a) serves for producing ^{44}Ti/^{44}Sc generators that provide the positron-emitting nucleus ^{44}Sc ($T_{1/2}$=3.9 h).

D. Radioisotope extraction from liquid spallation target

A huge diversity of spallation products is created in the targets of spallation neutron sources. When using liquid spallation targets and implementing suitable extraction methods, part of these radioisotopes could be extracted continuously or batch-wise.

For this purpose a spallation target made from mercury is strongly preferred over lead-bismuth or lead since it is compatible with more promising extraction methods [33] and avoids problems related to contamination with long-lived polonium isotopes. Regular extraction of spallation products from the target material could moreover help to limit the build-up of a large inventory of long-lived radioisotopes in the spallation target.

E. Conclusions on the therapeutic uses of neutrons

Neutrons are certainly very potent and can inflict serious damage to cancerous cells, either directly as in fast neutron therapy or indirectly as in BNCT, and there is evidence that for some indications, neutrons (perhaps in combination with other modalities) are very effective in cancer control. Issues with normal tissue toxicity, especially at low doses, need to be carefully taken into account in treatment planning.

Existing facilities, such as MEDAPP at FRM2, are not overbooked and could accommodate more patients from abroad (FRM2 is just 15 minutes from MUC airport). Thus the catchment area could be enlarged for those rare cancer types that are best suited for neutron therapy. Such an approach could improve the quality-of-life for more patients and would be more efficient in gathering statistically significant data on the superiority of neutron beam therapy than waiting for the construction of similar treatment facilities at other places.

---

[1] C. Vettier et al.. "Neutrons and Health", ESS Scandinavia, http://ess-scandinavia.eu/documents/Neutrons_and_Health-lowres.pdf

[2] D. Lewis, Eur. J. Nucl. Med. Mol. Imaging **36** (2009) 1371.

[3] F. Deconinck, B. Ponsard, Position Paper of the High Scientific Council of the European Nuclear Society, "The refmedical isotope crisis calls for political action". http://www.euronuclear.org;

[4] B. Loeper, F.M. Wagner; S. Büdel; M. Harfensteller, A. Voit, R. Henkelmann, Neutron News **21** (2010) 16.

[5] The Supply of Medical Radioisotopes, An Economic Study of the Molybdenum-99 Supply Chain, NEA-OECD report Nr. 6967 (2010), http://www.nea.fr/med-radio/

[6] K. Yoshinaga, R. Klein, N. Tamaki, J. Cardiol. **55** (2010) 163.

[7] K.P. Zhernosekov, D.V. Filosofov, R.P. Baum, P. Aschoff, H. Bihl, A.A. Razbash, M. Jahn, M. Jennewein, F Rösch, J. Nucl. Med. **48** (2007) 1741.

[8] C. Grignon et al., Nucl. Instr. Meth. A **571** (2007) 142.

[9] W.A. Wohlgemuth, G. Leissner, H. Wengenmair, K. Bohndorf, K. Kirchhof, J. Endovascular Surg. **51** (2010) 473.

[10] The ESS Project. Vol. III, Technical Report (2002).

[11] J.C. Reubi, H.R. Mäcke, E.P. Krenning, J. Nucl. Med. **46** (2005) 67S.

[12] C.A. Boswell, M.W. Brechbiel, Nucl. Med. Biology **34** (2007) 757.

[13] M. van Essen, E.P. Krenning, B.L. Kam, M. de Jong, R. Valkema, D.J. Kwekkeboom, Nature Reviews Endocrinology 5 (2009) 382.

[14] R. Henkelmann et al., Eur. J. Nucl. Med. Mol. Imaging **36** (2009) S267.

[15] L.F. Mausner, K.L. Kolsky, V. Joshi, S.C. Srivastava, Appl. Radiat. Isot. **49** (1998) 285.

[16] G.J. Beyer, M. Miederer, S. Vranjes-Duric, J.J. Comor, G. Künzi, O. Hartley, R. Senekowitsch-Schmidtke, D. Soloviev, F. Buchegger, the ISOLDE Collaboration, Eur. J. Nucl. Med. Mol. Imaging **31** (2004) 547.

[17] B.J. Allen, G. Goozee, S. Sarkar, G. Beyer, C. Morel, A.P. Byrne, Appl. Radiat. Isot. **54** (2001) 53.

[18] F. Buchegger, F. Perillo-Adamer, Y.M. Dupertuis, A. Bischof Delaloye, Eur. J. Nucl. Med. Mol. Imaging **33** (2006) 1352.

[19] EXFOR database; `http://www.nndc.bnl.gov/exfor`

[20] U. Köster, Eur. Phys. J. A **15** (2002) 255

[21] T. Mann, The Magic Mountain, S. Fischer Verlag (1924).

[22] M.J. Rivard, L.M. Bobek, R.A. Butler, M.A. Garland, D.J. Hill, J.K. Krieger, J.B. Muckerheide, B.D. Patton, E.B. Silberstein, Appl. Radiat. Isot. **63** (2005) 157.

[23] RCR document BFCO (03) 3, (2003), ISBN 1872599 90 7.

[24] R.R. Wilson, "Radiological uses of fast protons", Radiology **47** (1946) 487.

[25] F.M. Wagner et al., Strahlentherapie Onkologie **184** (2008) 643.

[26] A.J. Lennox, "High Energy Fast Neutron Therapy for Radioresistant Cancers", see `http://www.neutrontherapy.com/documents/Lennoxpaper.pdf` ; J. Forman et al., "A randomized prospective trial of sequential neutron-photon vs. photon-neutron irradiation in reforgan confined prostate cancer", Int. J. Radiation Oncology Biology Physics **54** (2002) 10.

[27] B. Jones, `http://medicalphysicsweb.org/cws/article/opinion/32466` (2008); see also W. Duncan, "An evaluation of the results of neutron therapy trials", Acta Oncol. **33** (1994) 299; R.D. Errington et al, "High energy neutron treatment for pelvic cancers: study stopped because of increased mortality", British Medical Journal, **302** (1991) 1045.

[28] G. E. Laramore et al, "Fast Neutron Radiotherapy for Locally Advanced Prostate Cancer", Am. J. Clin.. Oncol. **16** (1993) 164.

[29] G.L. Locher, "Biological effects and therapeutic possibilities of neutrons", Am. J. Roentgenol. Radium. Ther, **36** (1936) 1.

[30] L.E. Farr et al, Am. J. Roentgenol. Radium Ther. Nucl. Med. 71 (1954) 279; J.T. Goodwin et al., Cancer **8** (1955) 601.

[31] K. Kortelainen, "Radiography in BNCT treatments in Finland", ISRRT, Durban 2008.

[32] R.F. Barth et al, "Boron Neutron Capture Therapy of Cancer: Current Status and Future

Prospects", Clin Cancer Res. **3987** (2005) 11.

[33] J. Neuhausen, D. Schumann, R. Dressler, S. Horn, S. Lüthi, S. Heinitz, S. Chiriki, T. Stora, M. Eller, "Innovative Waste Management in the Liquid Hg-Loop", Final report of EURISOL Design Study (2009).